Doctoral Dissertation

Degradation control of oxidized dextran-based hydrogel via Michael addition for drug delivery application

Punnida Nonsuwan

Supervisor: Associate Professor Kazuaki Matsumura

School of Materials Science

Japan Advanced Institute of Science and Technology

December 2018

Referee-in-chief:

Associate Professor Dr. Kazuaki Matsumura

Japan Advanced Institute of Science and Technology

Referees:

Professor Dr. Masayuki Yamaguchi

Japan Advanced Institute of Science and Technology

Professor Dr. Tatsuo Kaneko

Japan Advanced Institute of Science and Technology

Professor Dr. Nongnuj Muangsin

Chulalongkorn University

Associate Professor Dr. Takumi Yamaguchi

Japan Advanced Institute of Science and Technology

Abstract

Previously the biomedical application of polysaccharide hydrogel that was derived from aldehyde-introduced dextran by periodate oxidation and polyamine was reported and the hydrogels showed rapid degradation through main chain scission in the oxidized dextran which was triggered by Schiff base formation with amine and subsequent Maillard reaction [1, 2]. However, the formation and degradation of this hydrogel was simultaneously occurred after multiple Schiff base formation reaction between aldehyde and amino groups, therefore the degradation timing control was difficult [1, 3]. To overcome this uncontrollable degradation of the hydrogel, the oxidized dextran hydrogel was prepared with the aldehyde groups preserved. In this thesis, the oxidized glycidyl methacrylate derivatized dextran (Dex-GMA)-based hydrogel formed via thiol-en cross-linking by Michael addition without using aldehyde group was prepared. The prepared hydrogel was stable in phosphate buffer solution (PBS) but degradation could be initiated by addition of amino compounds by causing Maillard reaction. These findings indicate that the degradation of hydrogel can be controlled by the amino group addition. In addition, the degradation speed of oxidized Dex-GMA-based hydrogel was also controlled independently of mechanical properties because the crosslinking points and degradation points are different. And by kinetic analysis with NMR measurement, molecular mechanism behind the crosslinking between thiol and aldehyde groups was observed to explain control of the degradation of dextran derivatives. To lead this hydrogel to a smart material, the release of amino source should be controlled for further controlling the degradation of hydrogel. In this part, amino compounds were functionalized on carrageenan chain (amino-CG) to act as dual-functioned material of being amino source and showing temperature-responsive behavior. The polydopamine microspheres (PDA), which is an NIR photothermal agent, were composited with carrageenan

derivative (amino-CG@PDA micromposite). The role of PDA is to convert NIR light to energy and then to transform it to heat. The amino-CG@PDA beads are sensitive to the temperature change, finding that the amino compounds were released at 40℃ via gel-to-sol phase transition but dissolution of beads were not observed at 37℃. The release of amino groups from the phase transition of amino-CG@PDA microcomposites was enhanced by increasing temperature and more greatly under external NIR light. Thus, the release rate of amino compounds can be controlled by switching NIR-light irradiation. In addition, the degradation of oxidized Dex-GMA by amino groups release from amino-CG@PDA was investigated. The amino-CG provides the ability to be the amino source for the reaction with aldehyde groups from oxidized Dex-GMA to introduce the main chain degradation. The release of doxorubicin (DOX) from oxidized Dex-GMA-based hydrogel was controlled under NIR irradiation due to the Schiff base reaction of amino compound release from amino-CG and the preserved aldehyde on hydrogel, consequently, the degradation occurred and drug can be released. Thus, this work presents an alternative way for controlling the degradation of hydrogel to potentialize in clinical applications for cell scaffolds in regenerative medicine and drug delivery system carriers.

Keywords: hydrogel, biodegradation, aldehyde dextran, NIR irradiation, drug delivery

References

1. Hyon, S.-H.; Nakajima, N.; Sugai, H.; Matsumura, K., Low cytotoxic tissue adhesive based on oxidized dextran and epsilon-poly-l-lysine. *J. Biomed. Mater. Res. A* **2014,** *102* (8), 2511-2520.

2. Chimpibul, W.; Nagashima, T.; Hayashi, F.; Nakajima, N.; Hyon, S.-H.; Matsumura, K., Dextran oxidized by a malaprade reaction shows main chain scission through a maillard reaction triggered by schiff base formation between aldehydes and amines. *J. Polym. Sci. A* **2016,** *54* (14), 2254-2260.

3. Matsumura, K.; Nakajima, N.; Sugai, H.; Hyon, S. H., Self-degradation of tissue adhesive based on oxidized dextran and poly-L-lysine. *Carbohydr. Polym.* **2014**, *113*, 32-38.

Contents

This dissertation was prepared according to the curriculum for the Collaborative Education Program organized by Japan Advanced Institute of Science and Technology and Chulalongkorn University.

Chapter 1

General introduction

1.1 Research background

Hydrogels are crosslinked polymer networks that are able to swell in many solvents and aqueous environments without dissolving. The development of hydrogel technologies has been more interested in biomedical fields. Hydrogels particularly polysaccharide degradable hydrogel now pay attention to many tissue engineering scaffolds, wound dressings and drug delivery system [1,2,3]. Among of these applications drug delivery has become attractiveness. Hydrogel degradation can be used to control the release rate of the delivered component and also be safety to body when it is no longer needed. In our laboratory, successfully prepared degradation hydrogel by the reaction between the aldehyde-dextran and amino groups [4,5]. The formation of Schiff base and multiple crosslinking points were formed leading to hydrogel formation and suddenly started degradation. However, the unfovourableness of this hydrogel is lack of control the degradation time of hydrogel after Schiff base is formed. Thus, to overcome an unexpected degradable time and prolong the stability of hydrogel, the preparation of oxidized dextran based hydrogel without amino groups was suggested for degradation control and applying in drug delivery system. The aldehyde groups are left after hydrogel formation and the degradation of this hydrogel was controlled by amino source addition dependently mechanical properties.

Another newly emerged system, namely, near-infrared (NIR) light-responsive materials, has been intensively explored for biomedical application owing to their greater penetration

abilities and less damage to the tissue [6]. NIR optical stimulus is attractive as it can be remotely applied for a short period of time with high spatial and temporal precision. It would be more advantageous to materials that show thermoresponsive ability upon NIR light exposure can be controlled stimuli-responsive release systems. Therefore, to be control the release of amino groups at the desired time, the amino-carrageenan was introduced. The temperature-responsive polymer, carrageenan, was functionalized by amine group to obtain the amino-carrageenan product. The control release of amino source was triggered by photothermal agent stimulated by NIR. Hence, the degradation of oxidized dextran based hydrogel by the release of amino groups when amino-carrageenan absorbs heat was studied and reported in detail in this thesis.

1.2 Hydrogel

1.2.1 Hydrogel in drug delivery

In recent years, the hydrogel technology has been an integral part of human health care. The pharmaceutical industry has been developing hydrogel based drug delivery system in an advanced manner by tuning the structure, shape and surface modifications of the biopolymers. The highlighted properties of some natural and synthetic polymers such as dextran, carboxymethyl cellulose, poly(acrylic acid), and poly(2- hydroxyethylmethacrylate) etc. as a highly water swollen, soft and elastic gel leading to the keen interest in hydrogels as a class of biomaterials and their application as drug delivery systems. Three dimensional network formation occurs by the cross linking of the polymeric chains via physical interactions, covalent bonding, hydrogen bonding and by van der walls interactions [7]. The presence of the specific functional groups such as -OH, -$CONH_2$, -SO_3H, -CONH, and -COOR which have a hydrophilic tendency lead to the high content of water and biological fluids absorption (typically 70–99%) [8,9]. The soft and rubbery surface, structure and physicochemical properties of hydrogels similarity to that

of human tissue and can give the hydrogels excellent biocompatibility and the capability to easily encapsulate drugs. These characteristic features make hydrogels potential candidate for drug delivery systems.

Potentiality of hydrogel for drug delivery have been explored to reduce the release rate of drug from hydrogels by enhancing the interactions between drug and hydrogel. Both physical and chemical strategies can be manipulated to enhance the binding between a loaded drug and the hydrogel matrix. In case of physical interactions, the charge interactions between ionic polymers and charged drugs have been employed to increase the binding strength of target drugs and hydrogel. For example, the modification of gelatin hydrogels with amino acid could prolong the release of lysozyme and trypsin inhibitor protein because of the charge interactions between the amino acid chain and the entrapped proteins [10]. The anionic polymer, phosphate-functionalized N-isopropylacrylamide-based hydrogels (PNIPAM-based hydrogel) showed high uptake of cationic lysozyme comparing to non-functionalized PNIPAM hydrogels [11]. Similarly, our hydrogel; oxidized Dex-GMA based hydrogel performed the charge interaction with positive charge drug, consequently, drugs can be entrapped by this hydrogel.

1.2.2 Hydrogel degradation

Hydrogels have been a focus of attention for many years and are widely used in a variety of bio-related applications since they are typically biocompatible; furthermore, their moisture content can mimic the natural water content of human tissue [12,13]. The controlling mechanical properties and degradation behavior of hydrogel have focused to design and tailor appropriate materials for drug delivery and tissue engineering [14,15]. The degradation behavior control has been one of critical topics in general biomaterials research, and widely investigated until now. In general, biomaterials need to be gotten rid of from the body once they complete their roles in the

body, and degradable materials could be ideal for this purpose. The degradable hydrogels were typically obtained by two approaches. In the first case, the backbone of design gelling polymer is degradable hydrolysis and/or enzymatic action such as the degradation of aliphatic polyester and collagen were undergone main chain scission by hydrolysis and enzymatic action, respectively [16,17]. The second approach involves introduction of degradable cross-linking points to systems that are comprised of non-degradable polymer chains, for instance, hydrogel formation by crosslinking four-arm amine-terminated poly(ethylene glycol) (4-arm-PEG-NH_2) using an azo-containing linker was rapidly degraded by NIR laser and photolysis with ultraviolet light [18].

1.3 Polysaccharides-based hydrogel

Polysaccharides are carbohydrate polymers in which monosaccharide ($(CH_2O)_n$) units are covalently joined by an O-glycosidic bond in either a branched or linear configuration. Polysaccharide can be a homopolysaccharide, in which all the monosaccharides are the same, or a heteropolysaccharide in which the monosaccharides vary. Depending on which monosaccharides are connected, and which carbons in the monosaccharides connects, polysaccharides take on a variety of forms. Due to their structure, polysaccharides can have a wide variety of functions in nature. Some polysaccharides serve as stores of energy, as in glycogen (branched polysaccharide of glucose), some for sending cellular messages and others as a structural component providing support to cells and tissues, as in cellulose (linear polysaccharide of glucose).

Polysaccharides are produced from different sources obtained from microorganisms, plants, and animals. Polysaccharides made by microrganisms are secreted from the cell to form a layer over the surface of the organism. Microbial polysaccharides such as xanthan, xylinan, gellan, curdlan, pullulan, dextran, scleroglucan, schizophyllan, and cyanobacterial polysaccharides are available in commercial using for food, pharmaceutical, and medical

applications [19,4,20]. Polysaccharides in plants such as starch (a polymer of glucose, being found in the form of both amylose and the branched amylopectin) and cellulose are well known plant polysaccharides which used as a storage and support polysaccharide in plants. Chitin, an example of animal polysaccharide, is the exoskeleton of many arthropods, and is the main component of cell walls in fungi, radulas of mollusks etc. The utilization of polysaccharide should consider the structure, properties, production and modification to potentialize its applications.

1.3.1 Dextran-based hydrogel and its degradation

Dextran is a bacterial polysaccharide consisting essentially of α-1,6 linked glucopyranoside residues with a small percentage of α-1,3 linked residues. It contains the large amount of hydroxyl groups leading to high hydrophilicity and capability for chemical functionalization [1,21]. Dextran has been chosen in many biomedical applications due to its biocompatibility [22], low toxicity [4], high abundant in nature and degradation by enzyme in various part of the human body such as spleen, liver and colon [1,23]. It is slowly degraded by human enzymes as compared to other polysaccharides (e.g. glycogen with α-1,4 linkages) and cleaved by microbial dextranases in the gastrointestinal tract. In addition, it has been used as macromolecular carrier for delivery of drugs and proteins to increase the prolongation of therapeutic agents in systemic circulation. The elimination of dextran depends on its molecular weight (Mw). Low Mw, Mw < 40 kDa can be eliminated through renal clearance and have a half-life of 8 h, in contrast molecules with Mw > 40 kDa have larger half-lives and would be shortened in the liver and spleen and then hydrolysed by endo and exodextranases [1,23]. Moreover, the control degradation of dextran by enzymes or other methods to the target site and desirable time has been widely studied for utilization in drug delivery system.

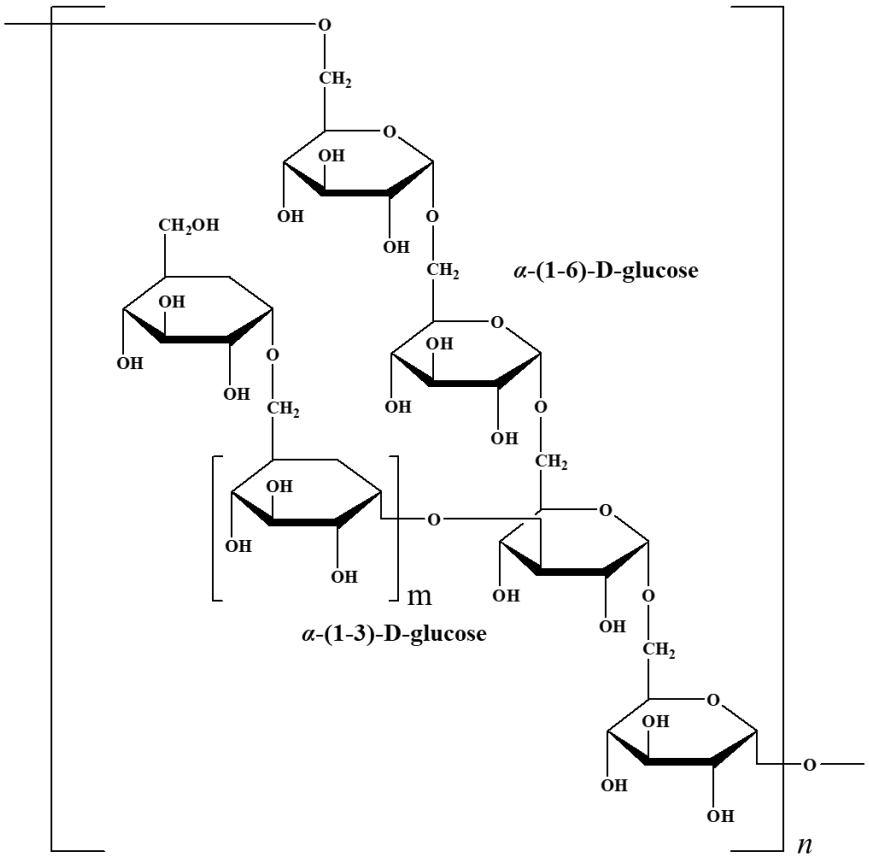

Figure 1.1 Dextran structure.

Focusing on dextran degradation, the main goal of this research has been descripted by both of two approaches. Enzymatic degradation of dextran and its derivatives were performed using dextranase and proceeds through the selective chain scission at the 1,6-*α*-glycosidic linkage between the saccharide units to generate D-glucose [24,23,25]. Enzymatically degradable nitric oxide (NO) releasing S-nitrosated dextran thiomers using for the treatment of drug resistant cancer cells was reported [26]. The release of NO under arterial blood conditions, followed by their sensitivity to undergo enzymatic degradation by dextranase presented in Figure 1.2. There is the reports on the degradation behavior of in situ gelling hydrogel matrices composed of positively and negatively charged dextran microspheres by hydrolysis of the carbonate ester bond

between the dextran backbone and the crosslinked HEMA side chains results in degradation of the dex-HEMA gels at physiological pH making them suitable for various biomedical applications in drug delivery, tissue engineering, and tissue adhesion [4,27]. The adhesive hydrogel formed by the Schiff base reaction of aldehyde dextran and epsilon-poly-L-lysine (**ε**-PL) was reported [4]. Its low cytotoxicity, good adhesive strength, and self-degradation were obtained which can be developed as a biological glues in wound healing process. Interestingly, the Schiff base formation between the reaction of aldehyde groups from oxidized dextran and the primary amino group showed the self-degradation of dextran chain which could be ascribed to a Maillard reaction (see 1.5.4) [4,28]. Chimpibul et al. (2016) suggested that the main chain degradation of oxidized dextran via Schiff base formation depended on the oxidation ratio and amino acid concentration and also descripted main chain scission mechanism of oxidized dextran triggered by reaction with amine which shows the degradation pathways in Figure 1.3. The degradation proceeded via Amadori rearrangement, Strecker degradation and melanoidin formation, leading to produces the brown color during polysaccharide degradation. The findings help to elucidate the reaction mechanism of polysaccharide degradation and develop novel biodegradable polysaccharide materials for biomedical applications.

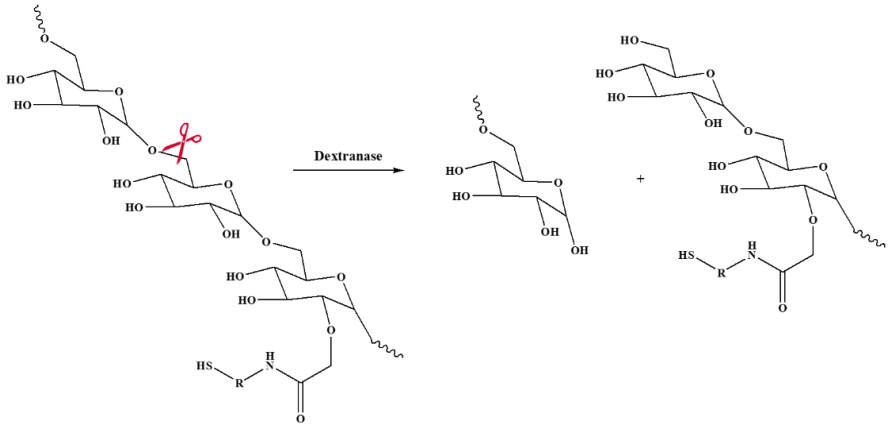

Figure 1.2 Schematic illustration of chain scission at 1,6-*α*-glycosidic linkage by dextranase [26].

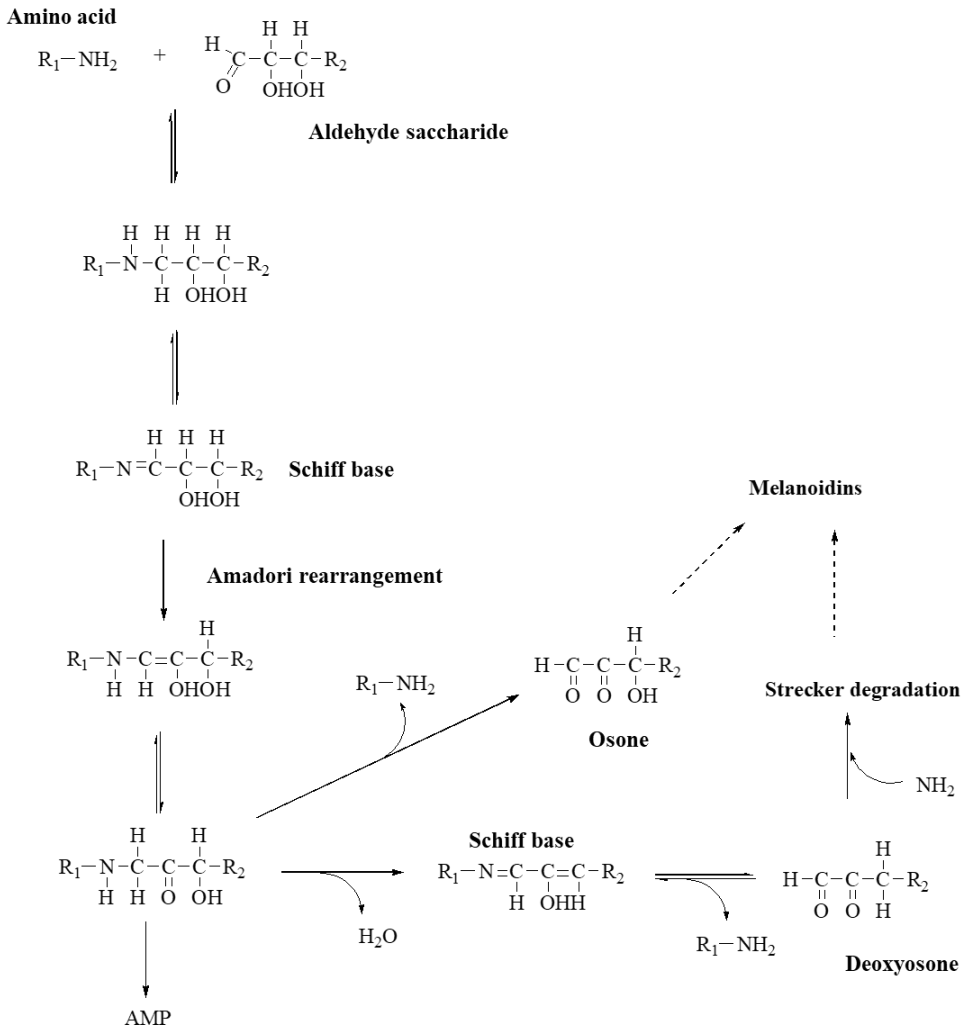

Figure 1.3 Degradation pathways for the reaction of aldehyde saccharides and amino acids via Maillard reaction [5].

1.3.2 Carrageenan thermo-sensitive gelation and its degradation

Carrageenan, a naturally occurring anionic sulfated linear polysaccharides extracted from edible red seaweeds [29]. The basic structure of carrageenan is based on alternating copolymers of 1,3-linked *β*-D-galactose and 1,4-linked *α*-D-galactose, with varying degrees of sulfatation.

The units are joined by alternating α-1,3 and β-1,4 glycosidic linkages forming the disaccharide repeating unit of carrageenans [30,31,32]. The most common types of carrageenan are traditionally labeled kappa (κ), iota (ι), and lambda (λ) (Figure 1.4) [33]. The structures of the three main forms of carrageenan differ only in the number of sulfate groups per disaccharide having one, two, and three for κ, ι, and λ, respectively [34,35]. The carrageenan biocompatibility has been increasingly used in the cosmetic and pharmaceutical industries, it does not induce a toxic reaction [30,36].

κ- and ι-carrageenan are known to undergo a thermally-induced disordered-ordered transition, both chains exist as random coils with a larger amount of conformational entropy when elevated temperature. Upon cooling, entropy is decreased and chains re-orient into a more ordered conformation, which is accepted to consist of various form such as a double helix, aggregated mono-helices or aggregated helical dimers [37]. κ- and ι-carrageenan also form gelation in the presence of mono- (such as KCl, LiCl, and NaCl) and di-valent cations (such as $MgCl_2$, $CaCl_2$, and $SrCl_2$). In contrast, λ-carrageenan does not show gelation in the presence of cation and displays only viscous behavior. It has been explained that the formation of ordered three-dimensional networks of κ- and ι-carrageenan compose of double helices resulting from crosslinking of the adjacent chains in which the sulfate groups are oriented externally [38,39].

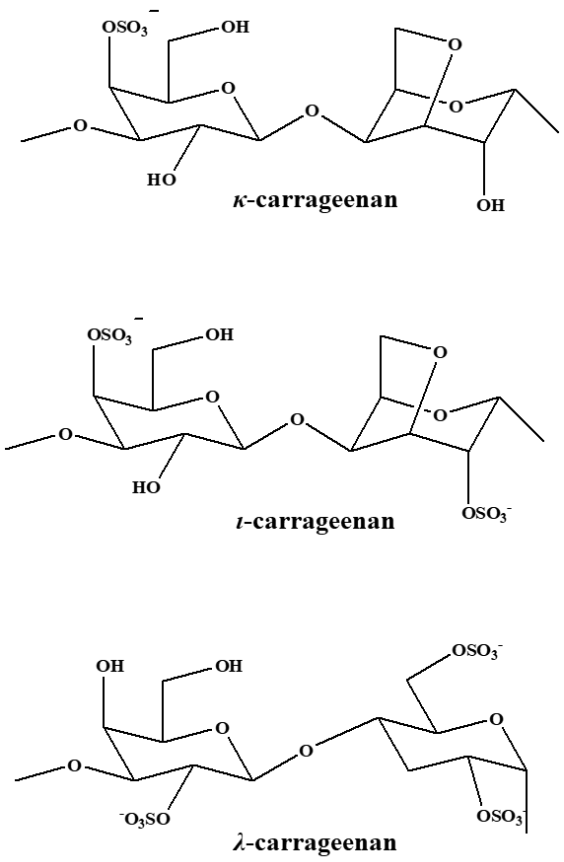

Figure 1.4 Idealized structures of the three types of carrageenan.

The degradation of carrageenan would appear in the stomach, which is only partially degraded and this limited degradation has no effect on the wall of the stomach, where the pH is very low and acid hydrolysis undoubtedly occurs [40]. The enzymatic degradation of *κ*-carrageenan was conducted using recombinant *Pseudoalteromonas carrageenovora κ*-carrageenase has been reported [41] which undertook the study of the effect of salt conditions on enzymatic degradation of carrageenan. The proposed that the presence of I^- binding is the main parameter which impedes carrageenan degradation by enzyme. The *κ*- carrageenan also be degraded by irradiation with gamma rays in the solid state, gel state or solution with various doses in air at ambient temperature [29]. The Mw of *κ*- carrageenan decreased continuously with

increasing the gamma ray intensity and the gel state needed lesser dose than solid state due to the indirect effect of radiation brought about by the water molecules.

In this research, *κ*-carrageenan was used to apply in the development of new carrier formulations because of its gelation properties. It can form gel when cooling or under appropriate salt conditions. *γ*-Carrageenan is either hot or cold soluble and forms soft elastic gels, while the κ-type dissolves only when heated and forms strong gels which is firm and brittle [34,42,43]. So, the *κ*-form could be the most appropriate type for releasing the carried substance when earning heat.

1.4 Photothermal agent triggered by near-infrared (NIR) for temperature-sensitive materials

Infrared radiation (IR) is electromagnetic radiation with longer wavelength than those of visible light, so, its higher energy allows the applications when using light. Among this region, near infrared (NIR) light have been strongly designed to utilize. NIR can penetrate up to 10 cm deep into tissue [44] with less damage and absorption or scattering and is more desirable for *in vivo* applications [45,46]. Thus, NIR laser was employed for photothermal therapy (PTT) to develop and encourage therapeutic strategy, especially advantages in cancer therapy. It shows high specificity, minimal invasiveness, precise selectivity and no systemic effects. The therapeutic efficacy of PTT significantly depends on the transformation of light to sufficient heat with photothermal agents, which absorb light-energy and then transform it to heat. In case of the tumor site, killing cancer cells via hyperthermia need the thermal energy 40-45 °C or higher [47]. The photothermal agents (PTA) such as noble metal nanostructures, carbon nanostructures, transition metal sulfide/oxides nanomaterials, and organic nanoagents have been extensively explored. For example, a trifolium like platinum nanoparticles were designed as a PTA for

photothermal ablation of bone metastasis by PTT treatment with effectiveness (Figure 1.5A) [48]. Considering the deeper tissue penetrating ability of laser and specific targeting of PTA, deep tumor-penetrating NIR probe (DiR) loaded DPN as a PTA for PTT of tumor progression and metastasis of breast cancer was developed (Figure 1.5B) [49]. Found that, the nanosized DPN could penetrate into the deep of tumor tissues and heat generated upon NIR irradiation for photothermal ablation of cancer cells which obviously inhibited the proliferation and migration activities of metastatic breast cancer cells.

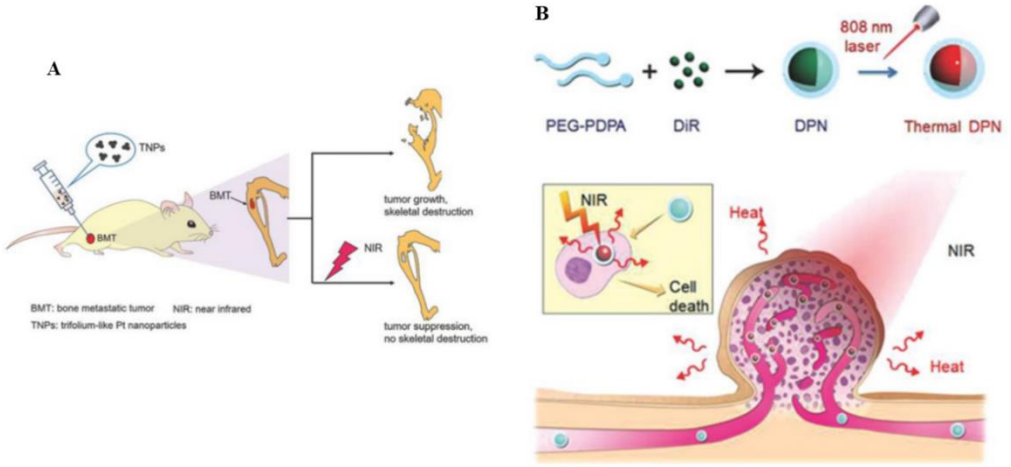

Figure 1.5 (A) The TPN-mediated PTA therapy in a bone metastasis model [48]. (B) DiR-loaded photothermal nanotherapeutics (DPN) for PTT of breast cancer [49].

Another application of NIR photothermal agent is to collaborate with the thermo-responsive polymer for remote activation and spatiotemporal control of the stimulation. The NIR light-responsive hydrogel that undergoing the gel to sol transition upon light exposure based on a photothermal effect was reported [50]. Gold nanorods (AuNRs) were loaded into an ABA-type triblock copolymer hydrogel in form of micelle whose constituted by thermoresponsive polymer

displaying an upper critical solution temperature (UCST). The hydrogel structure is stable at T<UCST while exposed to NIR light heat release from AuNRs can increase the temperature above UCST, resulting in gel-to-sol transition. The hydrogel became water soluble and the target drug molecules can be released. The organic agent such as polydopamine (PDA) were descripted to possess a PTA which shows higher photothermal efficiency than that of widely used gold nanorod [51]. Xu et al., 2017 reported the capping of PDA microspheres with a PNIPAm thermosensitive polymer shell, generating core−shell PDA@PNIPAm hybrid system. Its application was to use an NIR light-controlled release-targeted system for pesticide loaded [52]. In this research, we fabricated the new material, amino-CG@PDA, for control release the amine groups conjugated on carrageenan backbone by NIR light stimulus to induce the gel-to sol phase transition of carrageenan after getting enough heat. The intense information was detailed in chapter 3.

1.5 Polysaccharide chemical reactions

1.5.1 Thiol-Michael addition

The Michael addition reaction is the reaction of an enolate-type nucleophile in the presence of a catalyst to α, β- unsaturated carbonyl which involves reactions in a myriad of organic synthesis to yield highly selective products. It is a simple, and highly effective reaction that can result in C−C bond formation under relatively facile reaction conditions. One of the most attractive and longtime known of Michael addition reaction paradigm, thiol Michael reaction or thiol-ene addition reaction, has become popular in polymer chemistry [53,54]. Thiol Michael addition reactions can be readily actioned under base catalysis which can generate a thiolate anion by base abstract a proton from thiol. Then, the nucleophile thiolate anion attacks the electrophilic β-carbon of the C=C, forming the intermediate carbon-centered anion which, being a strong base,

abstracts a hydrogen from the conjugate acid to yield the thioether as a product [55,56]. The mechanism of base-catalyzed thiol Michael addition presents in Figure 1.6. In this thesis, glycidyl methacrylate (GMA) was introduced to oxidized dextran (oxidized Dex-GMA) and hydrogel was formed through thiol Michael addition when dithiothreitol (DTT) was added to oxidized Dex-GMA solution. The aldehyde groups from the oxidative cleavage of oxidized dextran were remained to react with primary amine for degradation trigger.

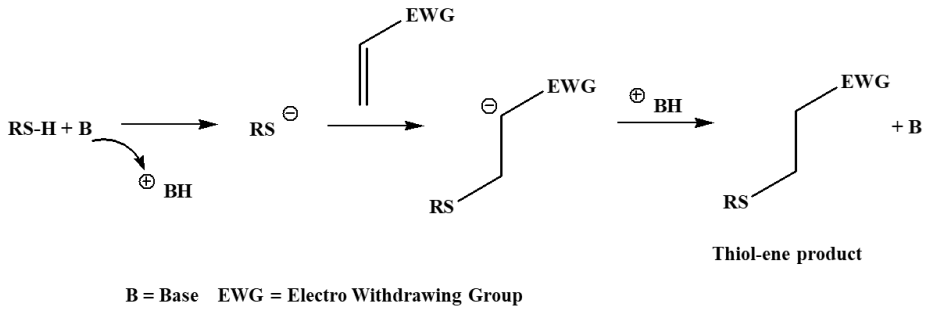

Figure 1.6 Schematic presentation of mechanism of base-catalyzed thiol Michael addition [56].

1.5.2 Malaprade reaction

Polysaccharide provide a profusion of compounds that contain hydroxyl groups on two or more adjacent carbon atoms, and its C-C bond can undergo oxidative scission selectively. Periodate oxidative cleavage of vicinal glycols was discovered by Malaprade as knows Malaprade reaction [57]. Malaprade reaction of carbohydrates by periodate ion was a classical method for a long time used for structure determination of complex carbohydrates. The using of periodate oxidation to introduce dialdehydes into polysaccharides (Figure 1.7) provides a number of interesting applications in tissue engineering, and drug delivery [58,59]. For drug carrier application, the degradation of hydrogel has been become interestingness. Thus, the scission of

aldehyde polysaccharide chain was developed by reaction with amino source to form Schiff base reaction, consequently, the main chain scission is started.

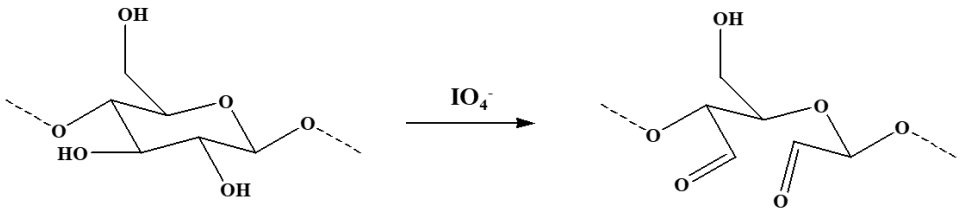

Figure 1.7 (1→4)-linked residues where cleavage occurs between C_2 and C_3 [60].

1.5.3 Schiff base reaction

Schiff bases (also known as imine or azomethine) is the reaction between any primary amine and an aldehyde or a ketone under specific conditions [61]. The electrophilic carbon atoms of aldehydes and ketones can be targets of nucleophilic attack by amines. The end result of this reaction is a compound in which the C=O double bond is replaced by a C=N double bond (Figure 1.8).

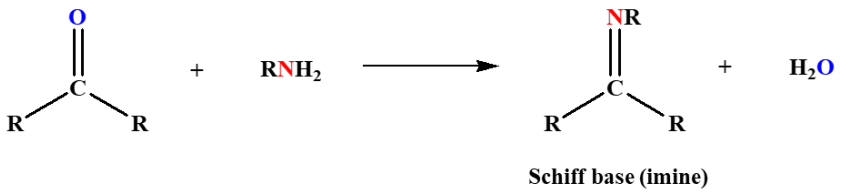

Figure1.8 Schiff base reaction.

Schiff base reaction has been exceedingly used in situ cross-linked hydrogel systems for tissue engineering and drug delivery applications. For example, Tan et al. reported the biocompatible and biodegradable composite hydrogels for cartilage tissue engineering [62]. The hydrogel derived from N-succinyl-chitosan (S-CS) and aldehyde hyaluronic acid (A-HA), upon mixing by the Schiff base reaction between amino and aldehyde groups. In addition, the other types of polysaccharides can be oxidized and used for Schiff base mediated cross-linking, such as dextran, gum arabic, and cellulose [5,63,64,65]. In previous study, our group reported the adhesive hydrogel formation between the aldehyde dextran and ε-poly-L-lysine (ε-PL) via Schiff base reaction [4]. The gelation time of the hydrogel was easily controlled by the extension of oxidation degree in dextran and of the acylation in ε-PL by anhydrides. The prepared hydrogel were lower cytotoxicity than that of glutaradehyde and poly(allylamine). Moreover, the self-degradation rate of this hydrogel bioadhesive through Maillard reaction can be controlled by its oxidation degree and type of anhydride species in the acylate poly-L-lysine which can develop in biomedical applications as a bioadhesive [66].

1.5.4 Maillard reaction

The Maillard or browning reaction, interaction between amino and carbonyl compounds, resulting in complex changes in biological and food systems, refers to a complex set of amino-carbonyl reaction with multiple mechanisms, pathways, and products. These reactions affect the color, taste, aroma, texture, nutritional value, and toxicity of foods during cooking [67]. The chemical aspects emphasize the importance of the amino-carbonyl reactions in food and biological systems which explore three types of the main constituents of all biological systems: proteins, polysaccharides, and lipids. The functional groups of their structural unit contained four groups of COOH, -OH, $-NH_2$, and –CHO. In case of the reaction of enzymatic mediation, the

formation of polymeric biological constituents by one-step reversible condensation such as enzymatic polymerization of amino acids, which goes as far as to form protein. However, the nonenzymatic reaction of -CHO and $–NH_2$ is quite different [68]. The first step of reaction between these groups is reversible process between formation and decomposition of glycosyl-amino products but its products undergo Amadori rearrangement to form ketosyl-amino products which undergo complex irreversible reactions involving dehydration, rearrangement, scission, and so on to yield decomposed products (Figure 1.9). It shows the unique features of the Maillard reaction involving irreversibility and complexity of the two functional groups -CHO and -NH and can recognizably different from the combinations formed by the other functional groups.

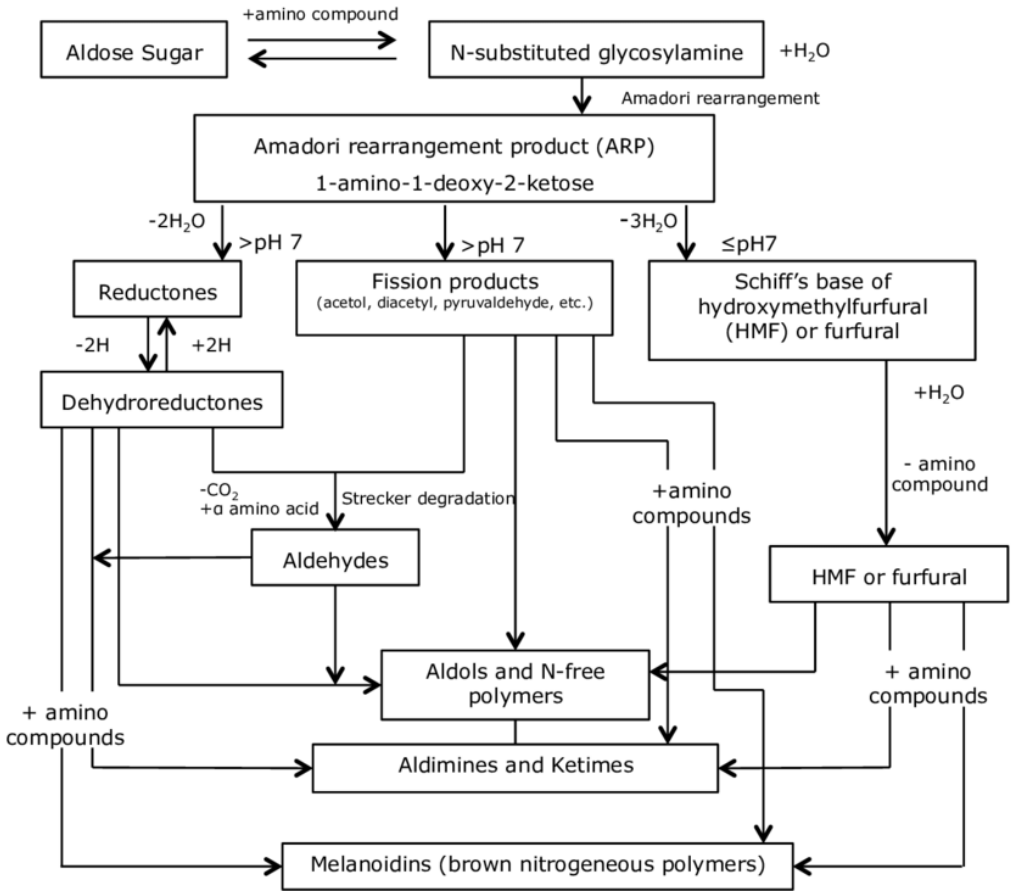

Figure 1.9 Scheme of Maillard reaction adapted from Hodge (1953) [69].

1.6 Research objective

The main goal of the study is to overcome the drawback of uncontrollable degradation timing of oxidized dextran-based hydrogel prepared by the reaction between aldehyde group in oxidized dextran and amino group in poly-L-lysine which was started degradation after Schiff based reaction form. And as mechanical property of the hydrogel was decided by the number of cross-linking points, degradation time also depended on the mechanical property. Hence, if the degradation time is independent with mechanical properties, the widely application in biomedical field will be provided. Therefore, the hydrogel formation of oxidized dextran without using aldehyde groups was prepared. The remaining aldehyde of hydrogel was reacted with amino groups and the degradation is stared. The posteriori degradation was controlled by addition of amine source to aim the controllable degradation independently of mechanical properties of hydrogels. Moreover, I also considered the control release of amino source which is stimulated by NIR light to irradiate the temperature-sensitive material (amino functionalized carrageenan or amino-CG) for release its amino group to react with aldehyde remaining. Thus, the degradation of oxidized dextran-based hydrogel was controlled.

References

1. Mehvar, R., Dextrans for targeted and sustained delivery of therapeutic and imaging agents. *Journal of controlled release : official journal of the Controlled Release Society* **2000**, *69* (1), 1-25.

2. Ferreira, L. S.; Gerecht, S.; Fuller, J.; Shieh, H. F.; Vunjak-Novakovic, G.; Langer, R., Bioactive hydrogel scaffolds for controllable vascular differentiation of human embryonic stem cells. *Biomaterials* **2007,** *28* (17), 2706-2717.

3. Van Tomme, S. R.; Hennink, W. E., Biodegradable dextran hydrogels for protein delivery applications. *Expert review of medical devices* **2007**, *4* (2), 147-164.

4. Hyon, S. H.; Nakajima, N.; Sugai, H.; Matsumura, K., Low cytotoxic tissue adhesive based on oxidized dextran and epsilon-poly-L-lysine. *Journal of biomedical materials research. Part A* **2014**, *102* (8), 2511-2520.

5. Chimpibul, W.; Nagashima, T.; Hayashi, F.; Nakajima, N.; Hyon, S.-H.; Matsumura, K., Dextran oxidized by a malaprade reaction shows main chain scission through a maillard reaction triggered by schiff base formation between aldehydes and amines. *Journal of Polymer Science Part A* **2016**, *54* (14), 2254-2260.

6. Fomina, N.; McFearin, C. L.; Sermsakdi, M.; Morachis, J. M.; Almutairi, A., Low Power, Biologically Benign NIR Light Triggers Polymer Disassembly. *Macromolecules* **2011**, *44* (21), 8590-8597.

7. Qiu, Y.; Park, K., Environment-sensitive hydrogels for drug delivery. *Advanced drug delivery reviews* **2001**, *53* (3), 321-339.

8. Arti Vashist, S. A., Hydrogels: Smart Materials for Drug Delivery. *Oreiental Journal of Chemistry* **2013**, *29* (3), 861-870.

9. Li, J.; Mooney, D. J., Designing hydrogels for controlled drug delivery. *Nature Reviews Materials* **2016**, *1*, 16071-16081.

10. Sutter, M.; Siepmann, J.; Hennink, W. E.; Jiskoot, W., Recombinant gelatin hydrogels for the sustained release of proteins. *Journal of controlled release* **2007**, *119* (3), 301-312.

11. Nakamae, K.; Nishino, T.; Kato, K.; Miyata, T.; Hoffman, A. S., Synthesis and characterization of stimuli-sensitive hydrogels having a different length of ethylene glycol chains carrying phosphate groups: loading and release of lysozyme. *Journal of biomaterials science* **2004**, *15* (11), 1435-1446.

12. Lee, K. Y.; Mooney, D. J., Hydrogels for Tissue Engineering. *Chemical Reviews* **2001**, *101* (7), 1869-1880.

13. A Peppas, N.; Zach Hilt, J.; Khademhosseini, A.; Langer, R., Hydrogels in Biology and Medicine: From Molecular Principles to Bionanotechnology. *Advanced Materials* **2006**, *18* (11), 1345-1360.

14. Behravesh, E.; Jo, S.; Zygourakis, K.; Mikos, A. G., Synthesis of in Situ Cross-Linkable Macroporous Biodegradable Poly(propylene fumarate-co-ethylene glycol) Hydrogels. *Biomacromolecules* **2002**, *3* (2), 374-381.

15. Meyvis, T. K. L.; De Smedt, S. C.; Demeester, J.; Hennink, W. E., Influence of the Degradation Mechanism of Hydrogels on Their Elastic and Swelling Properties during Degradation. *Macromolecules* **2000**, *33* (13), 4717-4725.

16. Eliaz, R. E.; Kost, J., Characterization of a polymeric PLGA-injectable implant delivery system for the controlled release of proteins. *Journal of biomedical materials research* **2000**, *50* (3), 388-396.

17. Olde Damink, L. H.; Dijkstra, P. J.; van Luyn, M. J.; van Wachem, P. B.; Nieuwenhuis, P.; Feijen, J., In vitro degradation of dermal sheep collagen cross-linked using a water-soluble carbodiimide. *Biomaterials* **1996**, *17* (7), 679-684.

18. Hu, J.; Chen, Y.; Li, Y.; Zhou, Z.; Cheng, Y., A thermo-degradable hydrogel with light-tunable degradation and drug release. *Biomaterials* **2017**, *112* (2017), 133-140.

19. Ahmad; Mustafa; Man, C., Microbial Polysaccharides and Their Modification Approaches: A Review. *International Journal of Food Properties* **2015**, *18* (2), 332–347.

20. Kar, R.; Mohapatra, S.; Bhanja, S.; Das, D.; Barik, B., Formulation and In Vitro Characterization of Xanthan Gum-Based Sustained Release Matrix Tables of Isosorbide-5-Mononitrate. *Iranian Journal of Pharmaceutical Research* **2010**, *9* (1), 13-19.

21. Levesque, S. G.; Shoichet, M. S., Synthesis of enzyme-degradable, peptide-cross-linked dextran hydrogels. *Bioconjugate chemistry* **2007**, *18* (3), 874-885.

22. Ferreira, L.; Rafael, A.; Lamghari, M.; Barbosa, M. A.; Gil, M. H.; Cabrita, A. M.; Dordick, J. S., Biocompatibility of chemoenzymatically derived dextran-acrylate hydrogels. *Journal of biomedical materials research. Part A* **2004**, *68* (3), 584-596.

23. Khalikova, E.; Susi, P.; Korpela, T., Microbial dextran-hydrolyzing enzymes: fundamentals and applications. *Microbiology and molecular biology reviews* **2005**, *69* (2), 306-325.

24. Jain, A.; Gupta, Y.; Jain, S. K., Perspectives of biodegradable natural polysaccharides for site-specific drug delivery to the colon. *Journal of pharmacy & pharmaceutical sciences* **2007**, *10* (1), 86-128.

25. Covacevich, M. T.; Richards, G. N., Frequency and distribution of branching in a dextran: an enzymic method. *Carbohydrate Research* **1977**, *54* (2), 311-315.

26. Damodaran, V. B.; Place, L. W.; Kipper, M. J.; Reynolds, M. M., Enzymatically degradable nitric oxide releasing S-nitrosated dextran thiomers for biomedical applications. *Journal of Materials Chemistry* **2012**, *22* (43), 23038-23048.

27. Van Tomme, S. R.; van Nostrum, C. F.; de Smedt, S. C.; Hennink, W. E., Degradation behavior of dextran hydrogels composed of positively and negatively charged microspheres. *Biomaterials* **2006**, *27* (22), 4141-4148.

28. Ding, Y. Q.; Cui, Y. Z.; Li, T. D., New views on the reaction of primary amine and aldehyde from DFT study. *The journal of physical chemistry. A* **2015**, *119* (18), 4252-4260.

29. Relleve, L.; Nagasawa, N.; Luan, L. Q.; Yagi, T.; Aranilla, C.; Abad, L.; Kume, T.; Yoshii, F.; dela Rosa, A., Degradation of carrageenan by radiation. *Polymer Degradation and Stability* **2005**, *87* (3), 403-410.

30. Francis, S.; Kumar, M.; Varshney, L., Radiation synthesis of superabsorbent poly(acrylic acid)–carrageenan hydrogels. *Radiation Physics and Chemistry* **2004**, *69* (6), 481-486.

31. Abad, L. V.; Relleve, L. S.; Aranilla, C. T.; Dela Rosa, A. M., Properties of radiation synthesized PVP-kappa carrageenan hydrogel blends. *Radiation Physics and Chemistry* **2003**, *68* (5), 901-908.

32. Chronakis, I. S.; Piculell, L.; Borgström, J., Rheology of kappa-carrageenan in mixtures of sodium and cesium iodide: two types of gels. *Carbohydrate Polymers* **1996**, *31* (4), 215-225.

33. Maolin, Z.; Hongfei, H.; Yoshii, F.; Makuuchi, K., Effect of kappa-carrageenan on the properties of poly(N-vinyl pyrrolidone)/kappa-carrageenan blend hydrogel synthesized by γ-radiation technology. *Radiation Physics and Chemistry* **2000,** *57* (3), 459-464.

34. Yuguchi, Y.; Thu Thuy, T. T.; Urakawa, H.; Kajiwara, K., Structural characteristics of carrageenan gels: temperature and concentration dependence. *Food Hydrocolloids* **2002,** *16* (6), 515-522.

35. Langendorff, V.; Cuvelier, G.; Michon, C.; Launay, B.; Parker, A.; De kruif, C. G., Effects of carrageenan type on the behaviour of carrageenan/milk mixtures. *Food Hydrocolloids* **2000**, *14* (4), 273-280.

36. Cohen, S. M.; Ito, N., A critical review of the toxicological effects of carrageenan and processed eucheuma seaweed on the gastrointestinal tract. *Critical reviews in toxicology* **2002**, *32* (5), 413-444.

37. Song, K.-H.; Eddington, N. D., The impact of AT1002 on the delivery of ritonavir in the presence of bioadhesive polymer, carrageenan. *Archives of Pharmacal Research* **2012**, *35* (5), 937-943.

38. Campo, V. L.; Kawano, D. F.; Silva, D. B. d.; Carvalho, I., Carrageenans: Biological properties, chemical modifications and structural analysis – A review. *Carbohydrate Polymers* **2009**, *77* (2), 167-180.

39. Running, C. A.; Falshaw, R.; Janaswamy, S., Trivalent Iron Induced Gelation in Lambda-Carrageenan. *Carbohydr Polym* **2012**, *87* (4), 2735-2739.

40. Necas, J.; Bartosikova, L., Carrageenan: A review. *Veterinarni Medicina* **2013**, *58* (4), 187-205.

41. Nyvall Collen, P.; Lemoine, M.; Daniellou, R.; Guégan, J.-P.; Paoletti, S.; Helbert, W., Enzymatic Degradation of κ-Carrageenan in Aqueous Solution. *Macromolecules* **2009**, *10* (7), 1757–1767

42. Özbek, H.; Pekcan, Ö., Critical exponents of thermal phase transitions in κ-carrageenan-water system. *Journal of Molecular Structure: THEOCHEM* **2004**, *676* (1), 19-27.

43. Bixler, H. J., The Carrageenan Connection IV. *British Food Journal* **1994**, *96* (3), 12-17.

44. Weissleder, R., A clearer vision for in vivo imaging. *Nature Biotechnology* **2001**, *19*, 316.

45. Braun, G. B.; Pallaoro, A.; Wu, G.; Missirlis, D.; Zasadzinski, J. A.; Tirrell, M.; Reich, N. O., Laser-Activated Gene Silencing via Gold Nanoshell-siRNA Conjugates. *ACS nano* **2009**, *3* (7), 2007-2015.

46. Arnold, M. A., Near-Infrared Applications in Biotechnology Edited by R. Raghavachari (Corning Microarray Technology, Corning, NY). Marcel Dekker: New York and Basel. *Journal of the American Chemical Society* **2001**, *123* (50), 12746-12747.

47. Li, Y.; Lu, W.; Huang, Q.; Huang, M.; Li, C.; Chen, W., Copper sulfide nanoparticles for photothermal ablation of tumor cells. *Nanomedicine* **2010**, *5* (8), 1161-1171.

48. Wang, C.; Cai, X.; Zhang, J.; Wang, X.; Wang, Y.; Ge, H.; Yan, W.; Huang, Q.; Xiao, J.; Zhang, Q.; Cheng, Y., Trifolium-like Platinum Nanoparticle-Mediated Photothermal Therapy Inhibits Tumor Growth and Osteolysis in a Bone Metastasis Model. *Small* **2015**, *11* (17), 2080-2086.

49. He, X.; Bao, X.; Cao, H.; Zhang, Z.; Yin, Q.; Gu, W.; Chen, L.; Yu, H.; Li, Y., Tumor-Penetrating Nanotherapeutics Loading a Near-Infrared Probe Inhibit Growth and Metastasis of Breast Cancer. *Advanced Functonal Materials* **2015**, *25* (19), 2831-2839.

50. Zhang, H.; Guo, S.; Fu, S.; Zhao, Y., A Near-Infrared Light-Responsive Hybrid Hydrogel Based on UCST Triblock Copolymer and Gold Nanorods. *Polymers* **2017**, *9* (6), 1-9.

51. Liu, Y.; Ai, K.; Liu, J.; Deng, M.; He, Y.; Lu, L., Dopamine-melanin colloidal nanospheres: an efficient near-infrared photothermal therapeutic agent for in vivo cancer therapy. *Advanced materials* **2013**, *25* (9), 1353-9.

52. Xu, X.; Bai, B.; Wang, H.; Suo, Y., A Near-Infrared and Temperature-Responsive Pesticide Release Platform through Core–Shell Polydopamine@PNIPAm Nanocomposites. *ACS Applied Materials & Interfaces* **2017**, *9* (7), 6424-6432.

53. J. Kade, M.; J. Burke, D.; J. Hawker, C., The Power of Thiol-ene Chemistry. *Journal of Polymer Science: Part A* **2010**, *48* (4), 743-750.

54. Liu, Z. Q.; Wei, Z.; Zhu, X. L.; Huang, G. Y.; Xu, F.; Yang, J. H.; Osada, Y.; Zrinyi, M.; Li, J. H.; Chen, Y. M., Dextran-based hydrogel formed by thiol-Michael addition reaction for 3D cell encapsulation. *Colloids and surfaces. B* **2015**, *128*, 140-8.

55. Nair, D. P.; Podgórski, M.; Chatani, S.; Gong, T.; Xi, W.; Fenoli, C. R.; Bowman, C. N., The Thiol-Michael Addition Click Reaction: A Powerful and Widely Used Tool in Materials Chemistry. *Chemistry of Materials* **2014,** *26* (1), 724-744.

56. Sun, Y.; Liu, H.; Cheng, L.; Zhu, S.; Cai, C.; Yang, T.; Yang, L.; Ding, P., Thiol Michael Addition Reaction: A facile Tool for Introducing Peptides into Polymer-based Gene Delivery Systems. *Polymer International* **2017**, *67* (1), 35-31.

57. Jackson, E. L.; Hudson, C. S., Application of the Cleavage Type of Oxidation by Periodic Acid to Starch and Cellulose1. *Journal of the American Chemical Society* **1937**, *59* (10), 2049-2050.

58. Inci, I.; Kirsebom, H.; Galaev, I. Y.; Mattiasson, B.; Piskin, E., Gelatin cryogels crosslinked with oxidized dextran and containing freshly formed hydroxyapatite as potential bone tissue-engineering scaffolds. *Journal of tissue engineering and regenerative medicine* **2013**, *7* (7), 584-8.

59. Li, X.; Weng, Y.; Kong, X.; Zhang, B.; Li, M.; Diao, K.; Zhang, Z.; Wang, X.; Chen, H., A covalently crosslinked polysaccharide hydrogel for potential applications in drug delivery and tissue engineering. *Journal of Materials Science* **2012**, *23* (12), 2857-2865.

60. Kristiansen, K. A.; Potthast, A.; Christensen, B. E., Periodate oxidation of polysaccharides for modification of chemical and physical properties. *Carbohydrate Research* **2010**, *345* (10), 1264-1271.

61. da Silva, C. M.; da Silva, D. L.; Modolo, L. V.; Alves, R. B.; de Resende, M. A.; Martins, C. V. B.; de Fátima, Â., Schiff bases: A short review of their antimicrobial activities. *Journal of Advanced Research* **2011**, *2* (1), 1-8.

62. Tan, H.; Chu, C. R.; Payne, K. A.; Marra, K. G., Injectable in situ forming biodegradable chitosan-hyaluronic acid based hydrogels for cartilage tissue engineering. *Biomaterials* **2009**, *30* (13), 2499-2506.

63. Ito, T.; Yeo, Y.; Highley, C. B.; Bellas, E.; Benitez, C. A.; Kohane, D. S., The prevention of peritoneal adhesions by in situ cross-linking hydrogels of hyaluronic acid and cellulose derivatives. *Biomaterials* **2007**, *28* (6), 975-983.

64. Maia, J.; Ferreira, L.; Carvalho, R.; Ramos, M. A.; Gil, M. H., Synthesis and characterization of new injectable and degradable dextran-based hydrogels. *Polymer* **2005**, *46* (23), 9604-9614.

65. Nishi, K. K.; Jayakrishnan, A., Preparation and in vitro evaluation of primaquine-conjugated gum arabic microspheres. *Biomacromolecules* **2004**, *5* (4), 1489-1495.

66. Matsumura, K.; Nakajima, N.; Sugai, H.; Hyon, S. H., Self-degradation of tissue adhesive based on oxidized dextran and poly-L-lysine. *Carbohydr Polym* **2014**, *113*, 32-38.

67. Baynes, J. W., The Maillard Reaction: Chemistry, Biochemistry and Implications By Harry Nursten. *Journal of the American Chemical Society* **2005**, *127* (41), 14527-14528.

68. Namiki, M., Chemistry of Maillard Reactions: Recent Studies on the Browning Reaction Mechanism and the Development of Antioxidants and Mutagens. *In Advances in Food Research*, *32*, 115-184.

69. Hodge, J. E., Dehydrated Foods, Chemistry of Browning Reactions in Model Systems. *Journal of Agricultural and Food Chemistry* **1953**, *1* (15), 928-943.

Chapter 2

Controlling degradation of oxidized dextran-based hydrogel

2.1 Introduction

Hydrogels are cross-linked polymer networks that have a high number of hydrophilic domains and are able to expand in many solvents and aqueous environments without dissolving due to the chemical or physical bonds formed between the polymer chains [1, 2]. Natural polymers, specifically polysaccharides, are often used for hydrogel preparation because of their biocompatibility and chemical structure that facilitates the development of desirable functionalized materials [3]. To date, low toxicity, biocompatible, and degradable hydrogels have been designed using polysaccharides and functionalized polysaccharides for biomedical applications, such as tissue engineering scaffolds, wound dressings, and controlled drug delivery systems [4-8]. For example, alginate and its derivative hydrogels are compatible with a variety of techniques to control gelling and possess desirable physical and chemical properties that can be used to facilitate cell adhesion and control the speed of degradation, all of which can be combined to promote cell transplantation [9]. The periodate oxidation of alginate, which can be cross-linked with multivalent cations (Ca^{2+}) to produce hydrogels, was observed to degrade *in vitro* in a phosphate buffer saline solution (PBS) (pH 7.4, 37 °C) within nine days [10]. These hydrogels can potentially be used in cartilage-like tissue formation. In drug delivery systems, an active

therapeutic agent is integrated with a polymeric network structure that can control its release rate by allowing the hydrogel to safely degrade in the body when it is no longer needed [11]. Biodegradable polysaccharides, such as chitosan, alginate, xanthan gum, and dextran, have been widely researched for potential applications in drug carriers [12-15]. Among these, dextran has received significant attention.

Dextran is a bacterial polysaccharide that is broadly applicable in the biomedical field due to its biocompatibility [16, 17], low toxicity [18], high natural abundance, and ability to degrade via enzymes in various parts of the human body, such as the spleen, liver, and colon, and is available in a wide range of molecular weights [4, 19]. Furthermore, dextran contains a large number of hydroxyl groups, which give it a high hydrophilicity and allow it to be used in chemical functionalization [3, 4, 20, 21]. The structure of dextran presents in Figure 1.1. In a previous report, Hyon et al. prepared hydrogels via the reaction between the aldehyde groups in the periodate oxidized dextran and the amino groups in the poly-L-lysine [18]. In that case, the hydrogels exhibited degradation in PBS and found that the degradation time could be controlled by the rate of aldehyde introduction and the amine concentration. The mechanism behind the degradation was reported as follows: the main chain of the oxidized dextran was degraded by the Maillard reaction that was triggered by the Schiff base formation between the aldehyde and amino groups. A two-dimensional (2D) nuclear magnetic resonance (NMR) scan revealed that the partial hemiacetal structures produced by the periodate oxidation reacted with the amino groups and underwent an Amadori rearrangement, which led to the scission of the glucose unit ring [22] (Figure 2.1). This study is based on and utilizes this reaction to overcome the following drawback. From the previous report, because the crosslink points formed by the reaction between the aldehyde groups in the oxidized dextran and the amino groups in the poly-L-lysine triggered the degradation of the hydrogel, the degradation speed was found to depend on the number of

chemical crosslink points during gelation [15, 23]. However, as the formation and degradation of this hydrogel occurred simultaneously after the Schiff base formation reaction between the aldehyde and amino groups, it was difficult to control the timing of the degradation. In addition, as the mechanical properties of the hydrogel were determined by the number of crosslinking points, the degradation time also depended on the mechanical properties, much like stiff hydrogels exhibit longer degradation times while soft hydrogels exhibit shorter degradation times. If a degradation control with respect to time and space can be identified that is independent of the mechanical properties, such as hard/fast or soft/slow combinations, these hydrogels could prove to be valuable platform materials for the fabrication of biodegradable scaffolds and drug carriers.

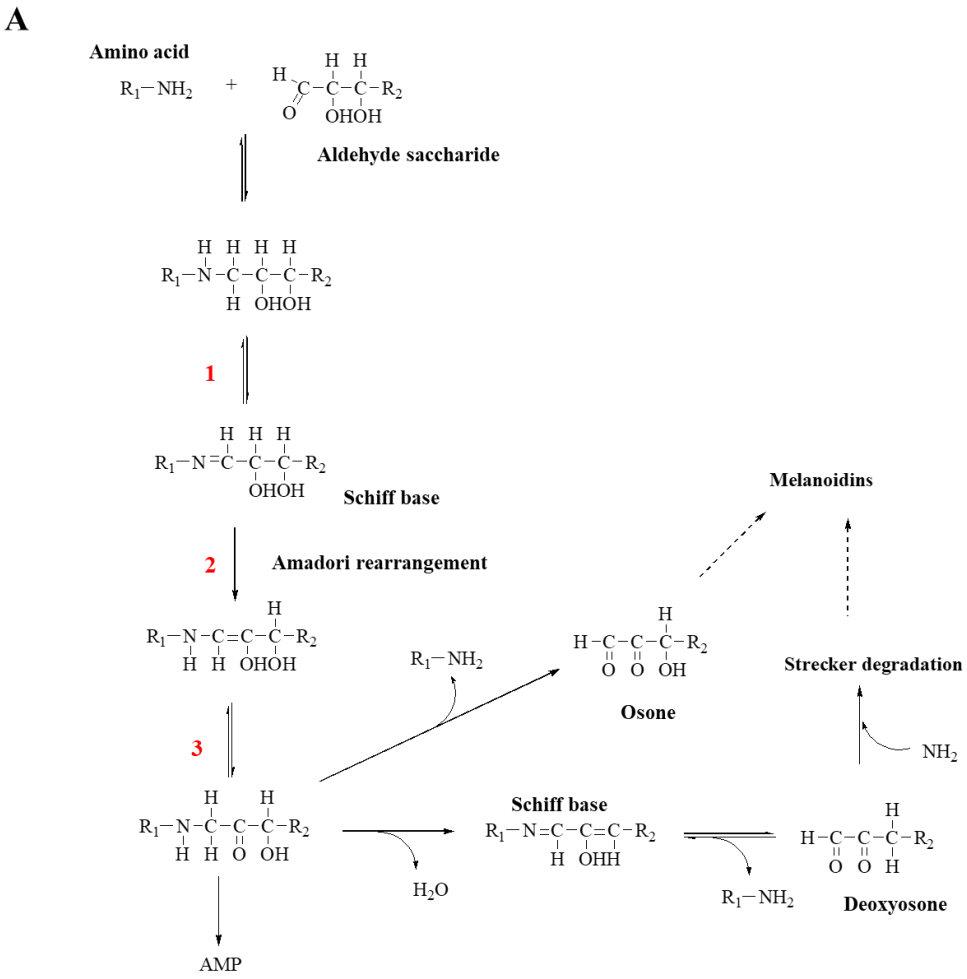

B

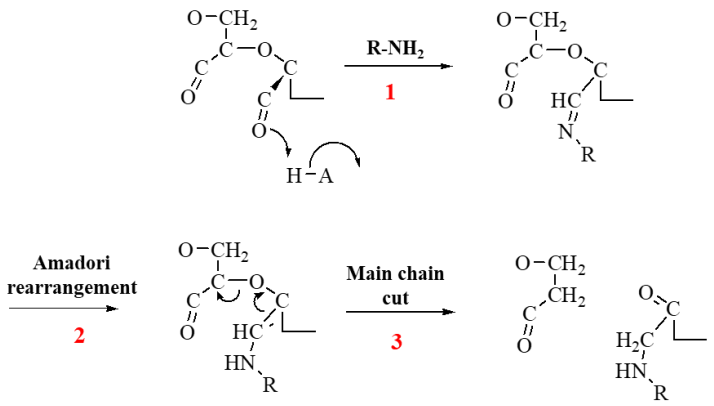

Figure 2.1 (A) Maillard reaction pathway for the reaction of aldehyde saccharides and amino acids. (B) Molecular scission mechanism of oxidized dextran by the reaction with amine [22].

In this study, glycidyl methacrylate (GMA) was immobilized into dextran (Dex-GMA) and oxidized by sodium periodate to introduce aldehyde groups, thereby creating oxidized Dex-GMA. The oxidized Dex-GMA was crosslinked with dithiothreitol (DTT) by a thiol-ene-Michael addition reaction to form a hydrogel with the remaining aldehyde groups. Then, the a posteriori degradation was controlled by the addition of an amine source so that the degradation was independent of the mechanical properties of the hydrogels. It was thought that this novel strategy may open new avenues of approach to create tissue engineering and drug delivery system materials via a unique chemical stimuli (amino group) responsive degradation control.

2.2 Materials and methods

2.2.1 Materials

Dextran (molecular weight (Mw) = 70 kDa) was acquired from Meito Sangyo (Nagoya, Japan), while GMA and DTT were purchased from TCI (Tokyo, Japan) and 4-

Dimethylaminopyridine (DMAP) was obtained from Sigma Aldrich (St. Louis, MO, USA). Acetyl cysteine (Ac-Cys-OH) was obtained from Watanabe Chemical Ind., Ltd. (Hiroshima, Japan) and sodium periodate ($NaIO_4$), disodium hydrogen phosphate (Na_2HPO_4), sodium dihydrogen phosphate (NaH_2PO_4), glycine, and other chemicals were purchased from Nacalai Tesque, Inc., (Kyoto, Japan). All chemicals were used without purification.

2.2.2 Synthesis and characterization of the oxidized Dex-GMA

Dex-GMA was synthesized by applying the method reported by Liu et al. [24]. In brief, 5 g of dextran was combined with 20 mL of dimethyl sulfoxide (DMSO) and the solution was stirred until the dextran was completely dissolved. The transparent solution was then stirred for 30 min under nitrogen gas. Then, 0.8 g of DMAP and 2.2 g of GMA were added to the solution under nitrogen gas for 30 min. The solution was stirred at 50 °C for 12 h before an equimolar amount of hydrochloric acid (HCl) was added to the solution mixture to neutralize the DMAP. The mixture was dialyzed against distilled water for one week using a dialysis membrane (MWCO = 3.5 kD). The resulting product was air dried for 48 h at 47 °C and vacuum dried for 48 h at 25 °C to obtain Dex-GMA derivative as a pale yellow-brown flake product.

Oxidized Dex-GMA was synthesized by the oxidation of dextran-GMA with sodium periodate [18]. Here, 2.5 g of Dex-GMA was dissolved in 10 mL of distilled water and various amounts of sodium periodate (0.375 to 1.25 g) were dissolved in 5 mL water. After dissolution, both solutions were mixed and the reaction was allowed to continue at 50 °C for 1 h. The mixture was dialyzed against running water overnight and water for one day using a dialysis membrane (MWCO = 3.5 kD). The resulting product was processed by air drying for 48 h at 47 °C and freeze drying for 48 h to obtain oxidized Dex-GMA, which was then characterized by ^{1}H nuclear magnetic resonance (NMR) (600, 700, and 900 MHz equipped with a cryogenic probe, Bruker). The results of the ^{1}H-NMR spectroscopy were used to investigate the degree of substitution (%

DS). In addition, oxidized dextran without GMA was synthesized by following the same method, except that dextran was employed as the starting material. The amount of aldehyde content in the functionalized dextran was determined using the fluorometry method [25]. Briefly, to prepare the mixture solution, 2.5 ml of 4.0 M ammonium acetate, 1.0 ml of 0.2 M acetoacetanilide (AAA), 1.0 ml of ethanol, and a series of standard glutaraldehyde solutions or samples were combined. Then, the mixtures were diluted to 5 mL with purified water and left for 10 min. The relative fluorescence intensities of the reagent blank, standard glutaraldehyde, and the sample solutions were measured at 470 nm with an excitation wavelength of 370 nm. The aldehyde content was determined from the standard calibration graph.

2.2.3 Gelation time measurement

Gels can form when oxidized Dex-GMA is crosslinked by DTT. The same volume of 10% (w/v) of oxidized Dex-GMA and 1.00, 1.36, or 2.72% (w/v) of DTT in PBS in which the molar ratio of C=C and thiol was equivalent at 1:0.74, 1:1, and 1:2, respectively, were mixed in a test tube and the gelation time was investigated by rheology analysis at a temperature of 37 °C. The molar ratio of the functional groups was varied by changing the concentration of the DTT to determine the gelling time.

2.2.4 Determination of the thiol content by Ellman's assay

To characterize the reaction of the aldehyde in the oxidized Dex-GMA with DTT, oxidized dextran without GMA was used as model to react with the mono-thiol reagent. Ellman's reagent, also known as 5,5'-Dithio-bis-(2-nitrobenzoic acid) or DTNB, was employed to evaluate the sulfhydryl group in the sample. Briefly, a set of test tubes was prepared, each of which contained 2.5 mL of reaction buffer (0.1 M phosphate buffer, pH 8), 1 mM of ethylenediaminetetraacetic acid (EDTA), and 50 μL of Ellman's reagent solution (created by

dissolving 4 mg of Ellman's reagent in 1 mL of reaction buffer). Then, standard cysteine (0–1.5 mM) or 250 μL of an unknown solution was added to a separate test tube. The solution was mixed and incubated at 25 °C for 15 min, and then the absorbance was measured at 412 nm. The concentration of the experimental sample was determined by comparison to the calibration graph of standard cysteine.

2.2.5 Rheological characterization

The rheological properties were evaluated using a rheometer equipped with a 24.99 mm, 2.069° cone (Rheosol G5000, UBM Co., Ltd., Kyoto, Japan). Briefly, 10% (w/v) of oxidized Dex-GMA (23% DS of GMA with varying degrees of oxidation) and 1 or 1.36% (w/v) of DTT in PBS with the same volume were mixed and placed into the gap between the lower plate and cone while the temperature was held at 37 °C. The dynamic storage (G') and loss (G") moduli of the hydrogels were determined via a frequency dispersion mode from 0.01 to 10 Hz.

2.2.6 Determination of the amount of quantitative gel degradation

To quantitatively evaluate the degradation of the gel, 0.5 mL of a 10% (w/v) oxidized Dex-GMA (23% DS of GMA with varying degrees of oxidation) aqueous solution and 0.5 mL of 1.36 wt% DTT were mixed in a centrifuge tube (15 mL capacity). The mixture was incubated at 37 °C for 30 min in water bath to allow for gelation. After the addition of 10 mL of PBS and an amino compound solution (1–10% (w/v) glycine solution), the tube was tightly sealed and incubated at 37 °C while being gently rotated. After the time interval had elapsed, the supernatant was removed and the remaining gel was rinsed with distilled water. Then, the remaining gel was freeze-dried (48 h) and vacuum dried (50 °C for 24 h). The weight of the remaining hydrogel was recorded versus the incubation periods. Samples were taken in triplicate (n = 3).

2.2.7 Determination of the molecular weight (Mw) by GPC

Oxidized dextran and oxidized Dex-GMA at the same %oxidation were dissolved in a phosphate buffer solution (pH 7.4, 0.1 M) to achieve the desired final concentration of 2% (w/v). In this section, a monothiol reagent (Ac-Cys-OH) was used instead of DTT so as to not form a hydrogel. The same volume of glycine (or Ac-Cys-OH) with a concentration of 0.6% and 5% (w/v) was added to the dextran derivatives solution, which was then incubated at 37 °C. Glycine was used as an amine source and Ac-Cys-OH was used as an SH source. Gel permeation chromatography (GPC) (Shimadzu, Japan, BioSep-s2000 column, Phenomenex, Inc., CA, USA) was employed to determine the molecular weight of the dextran derivatives at the desired time after the reaction. Here, PBS was used as the mobile phase (flow rate = 0.50 mL/min) and pullulan was used as the standard.

2.2.8 Kinetic analysis by NMR spectroscopy

The NMR data was recorded on a Bruker Avance III 600, 700 and 900 MHz spectrometer equipped with a cryogenic probe at 25 °C for use in a kinetic analysis of the reactions between the oxidized dextran-GMA and the Ac-Cys-OH or glycine. Two-dimensional NMR techniques, including $^{1}H–^{13}C$ hetero-nuclear single quantum correlation spectroscopy (HSQC), $^{1}H–^{13}C$ hetero-nuclear multiple-bond correlation spectroscopy (HMBC), total correlation spectroscopy (TOCSY), and double quantum filtered-correlation spectroscopy (DQF-COSY), were used to analyze the oxidized Dex-GMA. In the kinetic analysis experiments, oxidized Dex-GMA [10% (w/w)), oxidized with $NaIO_4$ (30% (w/w)], and 6% (w/w) Ac-Cys-OH or glycine, both in a PBS/D_2O solution at pH 7, were mixed at a 1:1 ratio in an ice bath to delay degradation. The final concentration was 5% oxidized Dex-GMA and 3% Ac-Cys-OH or glycine. As the peak was broadened due to the high concentration of Ac-Cys-OH, the reaction between the 5% oxidized

Dex-GMA and 0.75% Ac-Cys-OH (low concentration Ac-Cys-OH) was monitored via NMR. Once the solution was mixed, it was immediately transferred to the NMR spectrometer, and the first ^{1}H NMR spectrum was recorded 12 to 17 min later. Subsequently, one-dimensional ^{1}H NMR spectra with presaturation were recorded every 5 min, and 24 scans were accumulated with a recycle time of 12.5 s.

2.2.9 Cytotoxicity test

Cell viability was determined by measuring the ability of the cells to convert 3-(4,5-dimethyl thial-2-yl)-2, 5-diphenyltetrazalium bromide (MTT) to a purple formazan dye. L929 cells suspended in a 0.1 mL medium at a concentration of 1.0×10^{4}/mL were placed in 96-well culture plates. After 72 h incubation at 37 ℃, 0.1 mL medium containing different concentrations of oxidized Dex-GMA was added to the cells, followed by 48 h incubation. To evaluate the cell viability, 0.1 mL MTT solution (300 mg/mL in medium) was added to the cultured cells, which were further incubated for 4 h at 37 ℃. After removing the remaining medium, 0.1 mL DMSO was added to each well to dissolve the precipitation. The resulting color intensity, which was proportional to the number of viable cells, was measured by a microplate reader (versa max, Molecular Devices Co., CA, USA) at 540 nm. The cytotoxicity of the test substances was expressed as the 50% inhibition concentration of growth (IC50), which was defined as the concentration in the culture at which the cell activity was reduced to 50% of that of the untreated control cells.

2.3 Results and discussion

2.3.1 Characterization of the oxidized Dex-GMA

The concept of this study is depicted in Figure 2.2. The synthesis of the oxidized Dex-GMA was conducted in two steps, as shown in Figure 2.2A. In the first step, dextran was modified by GMA in DMSO as per the method described in the literature [24]. The reaction between the GMA and dextran proceeded via a nucleophilic attack of a hydroxyl group of dextran on the methylene carbon of the epoxy group of GMA [26, 27]. The dried Dex-GMA product was then oxidized by $NaIO_4$ to introduce aldehyde groups via Malaprade oxidation [18]. The formation of a hydrogel was accomplished by adding DTT to react with the C=C and SH via a Michael addition reaction with the remaining aldehyde groups (Figure 2.2B). In addition, an amine source was added to the hydrogel to react with the aldehyde to form a Schiff base and initiate the degradation of the hydrogels, which resulted in a Maillard reaction (Figure 2.2C). Assignments of the oxidized Dex-GMA were conducted with ^{1}H–^{13}C HSQC, ^{1}H–^{13}C HMBC, TOCSY, and DQF-COSY in ^{13}C and ^{1}H NMR. The ^{1}H–$1^{3}C$ HSQC NMR spectrum of the just prepared oxidized Dex-GMA is shown in Figure 2.3A. In the figure, it can be see that the $NaIO_4$ oxidized and cleaved the C2–C3 and C3–C4 bonds in the glucose unit in the dextran. Also, the aldehyde groups reacted with the adjacent hydroxyl groups to form hemiacetal structures [28, 29]. From the NMR measurements in our previous study, oxidized dextran contains many types of hemiacetal substructure units, of which at least four substructures, including a non-oxidized glucose unit, were observed. The existence of these structures is consistent with those proposed by Ishak [30]. The four types of partial structures, including GMA immobilized oxidized dextran, and the chemical shifts of the substructures are listed in Table 2.1. In terms of the C2–C3 bond cleavage, oxidized glucose was converted into hemiacetal substructure 3, and the C3–C4 cleavage was consistent with hemiacetal substructure 4. Then, when both the C2–C3 and C3–C4 bonds

were cleaved and the C3 was removed, the C2 and C4 aldehydic carbons with a water molecule were converted into hemiacetal substructure 2 (Figure 2.3A bottom schemes). The DS of the GMA in the oxidized Dex-GMA was calculated from the 1D ^{1}H-NMR (Figure 2.3B). The proton chemical shift of the Dex-GMA spectrum resulted in new proton peaks that exhibited resonances at 5.70–6.26 and 1.95 ppm, which are consistent with vinyl and methyl protons, respectively. The DS of the GMA into dextran was 23.1% ±1.3, which was calculated by comparing the ratio of the areas under the proton peaks at 2.0 ppm (methyl protons in GMA) to the peak at 3.3-4.2 (dextran sugar unit protons, H2-H6) based on the NMR spectra. The oxidized Dex-GMA spectrum should exhibit the proton chemical shift of aldehyde around 9–10 ppm; however, a peak with a low intensity at 9.6 ppm was observed instead, which is likely due to the very low concentration of aldehyde protons [3, 31] that was caused by the above mentioned hemiacetal formation.

A

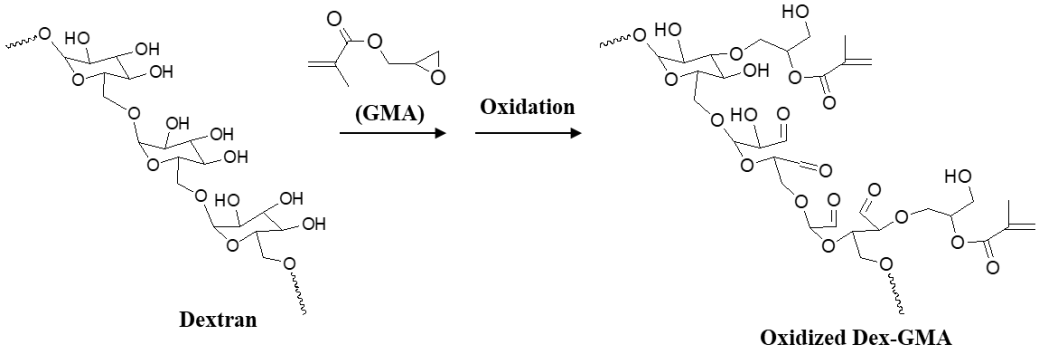

B

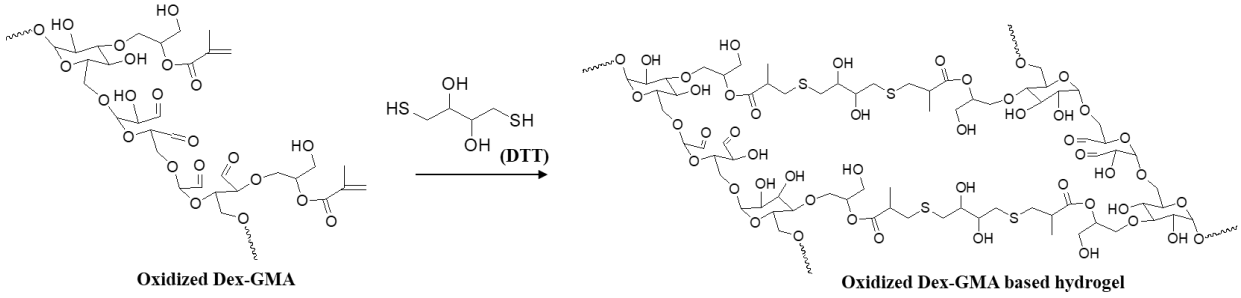

C

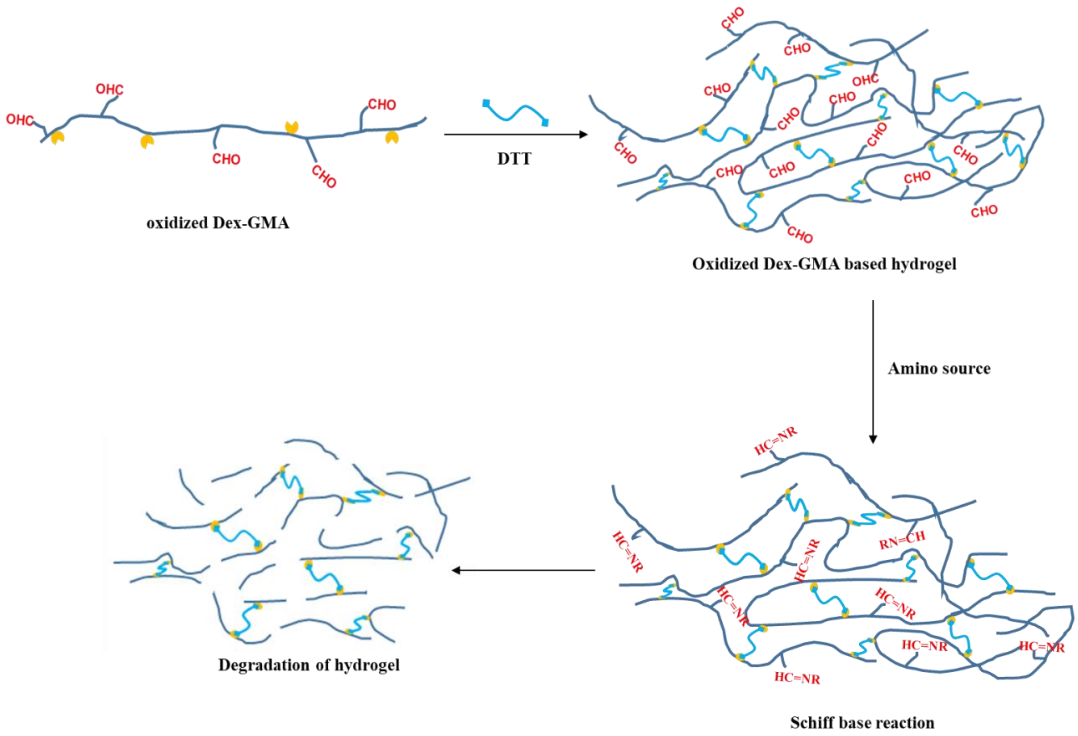

Figure 2.2 Syntheses of oxidized Dex-GMA based hydrogels. (A) The process used to synthesize oxidized Dex-GMA. (B) The proposed model of an oxidized Dex-GMA based hydrogel. (C) Schematic depiction of the formation of an oxidized Dex-GMA based hydrogel and its subsequent degradation by the addition of amino groups.

A

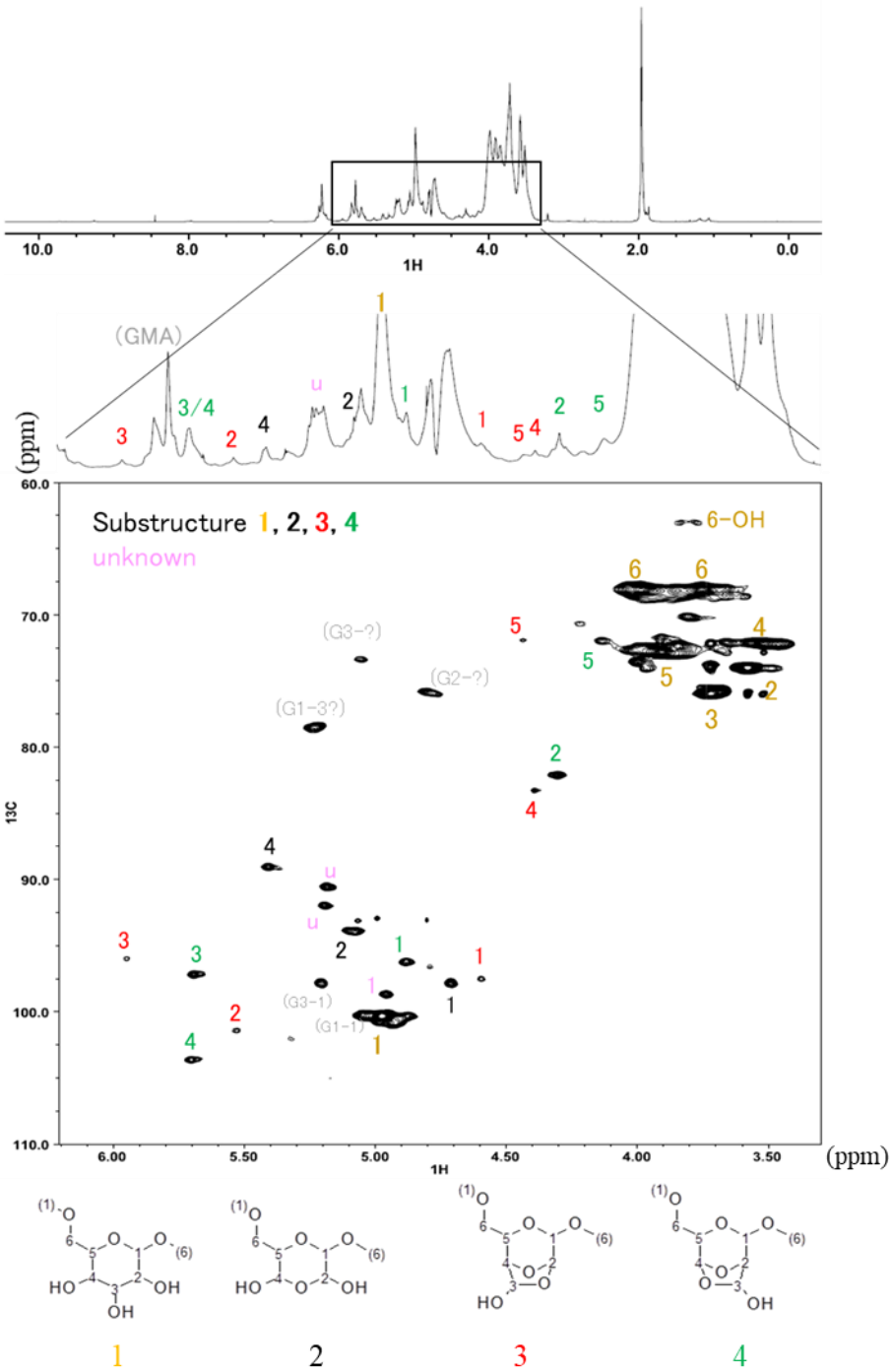
10.0
8.0
6.0
4.0
2.0
0.0
1H
(GMA)
3/4
u
(ppm)
60.0
70.0
80.0
90.0
100.0
110.0
13C
Substructure 1, 2, 3, 4
unknown
6-OH
(G3-?)
(G2-?)
(G1-3?)
(G3-1)
(G1-1)
6.00
5.50
5.00
4.50
4.00
3.50
1H
(ppm)
1
2
3
4

B

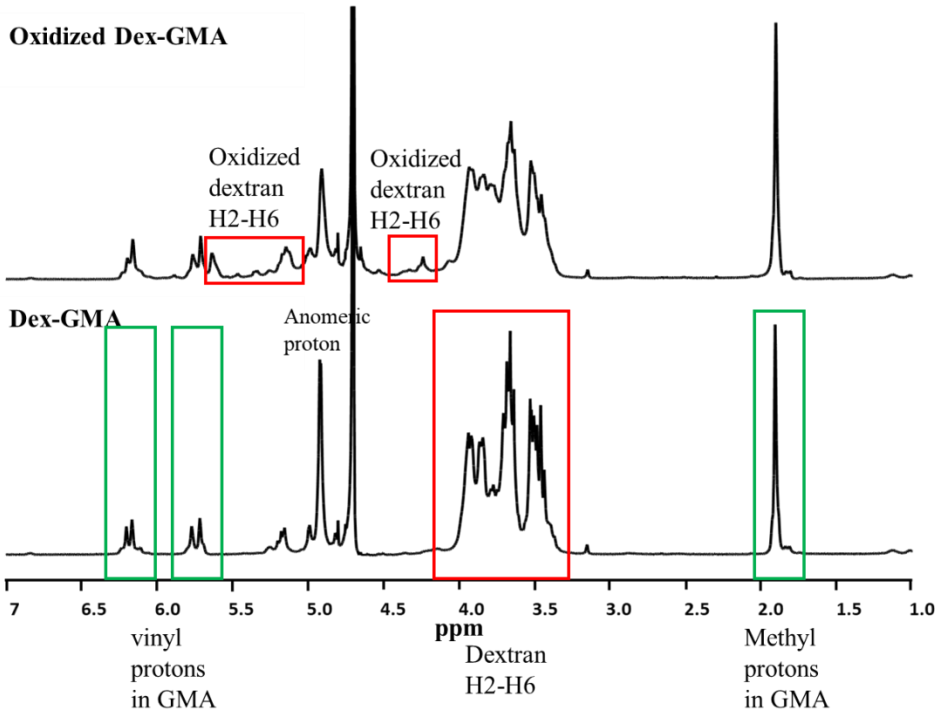

$$\textbf{Degree of substitution for GMA (\%)} = \frac{A_{\delta 1.7-2.0}}{3} / \frac{(A_{\delta 3.3-4.2})}{6} \textbf{ x 100}$$

Figure 2.3 NMR Spectra of the oxidized Dex-GMA. (A) ^{13}C–^{1}H HSQC NMR spectrum of newly oxidized Dex-GMA. Assignments of substructures 2 (black), 3 (red), and 4 (green), non-oxidized glucose (yellow), and GMA (gray) are indicated close to the NMR signals in the HSQC and 1D ^{1}H NMR. The assignment numbers represent the positions of the ^{1}H and ^{13}C in each substructure. The substructures that were identified in the oxidized Dex-GMA are 1: glucose, 2: C2–C3 and C3–C4 cleavage, C3 desorption, hemiacetal structure, 3: C2–C3 cleavage, hemiacetal structure, 4: C3–C4 cleavage, hemiacetal structure. (B) One-dimensional ^{1}H NMR of Dex-GMA and oxidized Dex-GMA for calculating the degree of substitution of the GMA.

Table 2.1 Chemical shift data* for substructure of oxidized Dex-GMA (23% DS of GMA and 24% oxidation)

substacture	position	^{1}H	^{13}C
1 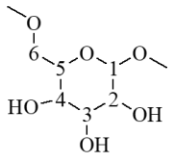	1	4.98	100.43
	2	3.58	74.11
	3	3.72	76.07
	4	3.52	72.26
	5	3.91	72.90
	6	3.99 / 3.76	68.25
2 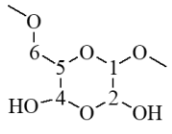	1	4.71	97.97
	2	5.07	93.98
	4	5.41	89.22
	5	Not identified	Not identified
	6	Not identified	Not identified
3 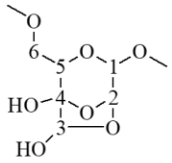	1	4.60	97.69
	2	5.53	101.54
	3	5.95	96.09
	4	4.39	83.38
	5	4.44	72.05
	6	Not identified	Not identified
4 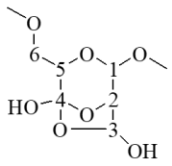	1	4.88	96.32
	2	4.30	82.23
	3	5.69	97.28
	4	5.70	103.75
	5	4.14	72.05
	6	Not identified	Not identified

* Relative to HOD signal at 4.77 ppm.

The aldehyde content could not be quantitatively detected via the iodometric method due to a disturbance in the reaction of the methacrylate groups in the oxidized Dex-GMA and iodine [32]. Hence, the aldehyde content was determined based on the reaction between acetoacetanilide (AAA) and formaldehyde in the presence of ammonia, which was reported by Li et al. [25]. The

aldehyde content in the oxidized Dex-GMA was then determined using the corresponding calibration curves. The degree of oxidation was evaluated from the oxidation percentage per glucose unit, which is defined as the number of C-C bonds cleaved in the 1,2-diol in each glucose unit. By way of the fluorescence intensity, the degree of oxidation of the oxidized Dex-GMA was well controlled from 10 to 41% (Figure 2.4), which is consistent with the results in previous report. In the remainder of this chapter, I denote the particular oxidized Dex-GMA as Ox(XX%)-GMA(YY%)-Dex, where XX is the degree of oxidation and YY is the DS of the GMA.

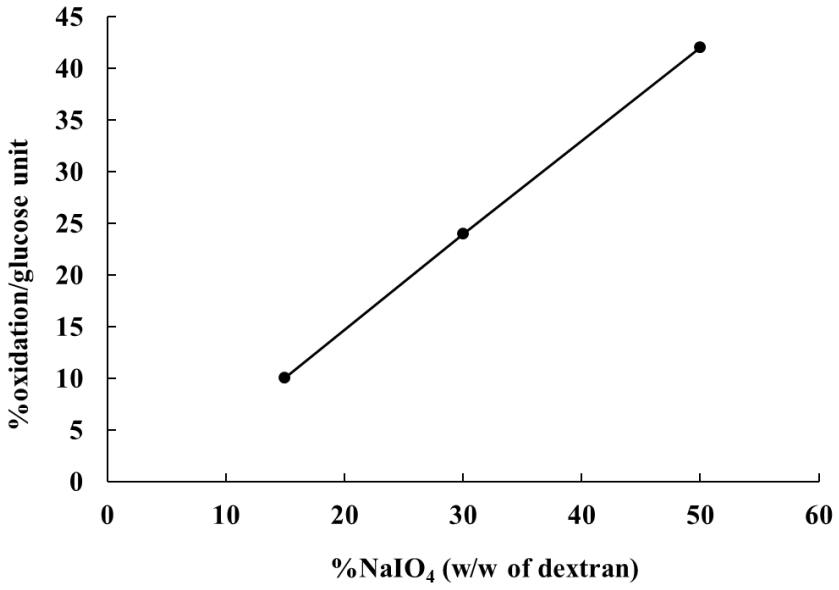

Figure 2.4 Effect of the periodate concentration on the oxidation of the Dex-GMA.

2.3.2 Cytotoxicity assay

The cytotoxicity of dextran, Ox-(24%)-GMA(23%)-Dex and glutaraldehyde to L929 cells was evaluated by the MTT assay and the results were given in Figure 2.5 and Table 2.2. IC50 of Ox(24%)-GMA(23%)-Dex was 15362±1353 μg/mL (1.5 w/w %), demonstrating lower

cytotoxicity than glutaraldehyde (IC50 was 5.6 μg/mL). Although the cytotoxicity of aldehyde dextran was enhanced by the oxidation and introduction of aldehyde, the cytotoxicity was still 1/3000 that of glutaraldehyde. Such low toxicity of oxidized dextran was consistent with our previous report [18]. The low cytotoxicity of aldehyde in the oxidized dextran was likely to ascribe to its low reactivity [18] with amine species due to the hemiacetal formation described in the further section.

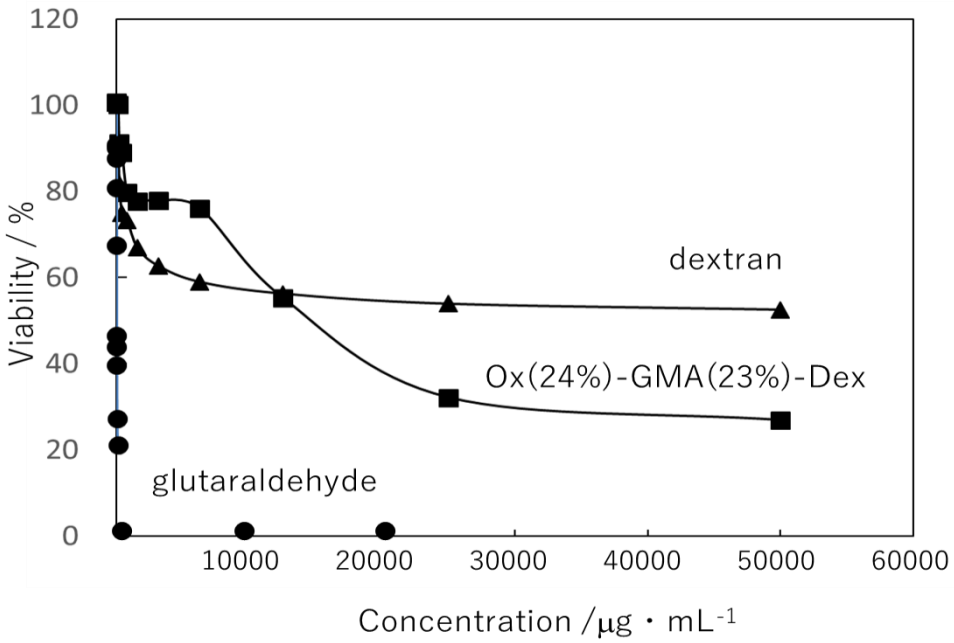

Figure 2.5 Cytotoxicity of dextran, Ox(24%)-GMA(23%)-Dex and glutaraldehyde.

Table 2.2. IC50 of dextran, Ox(24%)-GMA(23%)-Dex and glutaraldehyde to L292 cells.

Material	**IC50 (μg/mL)**	**IC50 (-CHO/10^{-6} M)**
Dextran	>50000	-
Ox(24%)-GMA(23%)-Dex	15362 ± 353	45471 ± 1044
Glutaraldehyde	5.6 ± 0.1	112.1 ± 3.1

2.3.3 Gelation time of the oxidized Dex-GMA with DTT

A hydrogel can be formed by mixing 10% (w/v) oxidized Dex-GMA and various concentrations of DTT in PBS at a temperature of 37 °C via a Michael reaction between the methyl acrylate (from oxidized Dex-GMA) and thiol groups (from DTT) [24]. An opaque white hydrogel was observed in all samples and the gelation time could be controlled by varying the molar ratio of the C=C and thiol groups (Figures 2.6A and 2.6B). The gelation time decreased as the amount of crosslinker DTT increased. For example, the hydrogel reached the gel point within 4.83 ± 0.53 min for a molar ratio of 1:2, which was approximately three times faster than that for a 1:0.74 ratio (13.83 ± 0.76 min). These results indicate that the gelation process can be accelerated by increasing the crosslinker concentration.

A

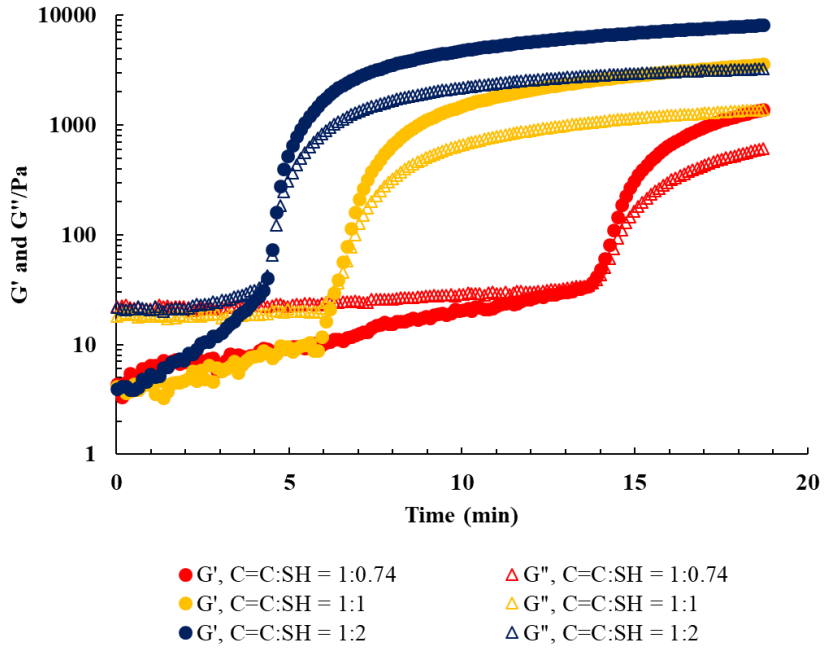

B

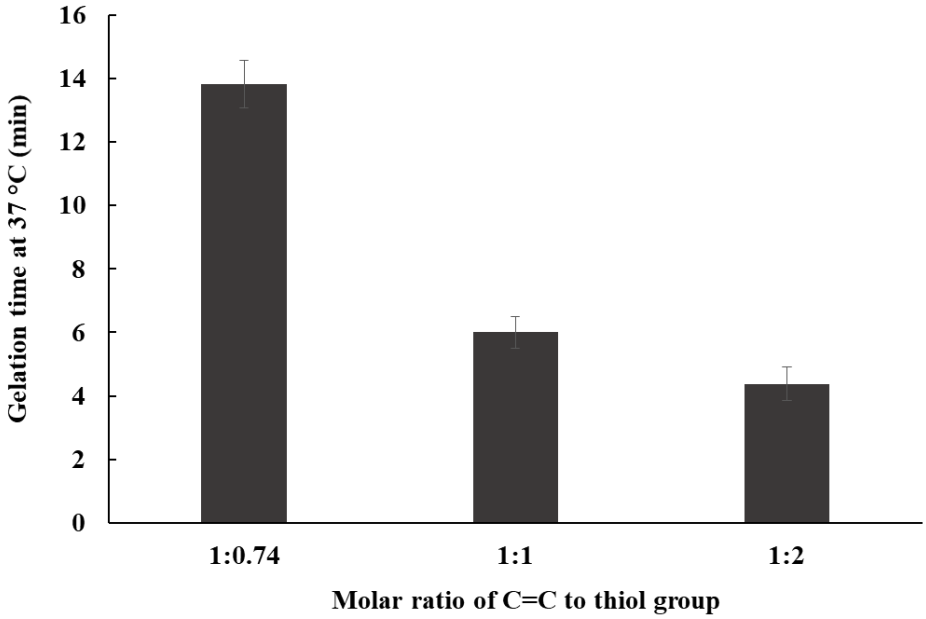

Figure 2.6 (A) Rheology analysis of oxidized Dex-GMA based hydrogels at different molar ratios of methyl acrylate to thiol. (B) Gelation time obtained from the rheology analysis.

2.3.4 Rheological measurements

To assess the effects of the mechanical properties on the strength of the oxidized Dex-GMA based hydrogel, a rheology test (Figure 2.7A and 2.7B) was performed on the hydrogels by mixing them with 1 or 1.36% DTT and 10% oxidized Dex-GMA (23% DS of GMA with varying degrees of oxidation). The addition of 1.36% w/v of DTT and a mole of thiol and methylacrylate are equivalent amounts, and the thiol content was less than the amount of methylacrylate when 1% w/v of DTT was added. Higher concentrations of DTT corresponded to higher levels of G' due to the increase in the crosslinking points. The oxidized Dex-GMA based hydrogel with same degree of oxidation showed dissimilar dynamic moduli when different concentrations of DTT were used. In the presence of 1.36% w/v DTT, the G' and G" were higher than those of the 1% w/v DTT addition because both the amount of thiol and the number of crosslinking points decreased, which caused a decrease in the dynamic moduli [33]. Interestingly, the degree of oxidation affected the storage moduli of various hydrogels. For example, the Ox(24%)-GMA(23%)-Dex hydrogels exhibited a higher G' value compared with the Ox(10%)-GMA(23%)-Dex hydrogels (the reasons for this are discussed in Section 2.3.8). Hence, these results demonstrate that the mechanical properties can be controlled by changing the degree of oxidation of the Dex-GMA and the concentration of the crosslinker.

In previous work, the dynamic moduli which were dependent on the degree of oxidation because crosslinking occurred in the reaction between the aldehyde and amine in the poly-L-lysine was reported [33]. However, in this report, the aldehyde content found to be not related to the crosslinking but the results indicated that the mechanical properties of the hydrogels depended on the aldehyde content. This means that the aldehyde groups may react with the thiol groups (this is analyzed in Section 2.3.8). The mechanical properties of the hydrogels were able to

control from 0.1 to 10 kPa by using DTT and oxidized Dex-GMA with varying degrees of oxidation.

A

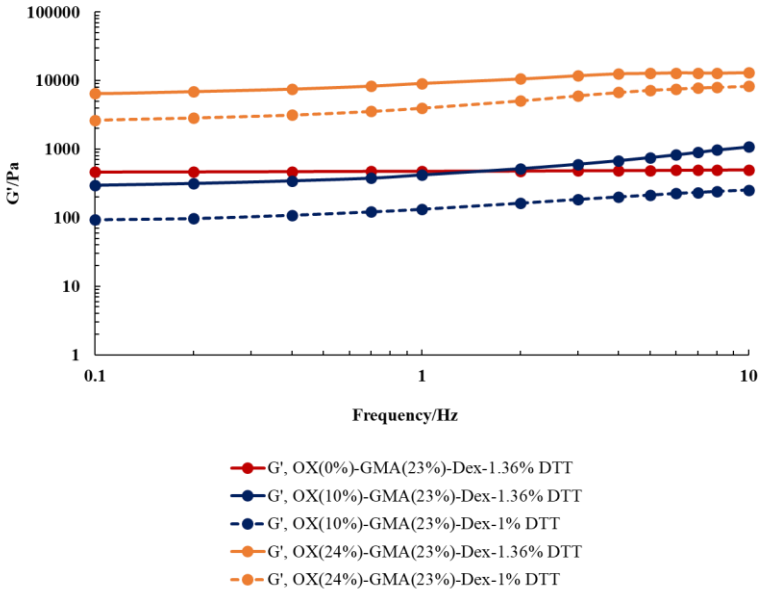

B

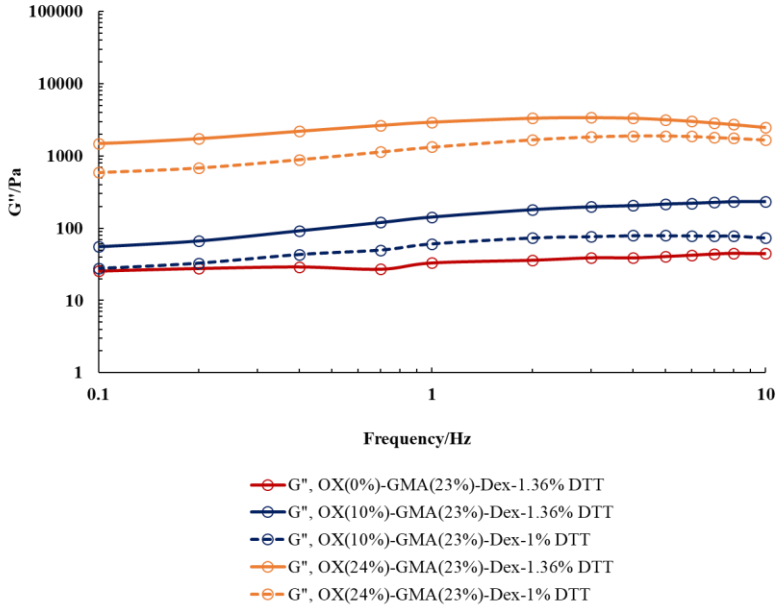

Figure 2.7 Dynamic moduli of various oxidized Dex-GMA based hydrogels: (A) G' and (B) G".

2.3.5 Quantitative gel degradation

The gel formulation of oxidized Dex-GMA was produced by crosslinking the oxidized Dex-GMA with DTT, which resulted in an opaque white hydrogel. In a previous study, glycine was used as a monoamine source to control the degradation of the oxidized dextran [22]. In this report, glycine was also used to react with the remaining aldehyde in the oxidized Dex-GMA hydrogel that had been prepared via DTT crosslinking. As shown in Figures 2.8A and 2.8B, the addition of glycine (an amine source) caused the gel to degrade. During the course of the degradation process, the color of the hydrogels after being left in a glycine solution changed to brown, which indicates that a Maillard reaction occurred after a Schiff base formed between the aldehyde and primary amino groups [22, 33, 34]. Figure 2.8A shows the gel degradation with different degrees of oxidation (0%, 10%, and 24% oxidation) and concentrations of DTT (1% and 1.36% w/v) in the presence of a glycine solution. The Ox(0%)-GMA(23%)-Dex and Ox(10%)-GMA(23%)-Dex hydrogels, after reacting with 1.36% w/v DTT, exhibited the same G', as shown in Figure 2.7A. The differences in the hydrogel degradations are represented by the solid red and blue lines (Figure 2.8A). Almost 100% of the remaining weight was observed in the Ox(0%)-GMA(23%)-Dex hydrogel but no hydrogel remained in the case of the Ox(10%)-GMA(23%)-Dex hydrogel after eight days. This was likely because there were no aldehyde groups in the gel to react with the amino groups from the glycine solution; thus, degradation did not occur. In addition, the hydrogels with 10% oxidation but different concentrations of DTT crosslinker exhibited the same degradation of the hydrogel but differing mechanical strengths, as indicated by the solid and dashed blue lines. This may be because the number of crosslinking points was different in the various concentrations of DTT that had differing mechanical properties; however, the number of degradation points (aldehyde groups) were the same. Therefore, the degradation pattern was the same. In the case of the Ox(24%)-GMA(23%)-Dex hydrogels, the mechanical

properties were different when the DTT concentrations were 1.36% and 1% (Figure 2.7A orange solid and dashed lines); however, the degradation after the glycine was added showed a similar trend (Figure 2.8A orange solid and dashed lines). For easier consideration, the summary of mechanical properties in term of crosslink density (ν) and degradation ratio of various hydrogels was showed in Table 2.3. The crosslink density can be estimated from the plateau storage modulus, G', of hydrogel as the following equation:

$$G' = \nu kT$$

Where k and T are the Botzmann constant (1.38×10^{-23} $m^2.kg.s^{-2}.K^{-1}$) and temperature (K), respectively.

These findings clearly suggest that the degradation speed can be controlled independently of the mechanical strength of the hydrogels.

In Figure 2.8B, the weight that remained of the Ox(24%)-GMA(23%)-Dex with 1.36% DTT hydrogels in the 0 to 10% glycine PBS solutions were plotted. After eight days, more than 80% of the Ox(24%)-GMA(23%)-Dex based hydrogel remained in the PBS that did not contain glycine, and the gradual decrease that was observed may have been due to the hydrolysis of the ester bonds. In contrast, the degradation of the hydrogels in the presence of glycine was found to be dependent on the concentration. The remaining weight of the Ox(24%)-GMA(23%)-Dex hydrogel after eight days of incubation in 1% glycine was 60.7% while complete degradation was observed in the 5% and 10% glycine solutions. In the latter cases, the majority of the degradation was observed in the first four days. This suggests that the degradation reaction was faster than the hydrolysis of the ester bonds, and that the degradation of the hydrogels was triggered by the reaction between the aldehyde and amino groups. The oxidized Dex-GMA based hydrogel was stable in PBS but degraded in the presence of glycine, which suggests the degradation of the oxidized Dex-GMA hydrogel can be controlled by adding an amino source and that the rate of

degradation can be accelerated by increasing the concentration of the amino source. To confirm the degradation of oxidized Dex-GMA, GPC was used to track the decreasing molecular weight of the polymer.

2.3.6 Determining molecular weight via GPC

In this section, the decreasing molecular weight of the oxidized Dex-GMA after reacting with the mono-thiol reagent, Ac-Cys-OH, and glycine is described. The molecular weight of various samples after reacting with Ac-Cys-OH and glycine solutions of various concentrations were recorded by GPC, as shown in Figure 2.9. As shown, when the Ox(24%)-GMA(23%)-Dex (1% w/v) reacted with 0.3 and 2.5% w/v of Ac-Cys-OH (here, the thiol amount was similar and eight times higher than C=C concentration, respectively), the molecular weight remained unchanged after 3 h. The molecular weight of the Ox(24%)-GMA(23%)-Dex decreased rapidly in the glycine solution during the first 30 min, and then reduced gradually until it became steady. This is consistent with the results of the previously reported molecular degradation of oxidized dextran by glycine, and suggests that the GMA conjugation did not affect the degradation. In this study, we conclude that the hydrogels via the Michael addition between the GMA and thiol was stable in the PBS. The degradation of the hydrogel was controlled by the a posteriori addition of amine sources by main chain scission via a Maillard reaction independent of the mechanical properties.

A

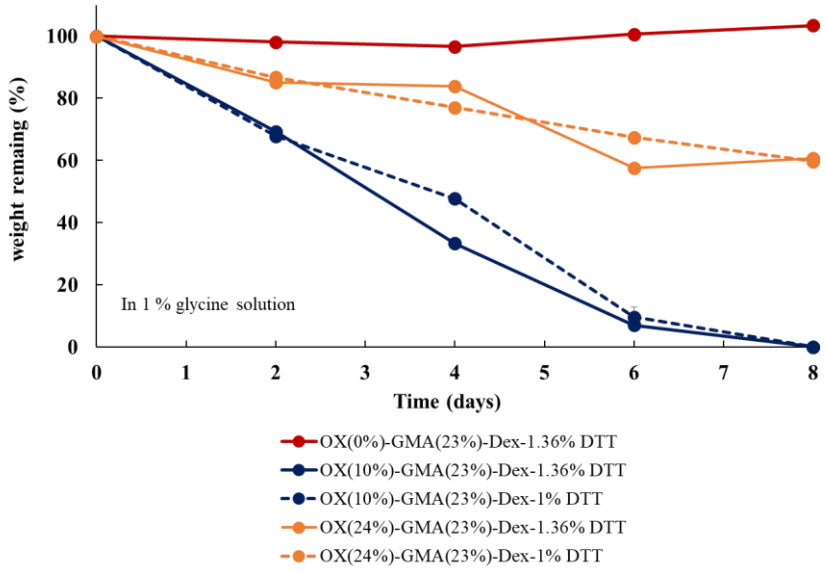

B

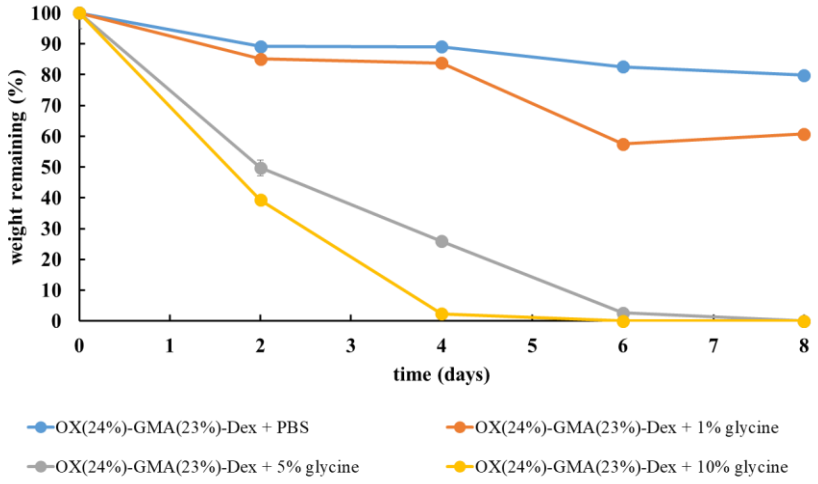

Figure 2.8 Degradation of the oxidized Dex-GMA (23% DS of GMA) hydrogel at 37 °C. (A) Gel degradation with different degrees of oxidation and different concentrations of DTT in a 1% w/v glycine solution. (B) Gel degradation of the oxidized Dex-GMA with 23% DS of GMA and 24% oxidation with different concentrations of glycine.

Table 2.3 Crosslink density and degradation pattern of various hydrogels with different oxidation degree and concentration of crosslinker

Sample name	**ν (x 10^{22} m^{-3})**	**Degradation ratio at 8 days (%)**
Ox(0%)-GMA(23%)-Dex – 1.36% DTT	12	~0
Ox(10%)-GMA(23%)-Dex – 1.36% DTT	12	100 ± 0.04
Ox(10%)-GMA(23%)-Dex – 1% DTT	3.8	100 ± 0.00
Ox(24%)-GMA(23%)-Dex – 1.36% DTT	304	40 ± 0.18
Ox(24%)-GMA(23%)-Dex – 1% DTT	140	40 ± 0.50

However, the addition of thiol into the Ox(24%)-GMA(23%)-Dex (green and orange lines in Figure 2.9) resulted in almost no molecular degradation. This suggests that the thiol and GMA reaction did not affect the degradation of the polymer chain. Interestingly, a slower degradation was observed when the Ox(24%)-GMA(0%)-Dex was mixed with thiol (black and yellow lines in Figure 2.9). This indicates that the aldehyde may react with the thiol and accelerate the molecular scission in the polymer main chain. To confirm this, detailed reaction kinetics analyses of the reaction between the thiol and aldehyde and the thiol and GMA were performed using the 2D NMR technique described in the following section.

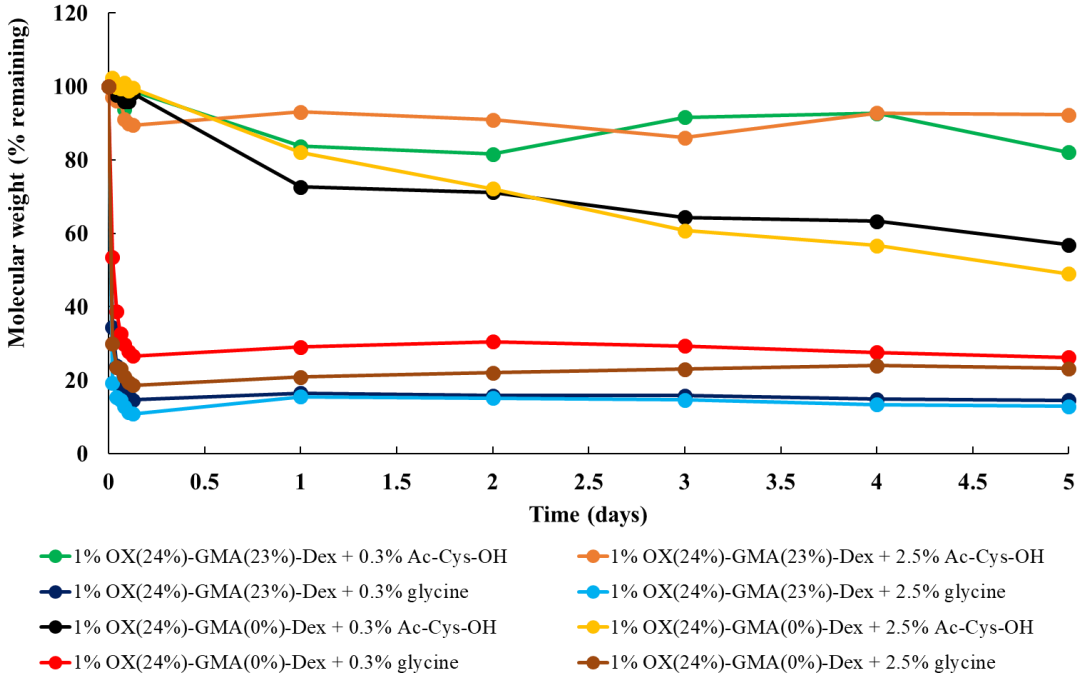

Figure 2.9 Changes in molecular weight of oxidized Dex-GMA (23% DS of GMA and 24% oxidation) and oxidized dextran (24% oxidation) in present of a monothiol reagent and glycine over the course of five days.

2.3.7 Determination of the reaction between the aldehyde and thiol

The aldehyde content in the Ox(24%)-GMA(23%)-Dex in the presence of thiol groups was determined via a fluorometry method in order to investigate the reactivity between the aldehyde and thiol. The aldehyde content of each of the samples is summarized in Table 2.4. Without the monothiol reagent, the volume of the aldehyde group in the Ox(24%)-GMA(23%)-Dex was 2.96 x 10^{-5} mole in 0.1 mL of solution. Interestingly, the amount of aldehyde showed a tendency to decrease when the mono-thiol concentration increased. When 3% (w/v) thiol was added, the volumes of the thiol and methacrylate were equivalent in the solution. When 1.5 and 3.0% Ac-Cys-OH were added, the amount of aldehyde did not significantly decrease; however,

when 5% of Ac-Cys-OH was added, the aldehyde amount did significantly decreased. This suggests that the thiol groups were able to react with the aldehyde.

To confirm the reaction of the aldehyde in the oxidized Dex-GMA with the thiol groups from the DTT, Ox(24%)-GMA(0%)-Dex (without introducing GMA) was used as model to react with the mono-thiol reagent, Ac-Cys-OH. Ellman's reagent was used to estimate the amount of sulfhydryl groups remaining in the sample. Here, a fixed amount of Ac-Cys-OH was added to the solution of oxidized dextran with various concentrations. The results showed that the concentration of the thiol groups decreased when the amount of oxidized dextran increased, as shown in Figure 2.10. From this, it can be concluded that the aldehyde can react with the thiol groups. From the literature, thiol reacts with aldehyde to produce hemithioacetal [35, 36]. However, from the result of Table 2.4, the thiol group reacts dominantly with the methacrylate group via a Michael addition reaction. Thus, less DTT should be added than immobilized GMA in the oxidized Dex-GMA to preserve the aldehyde groups after gel formation. The proposed model describing the formation of an oxidized Dex-GMA based hydrogel is shown in Figure 2.2B. The remaining aldehyde will react with the amine sources after gel formation, which will result in a degradation reaction (Figure 2.2C).

Table 2.4. Analytical results for determining the aldehyde content in the oxidized Dex-GMA

Sample	-CHO found in 0.1 mL of 10% Ox(24%)-GMA(23%)-Dex (x 10^{-5} mole)
Ox(24%)-GMA(23%)-Dex + 0% (w/v) Ac-Cys-OH	2.96 ± 0.41
Ox(24%)-GMA(23%)-Dex + 1.5% (w/v) Ac-Cys-OH	2.77 ± 0.15
Ox(24%)-GMA(23%)-Dex + 3% (w/v) Ac-Cys-OH	2.55 ± 0.35
Ox(24%)-GMA(23%)-Dex + 5% (w/v) Ac-Cys-OH	1.94 ± 0.81***

Different from 0% (w/v) of Ac-Cys-OH at *** $p < 0.035$

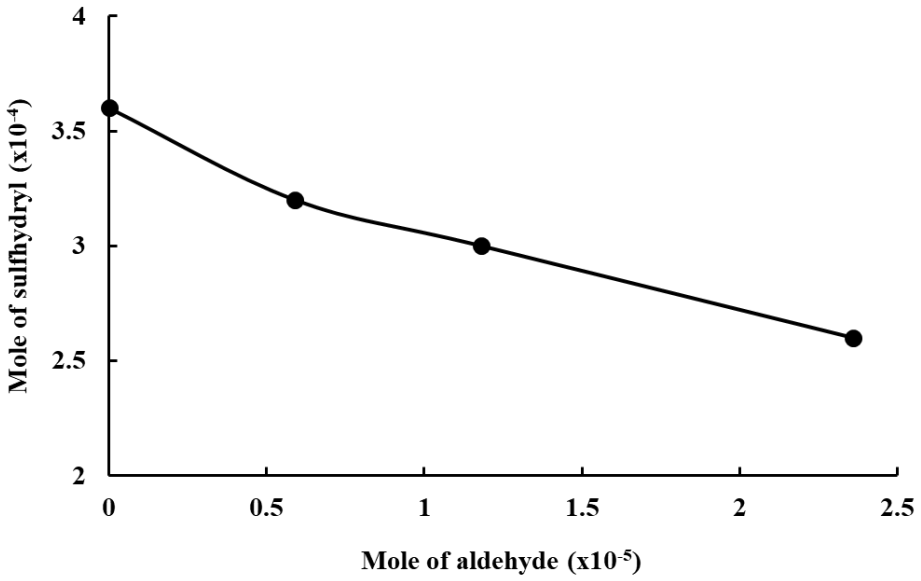

Figure 2.10 Sulfhydryl content of the reaction of oxidized dextran and Ac-Cys-OH.

2.3.8 Kinetic analysis of the reaction between the GMA and thiol, and the aldehyde and thiol by NMR

The identified time dependent NMR peak changes in the 5% Ox(24%)-GMA(23%)-Dex with 0.75% Ac-Cys-OH (low concentration condition) are shown in Figure 2.11. Under these conditions, there was more C=C than thiol. Figure 2.11A shows the time dependent peak intensity changes via the red to blue lines. The kinetics of the specific peaks are shown in Figures 2.11B–F. The aldehyde groups in the oxidized part reacted with adjacent hydroxyl groups to form hemiacetal substructures (substructures 2 to 4). Proton peaks in substructures 2 and 4 and the Ac-Cys-OH decreased (Figures 2.10B, C, and F). In contrast, the peaks of the GMA vinyl protons and substructure 3 showed no decrease in intensity (Figures 2.11D and E). These suggest that the thiol reacted quickly with aldehyde substructures 2 and 4, and not with the vinyl protons in the GMA. Substructure 3 did not react with the thiol under these conditions. The time dependent NMR peak changes in the 5% Ox(24%)-GMA(23%)-Dex with 3% Ac-Cys-OH (high concentration condition) are shown in Figure 2.12. Under these conditions, there was more thiol than C=C. The peak intensity of the vinyl protons in the GMA (5.8 and 6.2 ppm) rapidly disappeared after the reaction with the thiol groups (Figure 2.12B) after a time constant of 0.53 h.

Under these conditions, the protons from all substructures decreased after mixing with the thiol. Substructures 2 (H4 peak at 5.40 ppm) and 4 (H3/4 peak at 5.72 ppm) exhibited very rapid decomposition, which meant that the reaction was almost finished by the time the measurement started. However, substructure 3 (Figure 2.12C, H2 peak at 5.53 ppm) decomposed with a time constant of 4.33 h, which was slower than the time for the GMA peak to diminish, which had a time constant of 0.53 h. Comparing the speed of reaction with the thiol, it can be said that substructures 2 and 4 were faster than that for the GMA, and substructure 3 was later than the GMA.

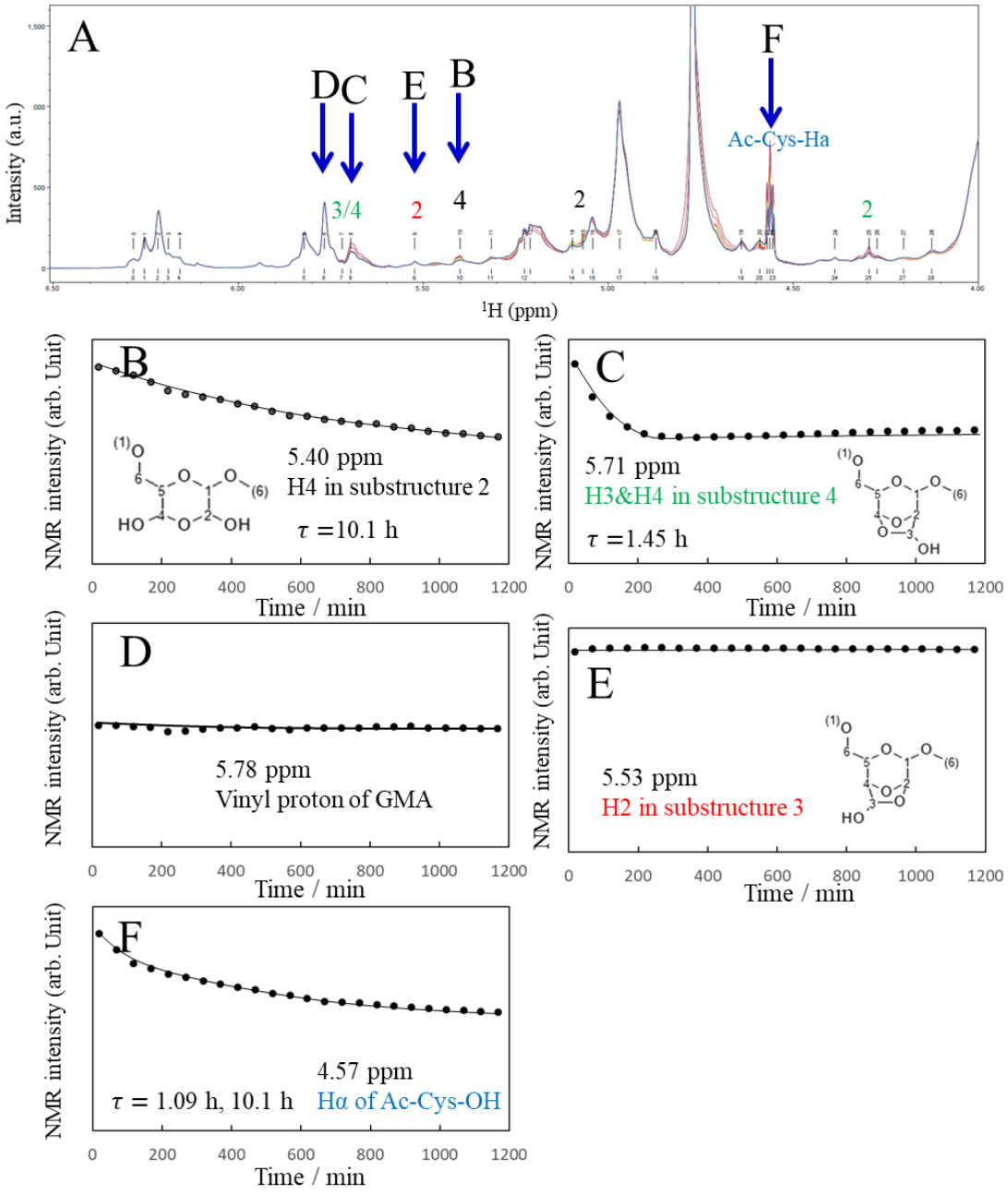

Figure 2.11 (A) One-dimensional ^{1}H NMR spectra of the reaction of 5% Ox(24%)-GMA(23%)-Dex and 0.75% Ac-Cys-OH (low concentration condition), and a kinetic analysis of the time-course NMR spectra for (B) substructure 2, (C) substructure 4, (D) vinyl group, (E) substructure

3, and (F) α proton of Ac-Cys-OH. The solid lines were computed by single-exponential curve fitting, and the time constants (τ) of the exponential function are shown.

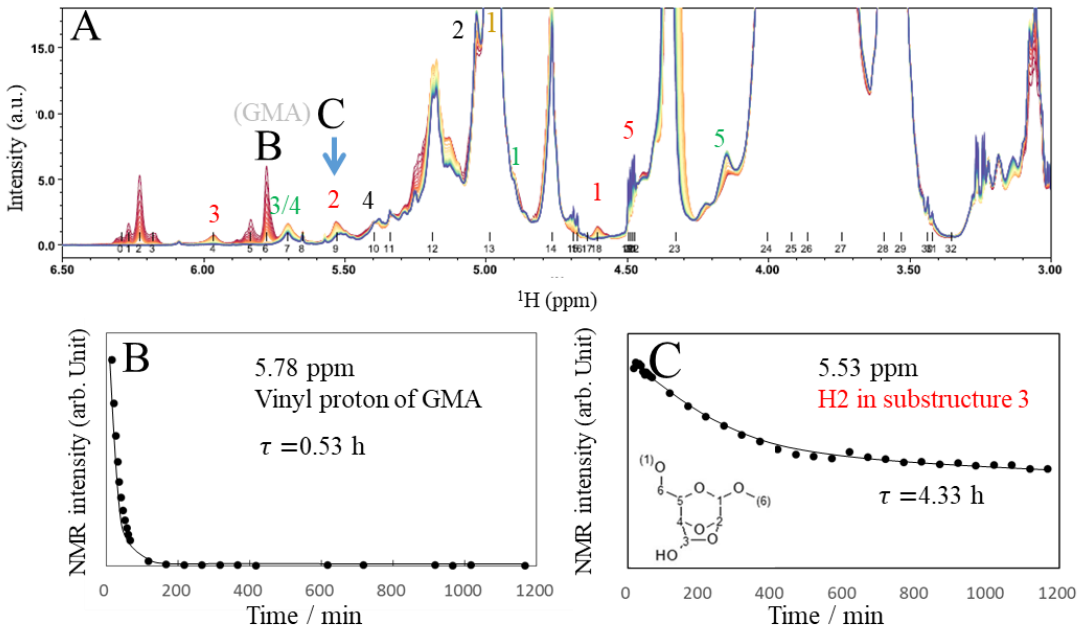

Figure 2.12 (A) One-dimensional ^{1}H NMR spectra of reaction of the 5% Ox(24%)-GMA(23%)-Dex and 3% Ac-Cys-OH (high concentration condition) and a kinetic analysis of the time-course NMR spectra for (B) the vinyl group, and (C) substructure 3. Solid lines are calculated by single-exponential curve fitting and the time constants (τ) of the exponential function are shown.

The reaction products of the thiol and aldehyde are shown in Figures 2.13A and 2.13B. These peaks were assigned to monothioacetal protons. Although, under high concentrations of thiol, the proton peaks of the reaction products were so broad they could not be assign to the structures, at low concentrations, the thioacetal production could be allocated between thiol and substructure 4 by HSQC and HMBC (Figure 2.14). In low concentration Ac-Cys-OH conditions, most of the thiol was consumed to produce thioacetal with aldehydes, which suggested fast

reaction aldehydes. This can be confirmed by thiocetal proton peak increasing (Figure 2.15). From this, it was determined that aldehyde (substructure 4), which reacted quickly with thiol, formed thioacetal, based on which the main structure of the product was assigned (Figure 2.13A). By comparing the production peaks between low and high concentrations of Ac-Cys-OH, I detected the same proton peaks in the high concentration condition, which indicates that thioacetal was produced even in high Ac-Cys-OH conditions (Figure 2.13B). It was determined that stable thioacetal [37] also contributed to the crosslinks in addition to the thiol-en crosslinking during hydrogel formation by the oxidized Dex-GMA and DTT. This is why the storage moduli in the Ox(24%)-GMA(23%)-Dex hydrogels were higher than those in the Ox(0%)-GMA(23%)-Dex or Ox(10%)-GMA(23%)-Dex hydrogels (Figure 2.7A). This was also supported by the observation that the oxidized dextran without GMA took the form of a hydrogel when mixed with DTT. However, the gelation time was very slow, which suggests the crosslinking by thioacetal may not be dominant.

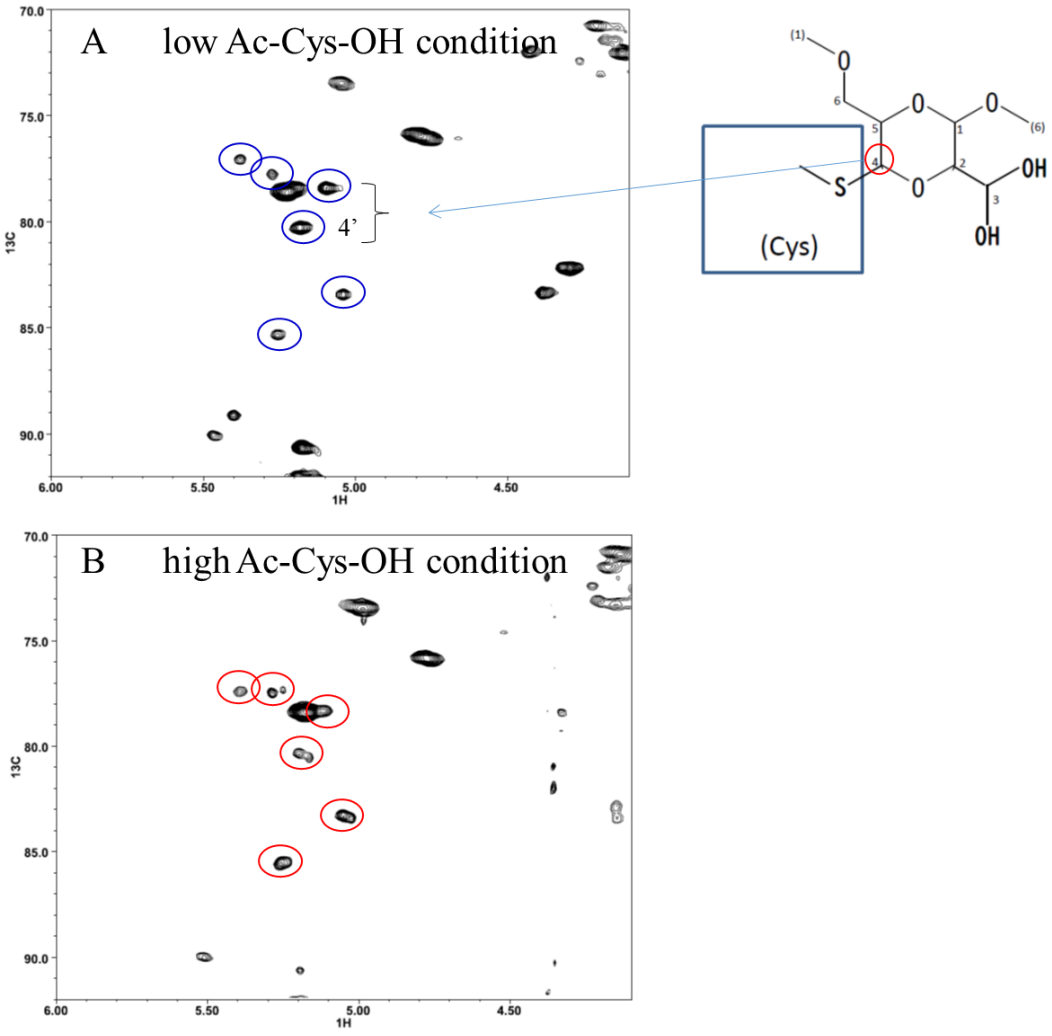

Figure 2.13 ^{13}C-^{1}H HSQC NMR spectrum of (A) 5% Ox(24%)-GMA(23%)-Dex and 0.75% Ac-Cys-OH and the estimated main structure of the thioacetal produced by the reaction between thiol and aldehyde (substructure 4), and (B) 5% Ox(24%)-GMA(23%)-Dex and 3% Ac-Cys-OH.

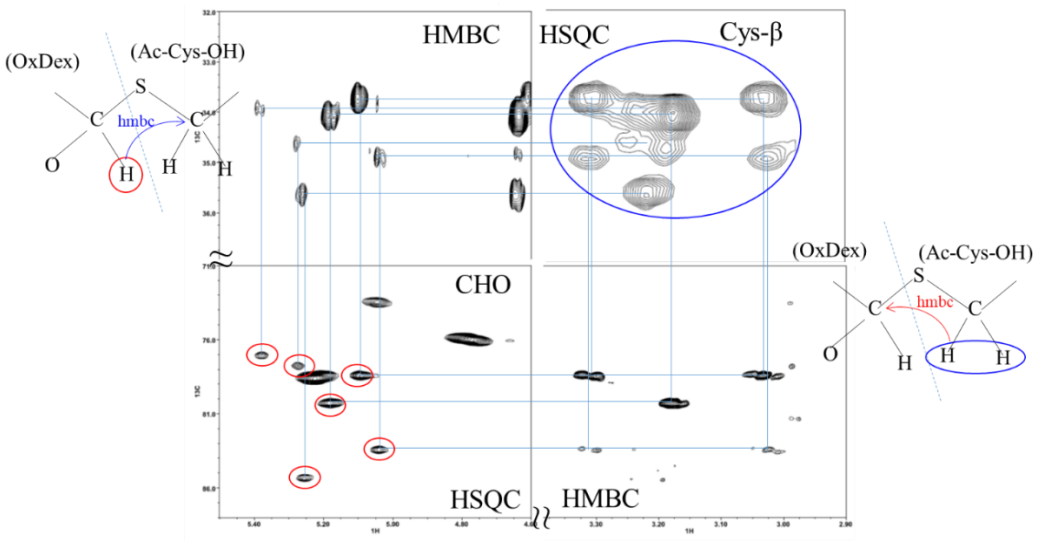

Figure 2.14 HMBC and HSQC for the assignment of thioacetal (substructure 4) of the reaction of 5 % Ox(24%)-GMA(23%)-Dex and 0.75 % Ac-Cys-OH (low concentration condition).

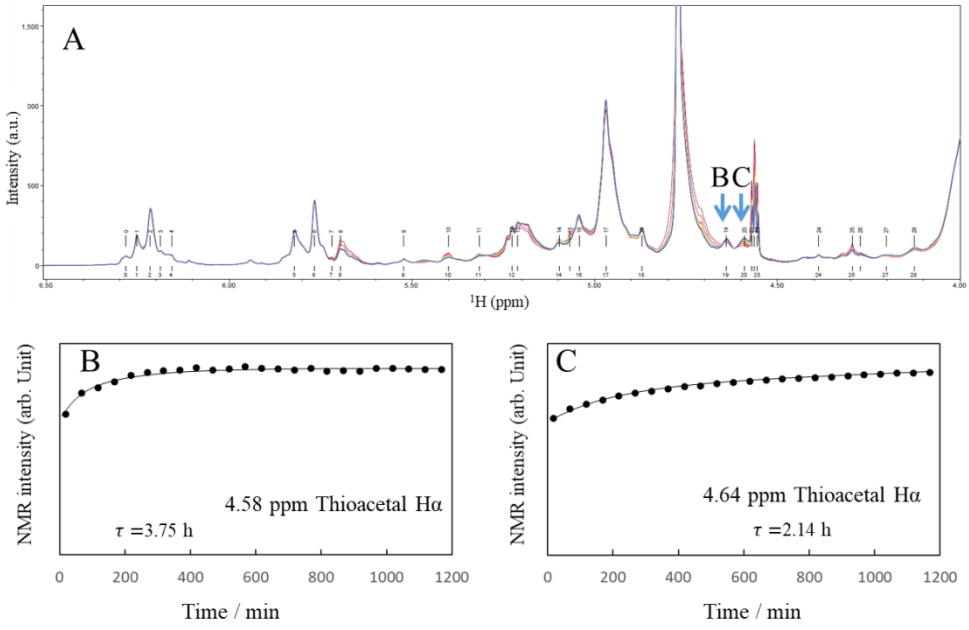

Figure 2.15 (A) One-dimensional ^{1}H NMR spectra of the reaction of 5 % Ox(24%)-GMA(23%)-Dex and 0.75 % Ac-Cys-OH (low concentration condition), and a kinetic analysis of the time-course NMR spectra for thioacetal Hα at (B) 4.58 and (C) 4.64 ppm.

As shown in Figure 2.16, the reduction in the end proton production only in high concentration Ac-Cys-OH conditions (black dots surrounded by circles) was detected. More rapid reductions in the number of end protons in the glucose unit was taken as evidence of main chain scission. This result suggested that the molecular degradation in the polysaccharide main chain also occurred after the reaction between the thiol and slow reacting aldehyde, which contradicts the GPC results. However, in Figure 2.9B, the yellow and black lines (Ox(24%)-GMA(0%)-Dex and thiol reaction) indicate a gradual degradation, which may be a result of the main chain scission after the aldehyde and thiol reaction, although a more detailed quantitative analysis will be required to confirm this. Also in Figure 2.8B, the Ox(24%)-GMA(23%)-Dex hydrogel exhibited slight degradation in PBS without an amine source, which may have been due to not only ester hydrolysis, but also to the main chain degradation caused by the thiol and aldehyde reaction. However, there were multiple crosslinking points of thiol-en and thiol-aldehyde, which should have delayed the degradation of the hydrogel. The rapid aldehyde reaction (substructure 2, 4) formed thioacetal with SH, followed by SH reacting with the GMA. Then, since SH reacted with substructure 3 and generated reducing ends, this suggests it was involved in the molecular decomposition.

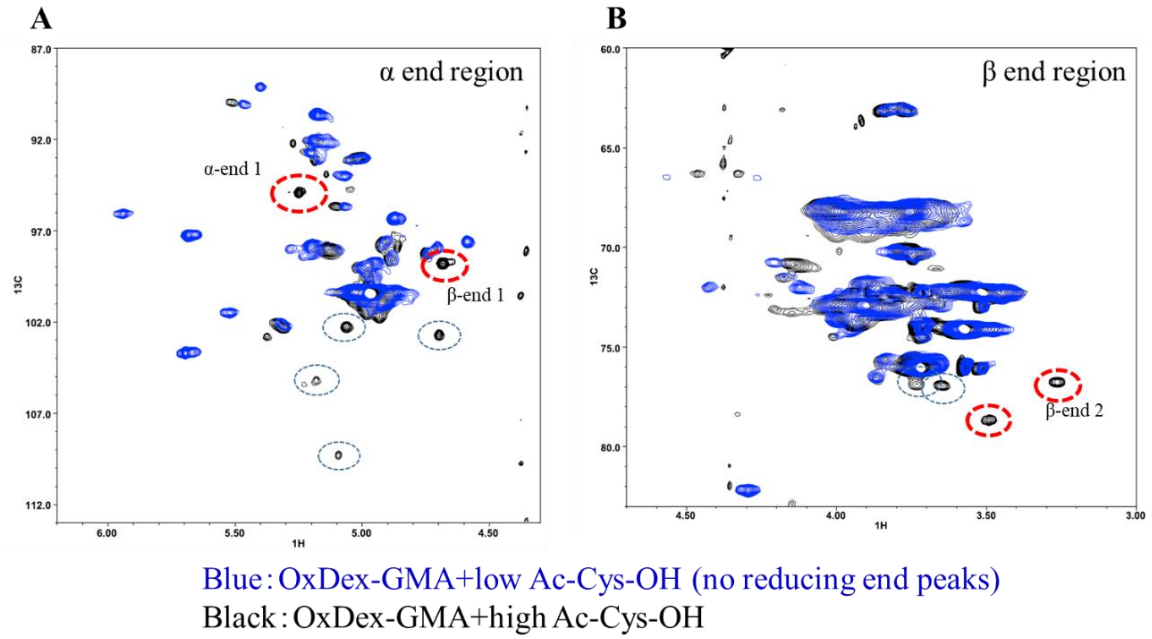

Figure 2.16 HSQC analysis of (A) α and (B) β end reducing protons after the reaction between oxidized GMA-Dex and low (blue) and high (black) concentration Ac-Cys-OH.

In Figure 2.17, the rapid decomposition of the aldehydes (hemiacetal substructure 2) in the Ox(24%)-GMA(23%)-Dex and glycine (model of amine source) mixture was confirmed. In addition, reducing the end proton signal suggested the main chain scission increased. Interestingly, based on the Figure 2.18 peak around 2.2 ppm, methylene groups were generated and this was ascribed to 3-deoxyosone during the progress of the Maillard reaction (Figure 2.1), which is consistent with the previous report [22], including the introduction of GMA. However, these methylene proton peaks were not observed in the mixture of Ox(24%)-GMA(23%)-Dex and Ac-Cys-OH, which suggested there was a different degradation pathway between the aldehyde and thiol, and aldehyde and amine reactions. This was also confirmed by the color change of the hydrogels, for example, the addition of glycine addition caused the hydrogel to turn brown. Therefore, the reaction mechanism was concluded as follows. There were fast and slow reactive

aldehyde substructures in the oxidized Dex-GMA, and the fast reactive ones reacted with the thiol to produce thioacetal, which resulted in crosslinking. Then, the thiol reacted with the GMA to produce dominant crosslinking points, followed by the slow reactive aldehydes reacting to the thiol and contribute to the main chain scission of the oxidized Dex-GMA. Finally, the a posteriori addition of amine resulted in a reaction with hemiacetal that led to a Maillard reaction via dexyosone production and accelerated the degradation. Considering these complicated reaction mechanisms, hydrogels were able to prepare in which the degradation timing was controlled independently of the mechanical properties.

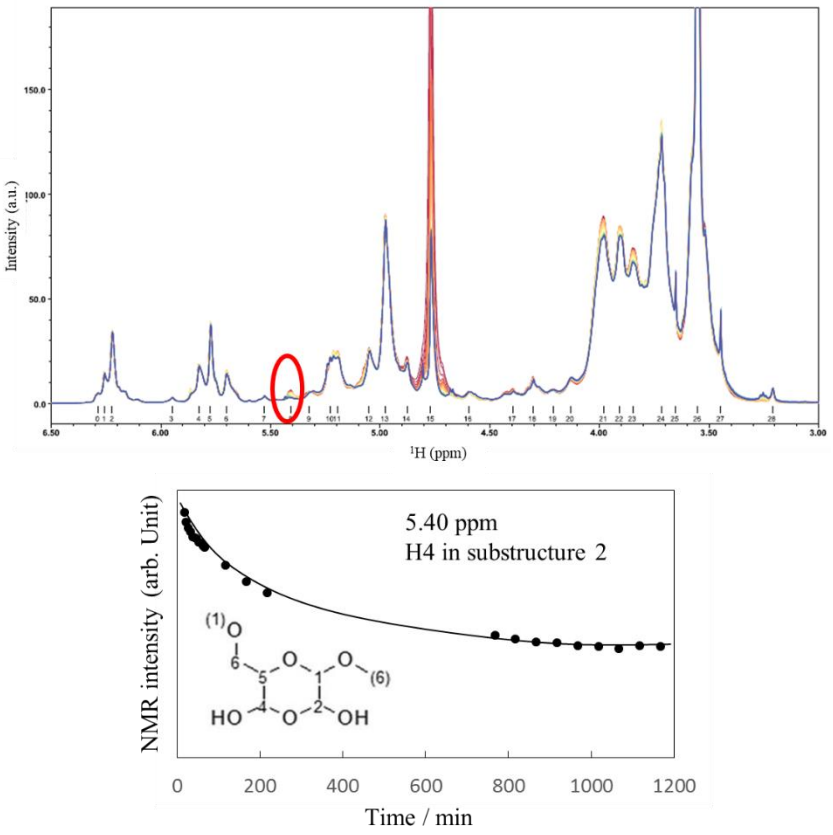

Figure 2.17 Kinetic analysis of time-course NMR spectra for substructure 2 for the reaction of Ox(24%)-GMA(23%)-Dex and glycine.

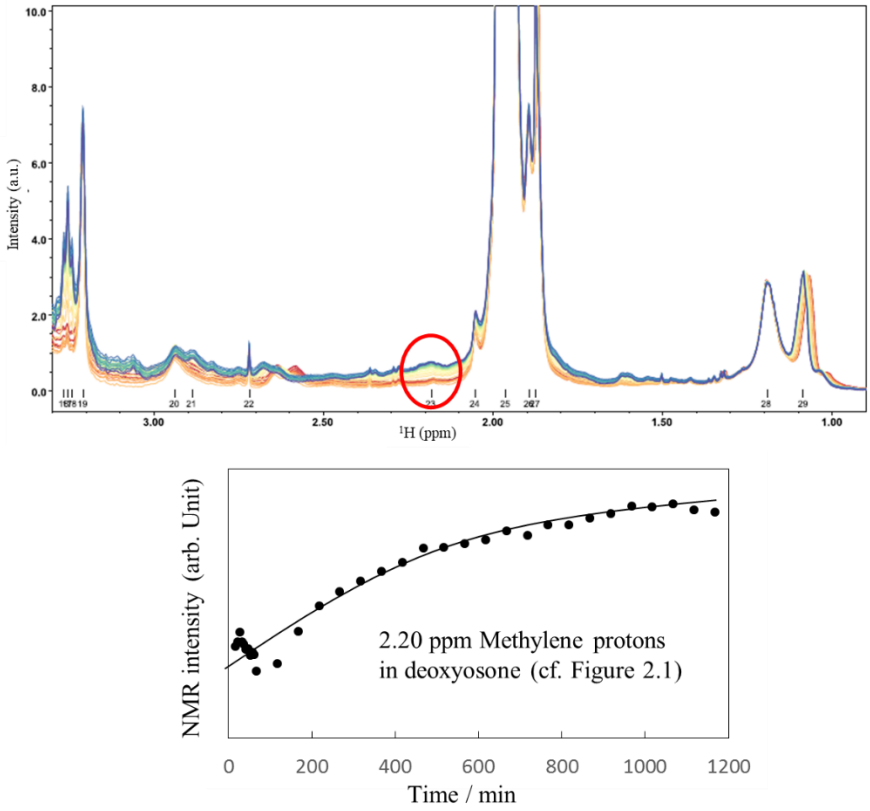

Figure 2.18 Kinetic analysis of time-course NMR spectra for methylene group for the reaction of Ox (24%)–GMA (23%)-Dex and glycine.

2.4 Conclusion

As described, by introducing GMA into oxidized dextran and then forming a hydrogel with DTT while preserving the aldehyde, the major drawback of oxidized dextran and polyamine hydrogels which was the uncontrollable degradation have overcome. In the proposed formulation, degradation did not occur immediately after the hydrogels were formed. Instead, the degradation could be controlled by the posteriori addition of an amine source, and interestingly, the degradation speed could be controlled independently of the mechanical properties of the hydrogel. The mechanical properties were found to depend on the number of crosslinking points, and NMR was used to determine that both the GMA and aldehyde groups react with thiol to form crosslinking points. Thus, the mechanical properties could be controlled by the numbers of both the GMA-thiol and aldehyde-thiol crosslinks. The addition of amine began a reaction with the remaining aldehyde, which triggering the degradation through a Maillard reaction via a Schiff base reaction. To the best of these knowledge, this is the first time the details of these degradation mechanisms have been elucidated at the molecular level. This level of understanding of the mechanism of molecular degradation is an important step toward the design of polymer materials in which the degradation can be precisely controlled. In the human body, there are many amine sources, such as proteins. This hydrogel must therefore be capable of biodegradation. For external stimuli responsive drug delivery applications, the study involving some combination of temperature responsive hydrogels that incorporate amine sources for control amino release manner should be studied. Therefore, in the next chapter, I prepare the novel system to temperature responsive materials to release amino compounds by external NIR light stimulation.

References

1. Hoare, T. R.; Kohane, D. S., Hydrogels in drug delivery: Progress and challenges. *Polymer* **2008**, *49* (8), 1993-2007.

2. Bhattarai, N.; Gunn, J.; Zhang, M., Chitosan-based hydrogels for controlled, localized drug delivery. *Adv. Drug Deliv. Rev.* **2010**, *62* (1), 83-99.

3. Maia, J.; Ferreira, L.; Carvalho, R.; Ramos, M. A.; Gil, M. H., Synthesis and characterization of new injectable and degradable dextran-based hydrogels. *Polymer* **2005**, *46* (23), 9604-9614.

4. Mehvar, R., Dextrans for targeted and sustained delivery of therapeutic and imaging agents. *J. Control. Release* **2000**, *69* (1), 1-25.

5. Ferreira, L. S.; Gerecht, S.; Fuller, J.; Shieh, H. F.; Vunjak-Novakovic, G.; Langer, R., Bioactive hydrogel scaffolds for controllable vascular differentiation of human embryonic stem cells. *Biomaterials* **2007**, *28* (17), 2706-2717.

6. Möller, S.; Weisser, J.; Bischoff, S.; Schnabelrauch, M., Dextran and hyaluronan methacrylate based hydrogels as matrices for soft tissue reconstruction. *Biomol. Eng.* **2007**, *24* (5), 496-504.

7. Van Tomme, S. R.; Hennink, W. E., Biodegradable dextran hydrogels for protein delivery applications. *Expert Rev. Med. Devices* **2007**, *4* (2), 147-164.

8. Jukes, J. M.; van der Aa, L. J.; Hiemstra, C.; van Veen, T.; Dijkstra, P. J.; Zhong, Z.; Feijen, J.; van Blitterswijk, C. A.; de Boer, J., A newly developed chemically crosslinked dextran-poly(ethylene glycol) hydrogel for cartilage tissue engineering. *Tissue Eng. Part A.* **2010**, *16* (2), 565-573.

9. Augst, A. D.; Kong, H. J.; Mooney, D. J., Alginate hydrogels as biomaterials. *Macromol. Biosci.* **2006**, *6* (8), 623-633.

10. Bouhadir, K. H.; Lee, K. Y.; Alsberg, E.; Damm, K. L.; Anderson, K. W.; Mooney, D. J., Degradation of partially oxidized alginate and its potential application for tissue engineering. *Biotechnol. Prog.* **2001**, *17* (5), 945-950.

11. Jogani, V.; Jinturkar, K.; Vyas, T.; Misra, A., Recent patents review on intranasal administration for CNS drug delivery. *Recent. Pat. Drug Deliv. Formul.* 2008, *2* (1), 25-40.

12. Morris, G.; Kok, S.; Harding, S.; Adams, G., Polysaccharide drug delivery systems based on pectin and chitosan. *Biotechnol. Genet. Eng. Rev.* **2010**, *27*, 257-284.

13. Liu, Z.; Jiao, Y.; Wang, Y.; Zhou, C.; Zhang, Z., Polysaccharides-based nanoparticles as drug delivery systems. *Adv. Drug Deliv. Rev.* **2008**, *60* (15), 1650-1662.

14. Debele, T. A.; Mekuria, S. L.; Tsai, H.-C., Polysaccharide based nanogels in the drug delivery system: Application as the carrier of pharmaceutical agents. *Mater. Sci. Eng. C.* **2016**, *68*, 964-981.

15. Togo, Y.; Takahashi, K.; Saito, K.; Kiso, H.; Huang, B.; Tsukamoto, H.; Hyon, S.-H.; Bessho, K., Aldehyded Dextran and ε-Poly(L-lysine) Hydrogel as Nonviral Gene Carrier. *Stem Cells Int.* **2013**, *2013*, 1-5.

16. Cadee, J. A.; van Luyn, M. J.; Brouwer, L. A.; Plantinga, J. A.; van Wachem, P. B.; de Groot, C. J.; den Otter, W.; Hennink, W. E., In vivo biocompatibility of dextran-based hydrogels. *J. Biomed. Mater. Res.* **2000**, *50* (3), 397-404.

17. Ferreira, L.; Rafael, A.; Lamghari, M.; Barbosa, M. A.; Gil, M. H.; Cabrita, A. M.; Dordick, J. S., Biocompatibility of chemoenzymatically derived dextran-acrylate hydrogels. *J. Biomed. Mater. Res. A.* **2004**, *68* (3), 584-596.

18. Hyon, S.-H.; Nakajima, N.; Sugai, H.; Matsumura, K., Low cytotoxic tissue adhesive based on oxidized dextran and epsilon-poly-l-lysine. *J. Biomed. Mater. Res. A.* **2014**, *102* (8), 2511-2520.

19. Khalikova, E.; Susi, P.; Korpela, T., Microbial Dextran-Hydrolyzing Enzymes: Fundamentals and Applications. *Microbiol. Mol. Biol. Rev.* **2005**, *69* (2), 306-325.

20. Massia, S. P.; Stark, J., Immobilized RGD peptides on surface-grafted dextran promote biospecific cell attachment. *J. Biomed. Mater. Res.* **2001**, *56* (3), 390-399.

21. Levesque, S. G.; Shoichet, M. S., Synthesis of enzyme-degradable, peptide-cross-linked dextran hydrogels. *Bioconjugate chemistry* **2007**, *18* (3), 874-885.

22. Chimpibul, W.; Nagashima, T.; Hayashi, F.; Nakajima, N.; Hyon, S.-H.; Matsumura, K., Dextran oxidized by a malaprade reaction shows main chain scission through a maillard reaction triggered by schiff base formation between aldehydes and amines. *J. Polym. Sci. A.* **2016**, *54* (14), 2254-2260.

23. Kirchhof, S.; Strasser, A.; Wittmann, H.-J.; Messmann, V.; Hammer, N.; Goepferich, A. M.; Brandl, F. P., New insights into the cross-linking and degradation mechanism of Diels-Alder hydrogels. *J. Mater. Chem. B.* **2015**, *3* (3), 449-457.

24. Liu, Z. Q.; Wei, Z.; Zhu, X. L.; Huang, G. Y.; Xu, F.; Yang, J. H.; Osada, Y.; Zrínyi, M.; Li, J. H.; Chen, Y. M., Dextran-based hydrogel formed by thiol-Michael addition reaction for 3D cell encapsulation. *Colloids Surf. B.* **2015**, *128*, 140-148.

25. Li, Q.; Sritharathikhun, P.; Motomizu, S., Development of novel reagent for Hantzsch reaction for the determination of formaldehyde by spectrophotometry and fluorometry. *Anal. Sci.* **2007**, *23* (4), 413-417.

26. Van Dijk-Wolthuis, W. N. E.; Franssen, O.; Talsma, H.; van Steenbergen, M. J.; Kettenes-van den Bosch, J. J.; Hennink, W. E., Synthesis, Characterization, and Polymerization of Glycidyl Methacrylate Derivatized Dextran. *Macromolecules* **1995**, *28* (18), 6317-6322.

27. Reis, A. V.; Fajardo, A. R.; Schuquel, I. T. A.; Guilherme, M. R.; Vidotti, G. J.; Rubira, A. F.; Muniz, E. C., Reaction of Glycidyl Methacrylate at the Hydroxyl and Carboxylic Groups

of Poly(vinyl alcohol) and Poly(acrylic acid): Is This Reaction Mechanism Still Unclear? The *J. Org. Chem.* **2009**, *74* (10), 3750-3757.

28. Barman, S.; Diehl, K. L.; Anslyn, E. V., The effect of alkylation, protonation, and hydroxyl group substitution on reversible alcohol and water addition to 2- and 4-formyl pyridine derivatives. *RSC Adv.* **2014**, *4* (55), 28893-28900.

29. Ouellette, R. J.; Rawn, J. D., *19 - Aldehydes and Ketones: Nucleophilic Addition Reactions*. In Organic Chemistry Study Guide, Elsevier: Boston, **2015**; pp 335-360.

30. Ishak, M. F.; Painter, T. J., Kinetic evidence for hemiacetal formation during the oxidation of dextran in aqueous periodate. *Carbohydr. Res.* **1978**, *64*, 189-197.

31. Liu, Y.; Chan-Park, M. B., Hydrogel based on interpenetrating polymer networks of dextran and gelatin for vascular tissue engineering. *Biomaterials* **2009**, *30* (2), 196-207.

32. Lacroix-Desmazes, P.; Severac, R.; Boutevin, B., Reverse Iodine Transfer Polymerization of Methyl Acrylate and n-Butyl Acrylate. *Macromolecules* **2005**, *38* (15), 6299-6309.

33. Matsumura, K.; Nakajima, N.; Sugai, H.; Hyon, S. H., Self-degradation of tissue adhesive based on oxidized dextran and poly-L-lysine. *Carbohydr. Polym.* **2014**, *113*, 32-38.

34. Shen, S.-C.; Tseng, K.-C.; Wu, J. S.-B., An analysis of Maillard reaction products in ethanolic glucose–glycine solution. *Food Chemistry* **2007**, *102* (1), 281-287.

35. Fife, T. H.; Anderson, E., Thioacetal hydrolysis. Hydrolysis of benzaldehyde methyl S-(substituted phenyl) thioacetals. *J. Am. Chem. Soc.* **1970**, *92* (18), 5464-5468.

36. Sakulsombat, M.; Zhang, Y.; Ramstrom, O., Dynamic asymmetric hemithioacetal transformation by lipase-catalyzed gamma-lactonization: in situ tandem formation of 1,3-oxathiolan-5-one derivatives. *Chemistry* **2012**, *18* (20), 6129-6132.

37. Kyprianou, D.; Guerreiro, A. R.; Nirschl, M.; Chianella, I.; Subrahmanyam, S.; Turner, A. P. F.; Piletsky, S., The application of polythiol molecules for protein immobilisation on sensor surfaces. *Biosens. Bioelectron.* **2010**, *25* (5), 1049-1055.

Chapter 3

Control release of amino source

3.1 Introduction

The design, development, fabrication and application of polymeric biomaterials have been designed and developed for improving human health and quality of life by using in biomedical application such as tissue engineering, artificial organs, regenerative medicine and controlled release system. The polymeric materials have been developed to create the smart, intelligent or stimuli-responsive materials [1,2,3]. There are various stimuli that can affect the alterable properties of smart polymers, such as temperature, pH, enzyme and light [4,5,6]. The thermoresponsive polymers are widely employed as a smart polymers which shows an important characteristic properties of alterable phase transition, occurring when response to a change in temperature [7]. This unique property can reach the smart polymers as on-off switchable control by temperature.

Thermoresponsive polymers are materials that undergo reversible phase transition by responding to an environmental temperature change. Temperature-sensitive hydrogel have gained considerable attention in the pharmaceutical field due to the ability of the hydrogels to swell or de-swell as a result of changing the temperature of the surrounding fluid. The sensitivity to the thermal environment of hydrogel have been used for various proposes, especially on-off release of drugs or other substances when temperature increased from physiological to higher or

decreased to lower. There are various type of polymers which show temperature-sensitive behavior, not only synthetic polymer but some chemical modified natural polymers also.

Poly(*N*-alkyl (meth)acrylamide)s are maybe the most studied temperature-sensitive polymer, particularly, homopolymers and copolymer of PNIPAM which have earned strong attention because of its well defined structure and property specially and its lower critical solution temperature (LCST) is closed to human body and can be improved its structure as well. The LCST polymers compress upon increase in temperature beyond their critical temperature [8]. PNIPAM contains amide (-CONH-) and propyl (-$CH(CH_3)_2$) moieties in the monomer structure which are an important part in response to temperature change. When temperature is low, the hydrophilic amide group is solvated by the water molecules thus their hydrogen bonding results in the structured hydration shell, as a result the polymer is soluble. When the temperature increase, the interactions among the hydrophobic groups (-$CH(CH_3)_2$) become strong because of the weakness of hydrogen bonding, leading to the release of water from the structure [8,9]. Due to the phase transition property, this polymer are more favorable for biomedical purposes which can release the substance at human body temperature or higher. However, PNIPAM possess some disadvantages, such as questionable biocompatibility, phase transition hysteresis, and a significant end group influence on thermal behavior [10,11].

The polypeptides and related artificial poly(amino acid)s have attracted interest recently in the drug delivery applications due to their biodegradability, biocompatibility and unique LCST-like behavior [12,13]. For instance, Elastin-like polypeptides (ELPs) which consist of repeating pentapeptide sequences Val–Pro–Gly–Xaa–Gly, where the guest residue (Xaa) can be any naturally occurring amino acid except proline [14]. These polymers undergo reversible phase transition that can be triggered by temperature. ELPs can be soluble in aqueous solution at low

temperatures but dehydration of the valine side chains took place when getting heat, leading to an aggregation of polypeptides [15]. To vary the transition temperatures of ELPs, the changing of amino acid residues presented in the pentapeptide was allowed. For example, by substitution of more hydrophobic such as oligoalanine and oligoglycine at the fourth position, the point of transition raised up to 40 °C [16]. However, the method to synthesize ELP is usually time consuming and expensive to scale up.

In addition, the natural polymers and their modification have been interested as a temperature-sensitive materials. Cellulose derivatives such as methyl cellulose show reverse thermogelation when an optimum balance of hydrophilic and hydrophobic moieties is established, with the methylcellulose solution gelling upon heating and returning to the liquid state upon cooling [17]. Another temperature sensitive polysaccharide is chitosan which can form a thermosensitive hydrogel when chitosan solution was neutralized with a polyol counterion salt, showing a liquid below room temperature and transformed into a gel at body temperature [18]. This system was successfully employed to deliver biologically-active compounds and applied for tissue engineering application. Kappa-carrageenan (κ-CG) is one kind of temperature sensitive polysaccharide that receiving an attention for pharmaceutical applications, however, this polysaccharide has not been extensively studying. Thus, this research is interested in themoresponsive carrageenan for utilization in the control release of active compounds.

κ-CG is a linear sulphated polysaccharide composed by D-galactose and 3,6 anhydrogalactose units (Figure 3.1) extracted from marine red algae. It shows the ability to form gel, which involves a coil to helix conformational transition followed by helix aggregation (Figure 3.2) [19]. The process to form gel is thermoreversible which can be induced by cooling and encouraged by monovalent cations such as potassium ions. The thermo-sensitive nature of κ-

CG hydrogels makes this biopolymer an interesting candidate for temperature activated drug delivery applications. In addition, the structure of κ-CG contains a lot of hydroxyl groups, providing the possibility for further derivatization and bioconjugation.

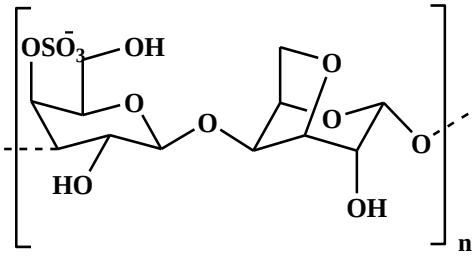

Figure 3.1 Kappa-carrageenan structure.

In this research, κ-CG was used to apply in the development of new carrier formulations because of its gelation properties. The carrageenan chain was funtionalized to create amino-CG derivative and its gelation beads were promote by K^+. The control release of amino groups was reached when amino-CG absorbed suitable heat. The details of this part was descrptied in this chapter.

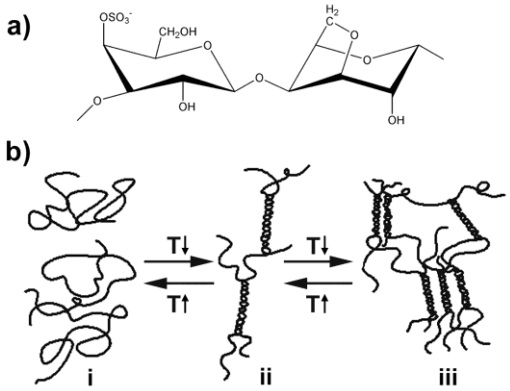

Figure 3.2 (a) The structural disaccharide unit of κ -carrageenan and (b) a schematic representation of the κ-carrageenan gelation mechanism: (i) random coil conformation, (ii) helix conformation, (iii) aggregation of helices. [19]

The external stimuli such as pH, temperature, microbe, γ-irradiation, and light have been developed for triggered the releasing of active substances. Among them, near-infrared (NIR) is especially attractive as it can be remotely applied for a short period of time with on-off switching and temporal precision. To enhance the potential of NIR, deal with NIR photothermal agents has been intensively explored. When exposed to NIR light, the photothermal agents can readily absorb and convert photo energy into thermal energy producing heat, leading to the response of the polymer matrices, realizing the triggered release of entrapped molecules [20]. Large number of light-sensitive materials responding to NIR have been reported recently. Xu et all., 2017 [20] reported polydopamine (PDA) microspheres as a photothermal agent capping with a PNIPAm thermosensitive polymer shell for control release of small pesticide molecules. The entrapped pesticide molecules from the core−shell PDA@PNIPAm nanocomposites was enhanced by increasing temperature under NIR-light irradiation. The hydrogel design relies on loading gold nanorods (AuNRs) in an ABA-type triblock copolymer that is able to undergo the gel to sol phase transition upon light exposure was reported by Zhang et al., 2017 [21]. The NIR light absorption of AuNRs could generate heat that raises the hydrogel temperature above upper critical solution temperature (UCST) and, consequently, the gel-to-sol transition.

In this chapter, the new platform of entrapment material by trapping a photothermal agent with thermo-sensitive polysaccharide, κ-CG and its derivative was created. After trigger by NIR laser the release of active compounds is carried out. Furthermore, the release rate can be controlled by on-off switching of NIR-light irradiation. Thus, the amino-CG was synthesized to provide the dual function of being amino source and showing temperature responsive behavior. The photothermal agent, PDA microspheres, were capped with carrageenan derivative to induce the phase transition when irradiation by NIR for control release of amino groups.

3.2 Material and method

3.2.1 Materials

Kappa-Carrageenan (κ-CG) and dopamine hydrochloride were obtained from TCI (Tokyo, Japan). 3-bromopropylamine hydrobromide was purchased from Sigma Aldrich (St. Louis, MO, USA). Ammonium hydroxide (NH_4OH, 28-30%) was acquired from Kanto Chemical Co. Inc., (Tokyo, Japan). Ethanol and other chemicals were purchased from Nacalai Tesque, Inc., (Kyoto, Japan). All chemicals were used without purification.

3.2.2 Synthesis and characterization of amino-CG

Amino-CG was synthesized by applying the method that reported by Tranquilan-Aranilla et al in 2012 [22]. κ-CG (1 g) was suspended in 10 mL of 80% (w/v) of 2-propanol in a 100 mL of round bottom flask equipped with a reflux cooler, and stirred vigorously at room temperature. NaOH (40%, 1.2 mL) was added dropwise to the mixture and stirring was continued for another 1 h at 40 ◦C. After alkaline activation, 3-bromopropylamine hydrobromide (0.11 to 1.4 g) was added. The reaction was allowed to proceed for 24 h at 40 °C. After the reaction was finished, the mixture was filtered, suspended in 80% (w/v) of 2-propanol (aq), and neutralized with 1 M HCl. The products were collected after filtration, washed several times with 80% (w/v) 2-propanol (aq) followed by pure 2-propanol, freeze-dried for a day, and kept in the refrigerator until use. The synthesized amino-CG was characterized by ^{1}H and ^{13}C NMR, differential scanning calorimetry (DSC), and zeta potential analysis.

FTIR analysis was conducted using FT/IR-4200 spectrophotometer in the range of 4000-600 cm^{-1} to investigate the functional groups of synthesized product. To confirm the structure of

products, ^{1}H NMR and ^{13}C NMR spectra were collected using a Bruker 400 MHz NMR spectrophotometer after dissolving the sample in D_2O.

The zeta potential was determined using a Zetasizer Nana-ZS (Malvern Instruments, UK) instrument. The samples were diluted to 0.1% (w/v) with DI water at pH 7. Three zeta potential measurements were taken for each sample.

DSC (Seiko SII Exstar6000) was used to determine the thermal transition of modified samples. The experiment was done under N_2 gas atmosphere from 35 to 150 °C at a heating rate of 10 °C/min.

3.2.3 Determination of amino content

2,4,6-Trinitrobenzene sulfonic acid (TNBS) is a rapid and sensitive assay reagent for quantitative determination of amino groups [23]. In brief, 1 mL of standard glycine (0–25 µg/mL) or analysis sample was added to 1 mL of 4% (w/v) $NaHCO_3$ (pH 8.5) and 1 mL of 0.1% (w/v) TNBS in water. The solution was then incubated at 40 °C in the dark for 2 h. After that, 1 mL of 10% (w/v) of SDS and 0.5 mL of 1 M HCl were added to each sample solution. The absorbance of the solution at 335 nm was read. A curve was generated using the measurement from standard samples, and used to determine the concentration in the analysis sample.

3.2.4 Synthesis and characterization of polydopamine (PDA) microspheres

PDA microspheres were synthesized by using a previously reported [20]. Dopamine hydrochloride (0.3 g) was dissolved in 5 mL of DI water. The prepared solution was slowly added to a mixture of 28−30% NH_4OH (1 mL), ethanol (20 mL), and DI water (45 mL). The reaction was allowed to proceed for 12 h at room temperature under mild magnetic stirring. Subsequently,

the prepared PDA microspheres were collected by centrifugation and washed with DI water several times. The synthesized products were dried and characterized.

The functional groups in the products were confirmed using a FT/IR-4200 spectrophotometer in 4000–600 cm^{-1}. The surface morphologies were observed by a Hitachi S-4100 SEM and a Hitachi H-7100 TEM systems. UV-vis spectra were obtained using a UV-1800 spectophotometer.

3.2.5 Preparation of amino-CG@PDA microcomposite beads

Concentrated κ-CG or amino-CG solutions in distilled water were prepared by heating the dispersion at 60 °C with constant stirring to obtain homogeneous solutions (2, 3, and 4% (w/v)). After that, 0.02% (w/v) of PDA microspheres were suspended into each of solution. The beads were prepared using an ionotropic gelation method. Briefly, 5 mL of the heated amino-CG solution was extruded dropwise through a syringe needle (0.838 mm of inner diameter) into 50 mL of KCl solution. The beads were allowed to harden for 30 min in KCl cross-linking solution. The gel beads were filtered, washed with DI water 3 times, and freeze dried until constant weight was achieved. The CG@PDA and amino-CG@PDA were obtained. Different types of processing parameters were varied; the polysaccharide concentration (2, 3 or 4% (w/v)), and the KCl concentration (5% or 10% (w/v)).

3.2.6 Swelling study

Water uptake of the prepared beads is defined as the weight percent with respect to that of the dried beads. To measure the swelling ratio of amino-CG@PDA, dried samples were weighted (W_{dry}) and immersed in PBS at 37 °C (or 40 °C) for different periods of time. The wet samples were carefully blotted with filter paper to absorb the

excess water, and then weighted again (W_{wet}). The water uptake is defined by the following equation (1):

$$\text{Water uptake (\%)} = [(W_{wet}-W_{dry})/W_{dry}] \times 100 \quad (1)$$

In this study, we used two temperatures (37 and 40 °C) to find the suitable condition to prepare amino-CG@PDA microcomposite that is stable at 37 °C but undergoes gel-to-sol phase transition at 40 °C. Beads prepared under this condition will be further used to prepare the NIR-induced temperature-responsive microcomposite.

3.2.7 Temperature and light-responsive amino releasing test

To evaluate thermoresponsive amino release, amino-CG@PDA microcomposites were suspended in PBS and incubate at 37 °C or 40 °C for 24 h. At different time intervals, the suspension was collected for the amino quantification. For NIR trigged amino release, the suspension of amino-CG@PDA was exposed to the 808 nm NIR light (at a power density of 1 W/cm^2) for 30 min at different time point (0.5, 1.5, 2.5, 3.5, and 4.5 h One milliliter of the supernatant was collected at each predetermined time to analyze the amino group amount by TNBS assay. Then, the sample was re-dispersed for further irradiation. A suspension incubated in dark condition was used as a negative control. The cumulative amount of amino-CG released from the composite beads was calculated according to the following equation (2):

$$\text{Amino release efficiency (\%)} = (W_t/W_i) \times 100 \quad (2)$$

Where W_i and W_t are the amino content in the obtained microcomposites at equilibrium state and released from the loaded nanocomposites at time t during the release process, respectively.

3.3 Results and discussion

3.3.1 Synthesis and characterization of amino-CG

The amino-CG was synthesized in a simple reaction as shown in Figure 3.3. The κ-CG was activated by NaOH and the varied amount of 3-bromopropylamine hydrobromide was then added to form amino-derivatized carrageenan with various degree of substitution (DS). The ^{1}H and ^{13}C NMR spectra of κ-CG and modified CG are shown in Figures 3.4A and 3.4B, respectively. The disaccharide polymer κ-CG contains 3-linked β-D-galactopyranose (G unit) and 4-linked 3,6-anhydro-α-D-galactopyranose (DA unit) as a repeating unit which showed the ^{1}H chemical shifts in Figure 3.4A-b [24]. In the spectrum for amino-CG (Figure 3.4A-c), new proton peaks appeared at the chemical shift of 2.25–3.20 ppm, possibly due to the mixing of shifted chemical shift of the methylene protons in the propylamine and that of amino proton of amino-CG. The proton decoupled ^{13}C NMR analyses gave more information on the structural properties of amino-CG derivatives. The spectrum of untreated κ-CG (Figure 3.4B-a) shows strong signals of the twelve carbon atoms in the disaccharide repeating unit [24,22]. New signals were present in the amino-CG spectrum (Figure 3.4B-b), namely additional resonances at the chemical shifts of 31.05 and 30.08 ppm, which were assigned to the methylene carbon from propylamine substitution. The intensities of the new signals are very weak due to the low amount of DS.

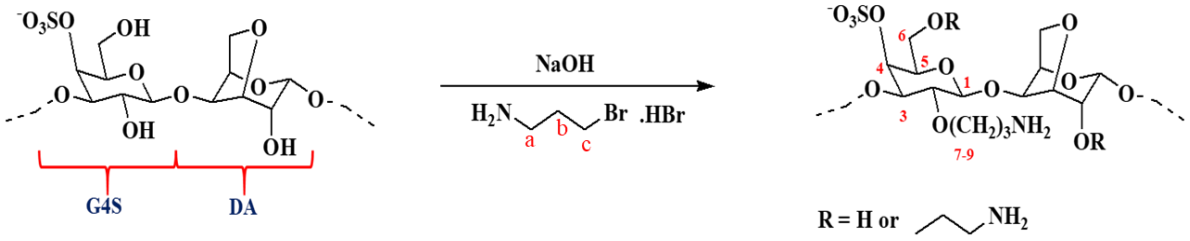

Figure 3.3 Schematic presentation of the synthesis of amino-CG.

A

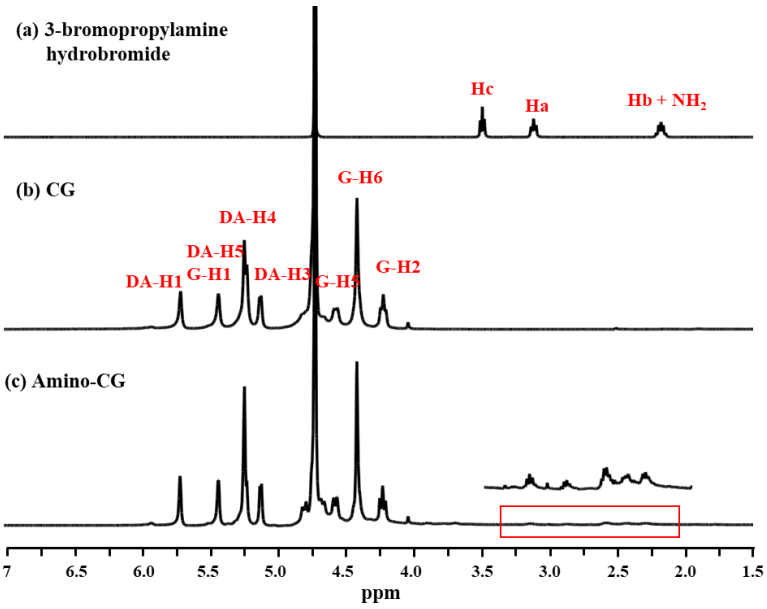

B

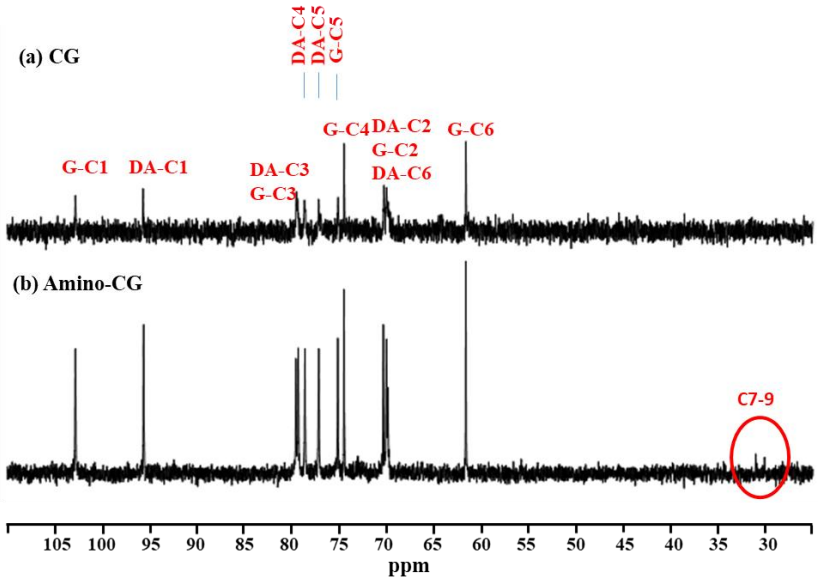

Figure 3.4 (A) ^{1}H NMR spectra of 3 bromopropylamine hydrobomide (a), original κ-CG (b) and amino-CG (c). (B) ^{13}C NMR spectra of original κ-CG (a) and amino-CG (b).

The FTIR characteristic signals of product was depicted in Figure 3.5, in the κ-CG, the band at 850 cm^{-1} and 1227 cm^{-1} were attributed to vibration of O=S=O and to $–O–SO_3$ stretching at C-4 of β-D-galactose residue (G4S), respectively. The signal at 927 cm^{-1} was related to the C-O-C vibration of the 3,6-anhydro-D-galactose residue (DA) [25,22]. The sharp peak at 1641 cm^{-1} was assigned to the structural water deformation band [26]. In the spectrum of amino-CG, it showed the new band of N-H bond of 1° amine at 1563 cm^{-1} but the intensity was very weak because the %DS was very low. The %DS was calculated from the number of amines contained within amino-CG sample which experimented using a rapid and sensitive assay reagent, TNBS [23]. Table 3.1 presented the different % DS when addition various amount of 3-bromopropylamine hydrobromide into 1 g κ-CG. Thus, the amino-CG with 0.87 %DS was used in the further experiment.

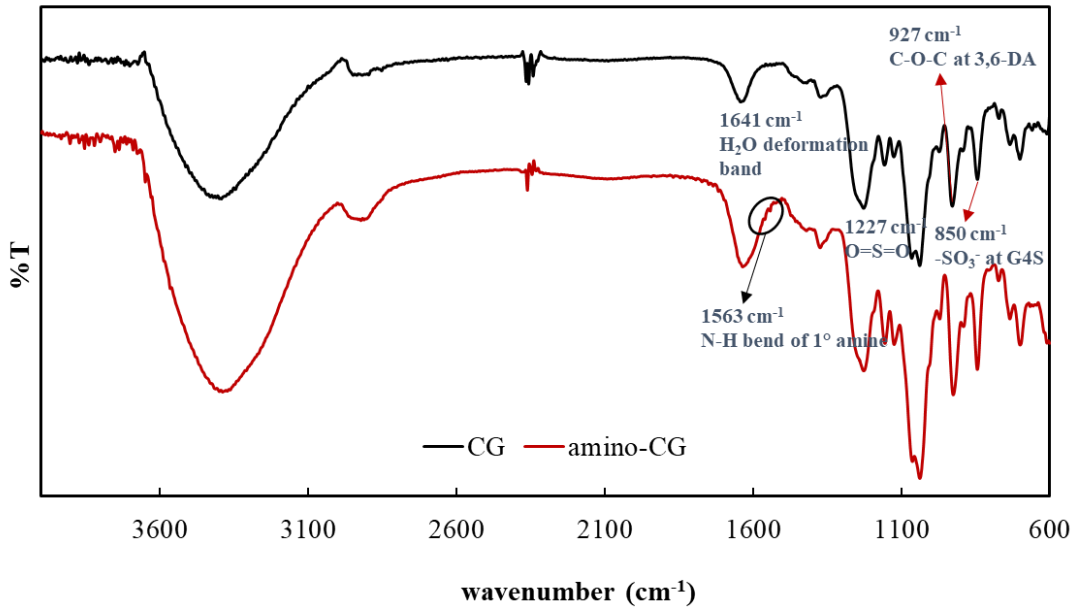

Figure 3.5 FTIR spectra of untreated κ-CG (black line) and amino-CG (red line).

Table 3.1 %DS of $–NH_2$ when varying the added amount of 3-bromopropylamine hydrobromide into 1 g of κ-CG

g of 3-bromopropylamine hydrobromide/1 g of κ-CG	**%DS**
0.11	Cannot detect $–NH_2$
0.55	0.87
0.80	0.9
1.36	Cannot dissolve

The charge of polysaccharide is reflected by the zeta potential of the solution, determined as the electrical potential produced around the surface of particles dispersed in solvent. The zeta potential results can help to confirm the synthesized product (Table 3.2 and Figure 3.6). The negative zeta potential of -58.6 ± 0.8 mV in the original κ-CG can be explained by the anionic structure which contains $–SO_3^-$ groups. However, the functionalized amino-CG showed a relatively higher zeta potential (-37.3 ± 1.4 mV), because the functionalized amino groups carry positive charge to partially neutralize the high negative value of unmodified κ-CG. Consequently, a higher zeta potential was observed.

Table 3.2 The zeta potential of κ-CG and amino-CG

Polysaccharide solution	**Zeta potential (mV)**
κ-CG	-58.6 ± 0.8
amino-CG (0.87% DS)	-37.3 ± 1.4

* Concentration of the polysaccharides was 1 mg/ml;

**average of three measurements at 25°C

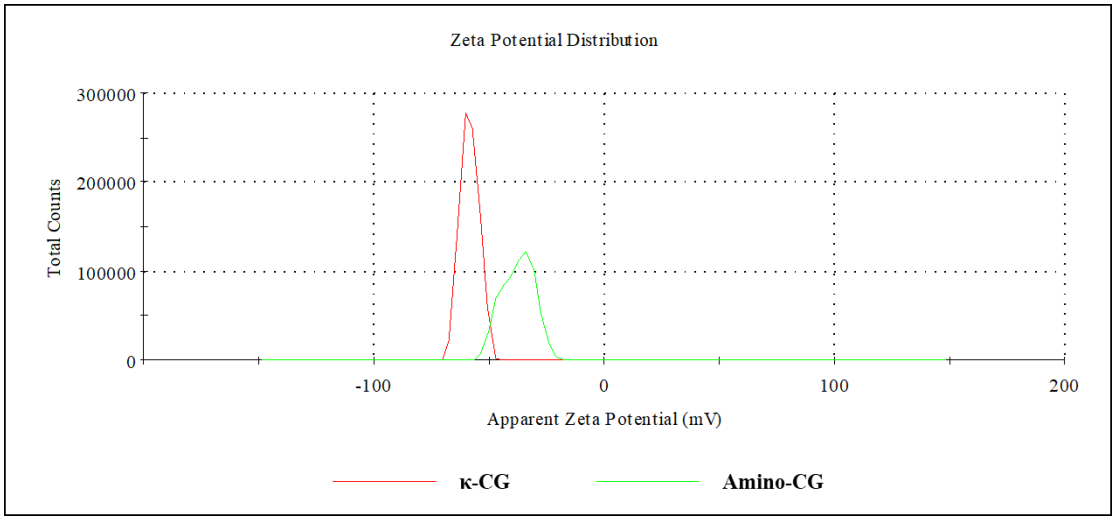

Figure 3.6 Zeta potential distribution of κ-CG and amino-CG.

The thermal analysis results also supported the successful synthesis of amino-CG. Figure 3.7 showed DSC thermograms of pure CG and amino-CG for detecting the glass transition temperature (T_g). The T_g of amino-CG was 102.2 °C whereas that of CG was lower (70.7 °C), because in amino-CG the intra- and/or intermolecular interaction is enhanced by the methylene groups [27, 28]. Consequently, restricted segments of polymer chains were formed, and hence it

takes more energy to break the bonds. All these results confirmed the successful modification of κ-CG with amino groups.

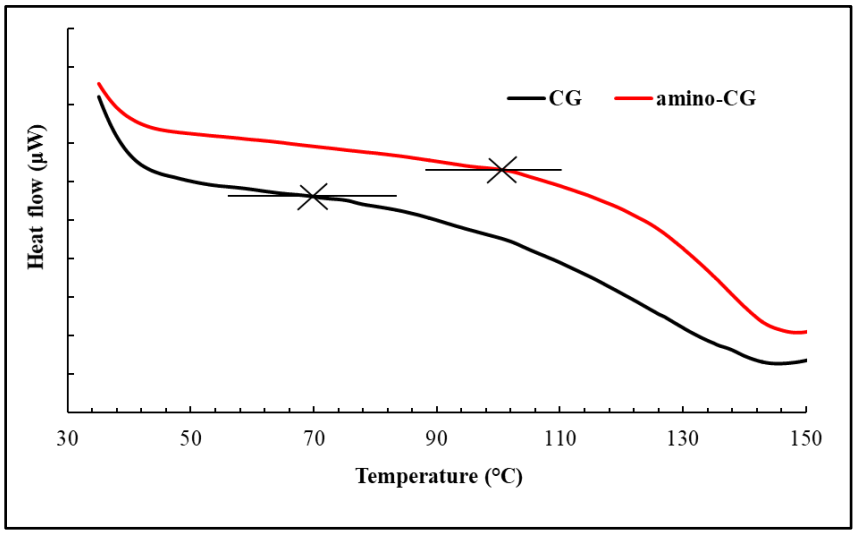

Figure 3.7 DSC thermograms of κ-CG and amino-CG.

3.3.2 Synthesis and characterization of PDA microspheres

This study reports a delivery system based on amino groups using NIR light and temperature for remote triggering, using PDA as a photothermal agent. The synthesis of PDA is presented in Figure 3.8, where the dopamine monomer was oxidized and then cyclized to form dopaminechrome in a mixture of water, ethanol, and ammonia. After that, the molecular structure of dopaminechrome was rearranged to produce an 5,6-dihydroxyindole intermediate, which further formed PDA microspheres by intermolecular polymerization (which is clearly seen by the solution color change from pale to dark brown).

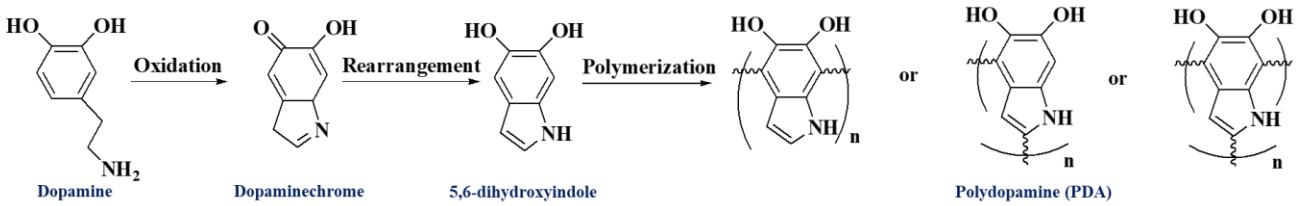

Figure 3.8 Schematic presentation of the production of PDA.

To verify the successfully synthesized PDA microspheres, SEM and TEM images were manipulated to characterize the product. Figure 3.9, SEM observation of the obtained PDA microspheres indicated that PDA microspheres had regular spherical structure with an average size range of 150-300 nm (Figure 3.9a,b) and showed good dispersibility. Moreover, TEM image confirmed the synthesized product, presenting the uniform spherical shape of PDA microspheres (Figure 3.9c).

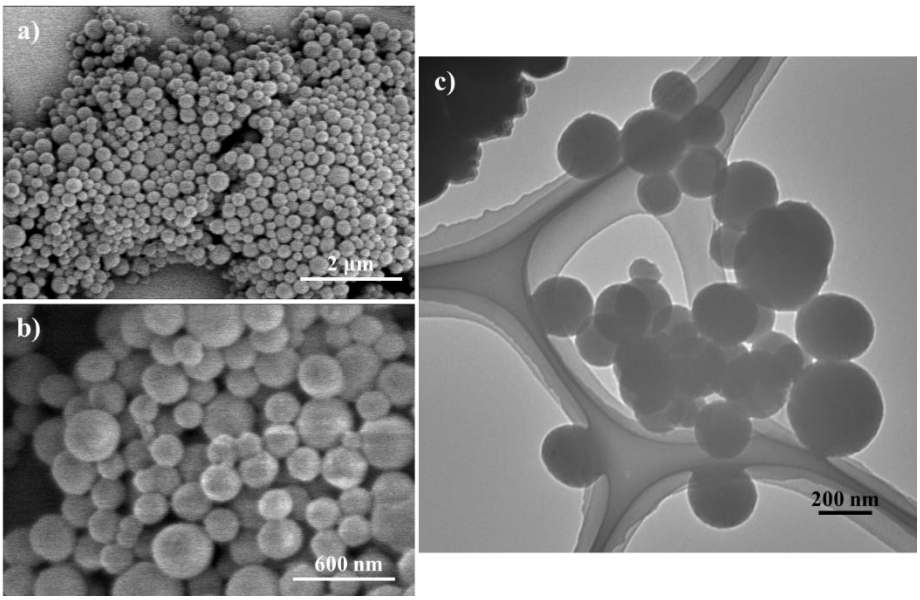

Figure 3.9 SEM images of the PDA microspheres (a (15k magnification) and b (50 k magnification)) and TEM image of the PDA microspheres (c).

The chemical composition of free dopamine and PDA were characterized by FTIR spectrometry. Unlike pure dopamine, the FTIR spectrum of PDA showed absorption bands at 1520 and 1615 cm^{-1}, corresponding to the vibration of N−H in the aromatic rings. The signal at 3265 cm^{-1} revealed the existence of –OH groups in 1,2-dihydroxybenzene or catechol (Figure 3.10a) [29]. In the UV-Vis spectra (Figure 3.10b), characteristic absorption peak of free dopamine was observed at 280 nm [20]. The curves of dopamine and PDA were dissimilar. PDA showed an absorption ranging from UV to NIR in wavelength, due to the oxidation of dopamine into dopaminechrome and dihydroxyindole, which subsequently self-polymerized [30]. A change in the solution color from colorless to deep brown was detected (the inset image of Figure 3.10b), suggesting the successful synthesis of polydopamine, which can function as a photothermal agent in the NIR range.

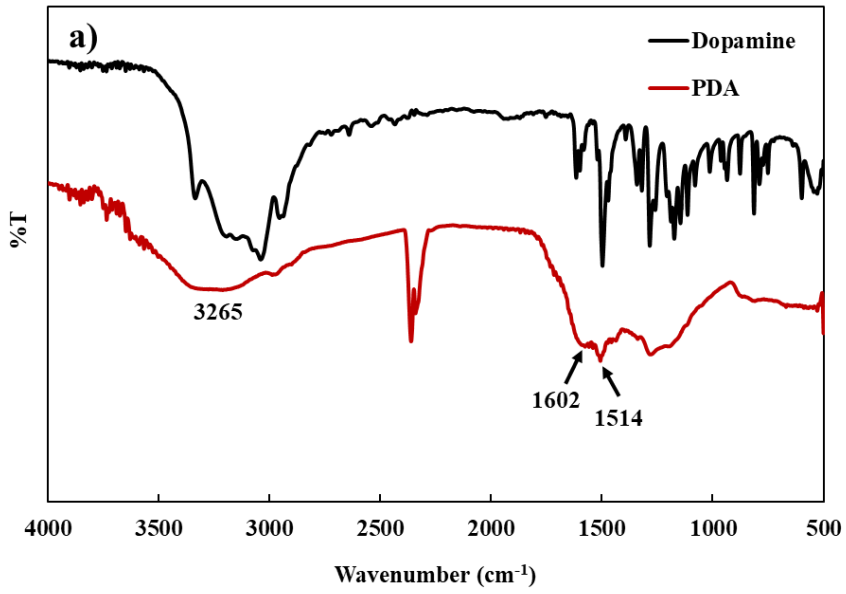

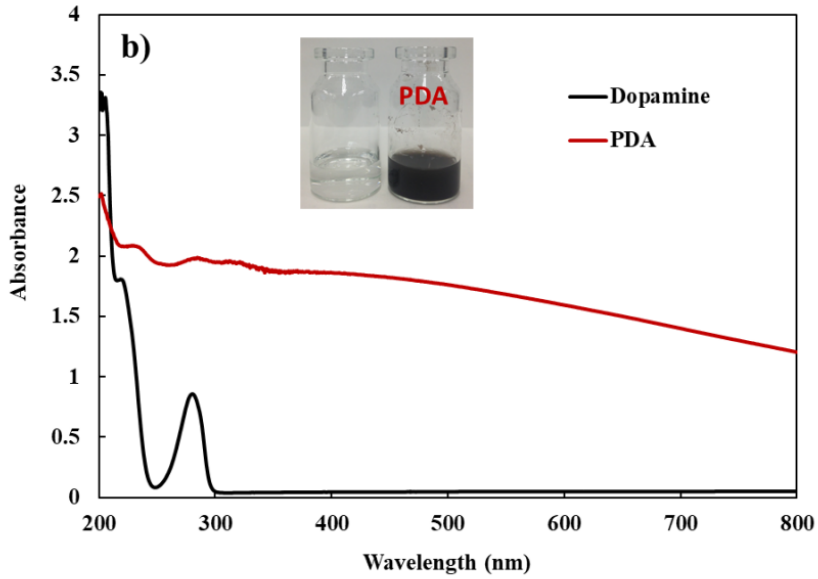

Figure 3.10 FT-IR spectrometry analysis (a) and UV−vis spectra of dopamine and PDA (b).

3.3.3 Amino-CG@PDA beads preparation and characterization

The PDA@amino-CG microcomposite can be easily prepared by using an ionotropic gelation method. κ-CG is an anionic polyelectrolyte hydrogel due to its sulfate groups. In aqueous solutions and in the presence of cations such as K^+, Na^+, or Ca^{2+}, κ-CG easily forms thermoreversible gels. In this process, there is an initial coiling to produce the helical conformation, and then the helices aggregate to form infinite networks [31, 32]. The cations can induce conformational changes in the polymer [33]. Due to the instantaneous nature of such ionic gelation, drugs, enzymes, and other substances can be encapsulated in carrageenan. In this study, a κ-CG derivative, amino-CG, was used for encapsulation of PDA microspheres in the presence of K^+ to form thermoreversible gel. SEM allows the investigation of the morphology of dried beads samples which showed in Figure 3.11 and 3.12. It was observed that samples produced by

κ-CG display spherical form showing that SEM image of pure carrageenan (Figure 3.11a-c) provides a smoother surface compared to the CG@PDA (Figure 3.11d-f) which showed a rough surface morphology since the PDA microspheres prevented the carrageenan chains from approaching each other. These results are similar to the SEM images from the beads prepared from amino-CG showing that the higher roughness of outer surface is presented in amino-CG@PDA (Figure 3.12d-f).

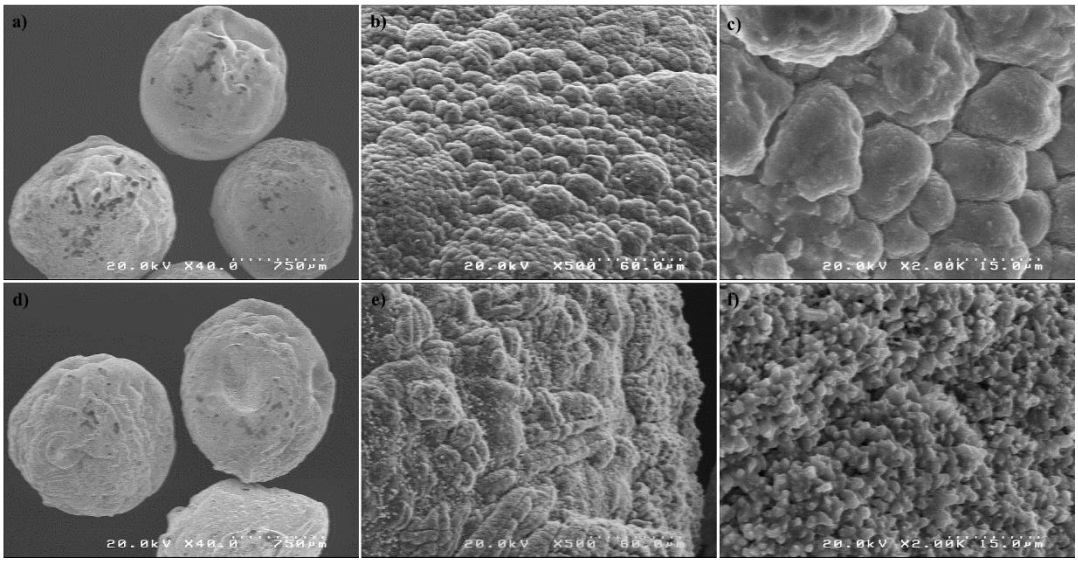

Figure 3.11 SEM image of 4% κ-CG (a-c) and 4% κ-CG@PDA (d-f) prepared with 5% KCl.

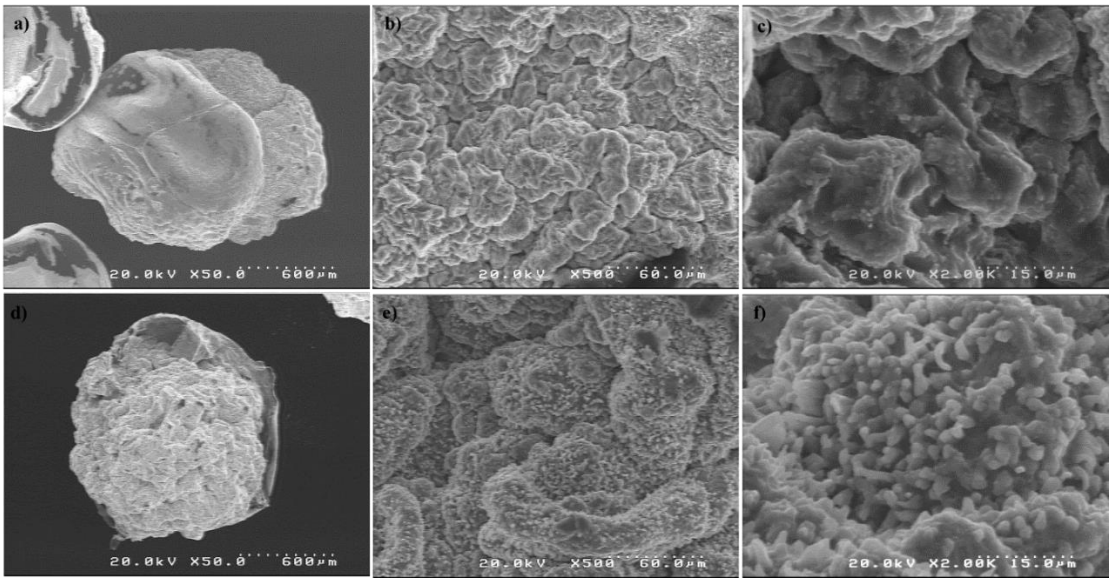

Figure 3.12 SEM images of 4% amino-CG (a-c) and 4% amino-CG@PDA (d-f) prepared with 5% KCl.

Water uptake is an important property in release studies. The swelling of hydrogel promotes the release of substances, because water molecules penetrate the structure of dry hydrogel and boost the relaxation of chains. This increases the pore size of porous hydrogel for the release of drugs or other target substances [34, 35]. In case of thermorevesible hydrogel, the strategy that I seek to develop the release molecule after swelling was being stable at body temperature (37 °C) but allowed the temperature-sensitive hydrogel to dissolve after reach to a desirable temperature. Thus, the water uptake of CG@PDA and amino-CG@PDA beads at 37 and 40 °C in PBS as the immersion solution was studied (Figure 3.13a and b). The different types of processing parameters; the polysaccharide concentration (2, 3 or 4% (w/v)), and the KCl concentration (5% or 10% (w/v)) affected the swelling ratio, due to the changing of gel charges and network density. From the swelling ratio in Figure 3.13, an initial burst of quick water

penetration occurred within the first 3 h at both temperatures. The higher of crosslinking beads prepared with 10% KCl (dash lines) provides a lower swelling ratio compared to the gel beads hardened in 5% KCl (solid lines). Higher concentration of KCl contains more K^+ to crosslink with SO_3^- on carrageenan backbone, resulting in high crosslinking degree. Focusing on Figure 3.13a, the thermoreversible gel beads samples can be stable at 37 °C with constant swelling ratio after 10 h, except 2% and 3% of amino-CG@PDA beads prepared with 5% KCl which demonstrated the dissolving within 5 h. Beads rapidly dissolve, because the $–SO_3^-$ contents are lower than 4% amino-CG@PDA beads prepared with 5% KCl, providing low ionic crosslink. The water uptake of beads samples at 40 °C displays in Figure 3.13b. I did not observe the dissolving of the beads prepared from all concentration of κ-CG and KCl. However, the water uptake of 2% κ-CG beads (5% KCl crosslinking) at 40 °C was 1/3 time lower than that of 37 °C because its low crosslink degree maybe enhanced some parts of beads to dissolve when more water was penetrated at high temperature. In addition, besides 2% and 3% of amino-CG@PDA beads prepared with 5% KCl, the 4% amino-CG@PDA thermoreversible gel bead with 5% KCl allowed to dissolve at 40 °C incubation within 5 h but the amino-CG@PDA beads prepared with 10% KCl were still remaining. Thus, a thermoreversible 4% amino-CG@PDA prepared with 5% KCl was selected for further experiments, since it formed stable swelling beads at body temperature and became a liquid at 40 °C.

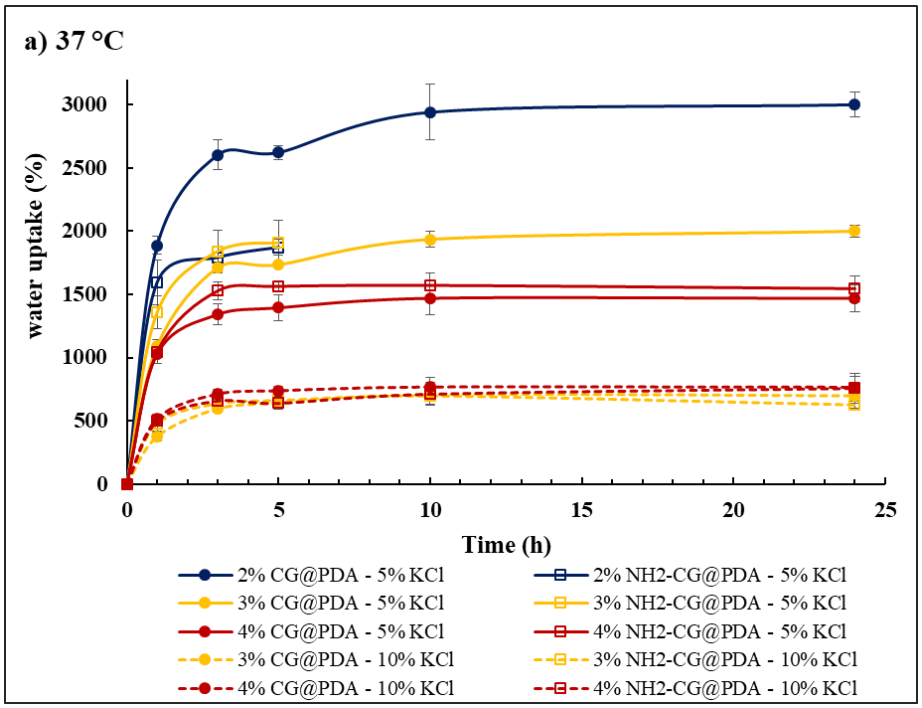

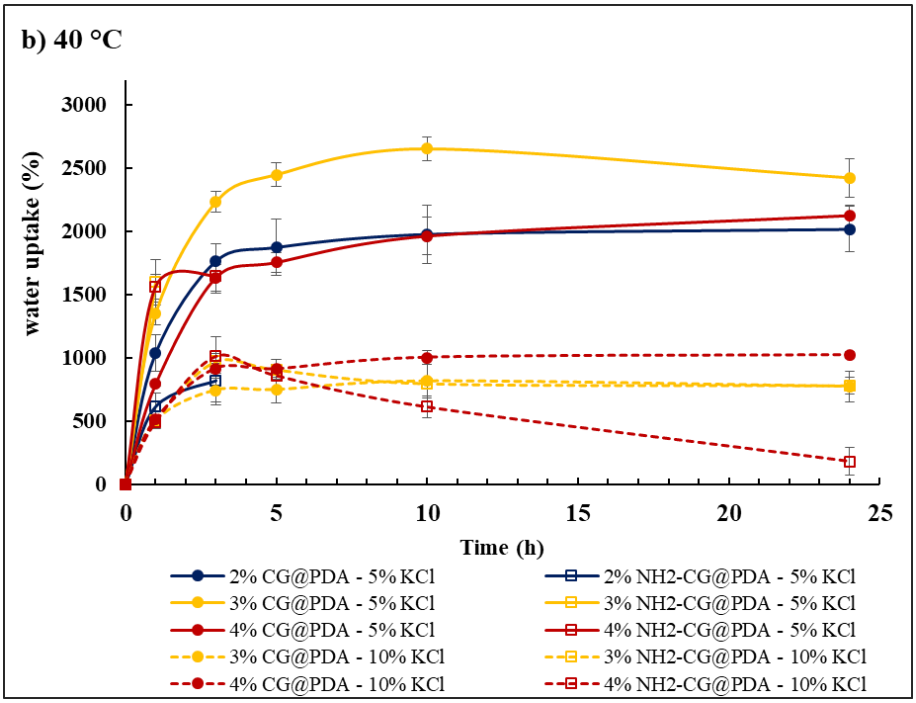

Figure 3.13 Water uptake studies for different formulation of beads at 37 °C (a) and 40 °C (b).

3.3.4 Temperature responsive amino release test

In this study, the hydrogel beads of 4% amino-CG@PDA crosslinked with 5% KCl were chosen for use in thermo-sensitive sol-gel transition. Since the driving force for dissolving the amino-CG should be controlled precisely by small temperature changes, the supernatant amino group concentration is plotted in Figure 3.14 after immersing amino-CG@PDA in PBS at 37 or 40 ℃. As shown in Figure 3.14, the amount of released amino group was negligible at 37 ℃, since at this temperature the beads just swelled without dissolution. In comparison, the amino release was much faster at 40 ℃, up to 70% after 5 h and 100% at around 10 h. Under this higher temperature, the gel dissolved into a sol after reaching swelling equilibrium. These results agree with the swelling behavior studies. It exhibits that the 4% amino-CG@PDA thermoreversible gel beads could dissolve at 40 ℃ incubation within 5 h, while it can remain stable at 37 ℃ with a constant swelling ratio after 10 h. To sum up, the beads prepared by 4% amino-CG@PDA crosslinked with 5% KCl indeed showed a thermosensitive releasing capability, and the release behavior could be easily managed via controlling the environment temperature.

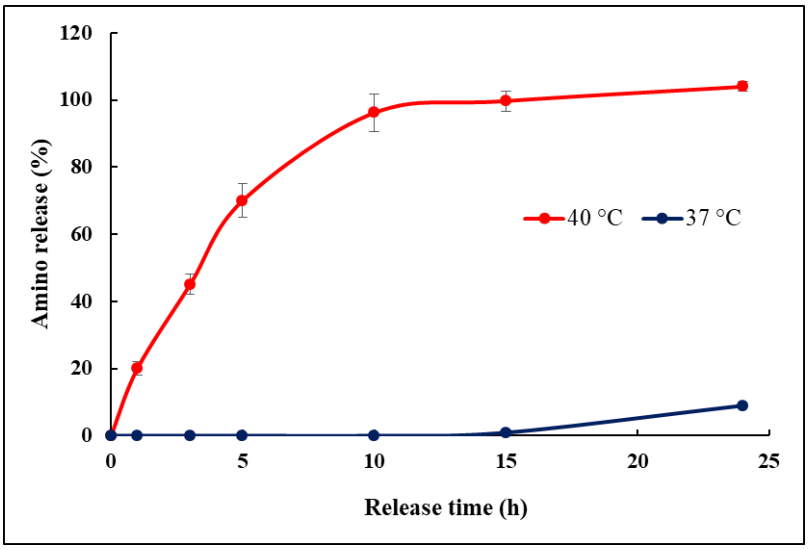

Figure 3.14 Release profiles of 4% amino-CG@PDA microcomposites prepared with 5% KCl under direct heating to various temperatures (37 and 40 °C) for different periods of time.

3.3.5 NIR light-responsive amino release test

In the temperature-responsive release test, the amino-CG@PDA is sensitive to high temperature above the body temperature. To further confirm the ability of external stimulus (NIR light) to trigger the amino-CG release, amino-CG@PDA microcomposites were exposed to NIR light irradiation, and the cumulative amino release was evaluated by using a UV−vis spectrophotometer. As plotted in Figure 3.15A, the amino-CG release was negligible in the absence of NIR light. When the NIR light was turned on, the temperature of the suspension increased to 42 °C as shown in in Figure 3.15B, and thus the amino release was greatly enhanced. When the external trigger (NIR light) was turned off, a slower release was observed. For example, the measured cumulative release of amino groups was 40.14% after 30 min of NIR irradiation. After the light was turned off, the release increased by another ~20% within 30 min

later (to 59.68%). Either with or without NIR light, the release of amino groups gradually increased after 2 h. The reason is the prominent gel-to-sol phase transition of amino-CG@PDA gel beads when the PDA converted NIR light to heat, leading to the re-dissolution of amino-CG chain. As a result, the encapsulated PDA microspheres were liberated and dispersed in the solution. Now, with less encapsulated PDA in the amino-CG@PDA microcomposites during the subsequent irradiation, the temperature of the suspension clearly decreased in the third cycle of irradiation to 38 °C, leading to less amino compounds being released. This amino release pattern occurred periodically, suggesting that the amino-CG@PDA beads possess the continuous photothermal-responsive ability, and that the release rate of amino compounds can be controlled by switching NIR-light irradiation.

A

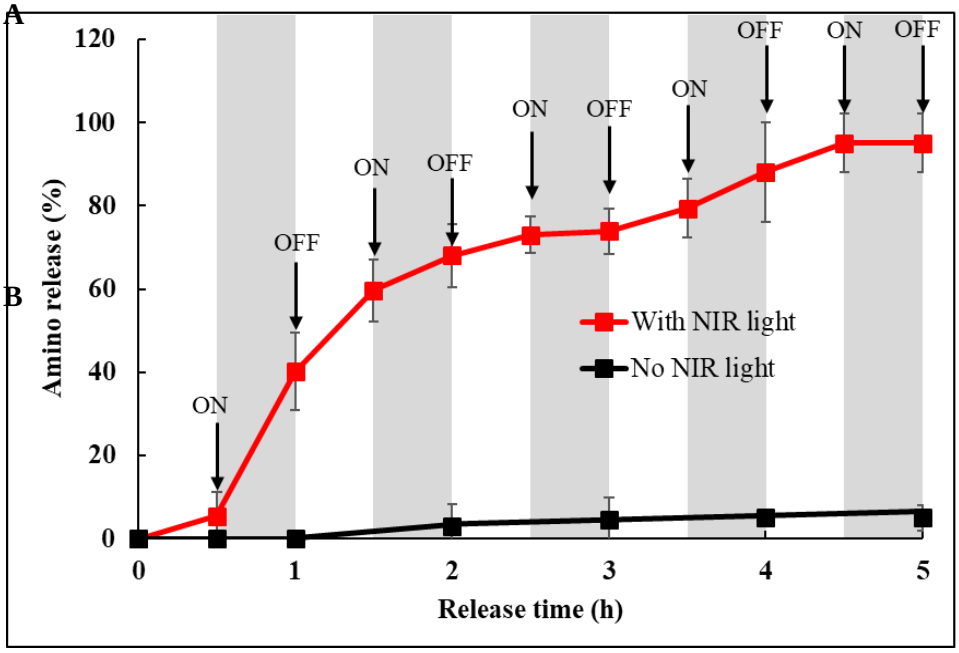

B

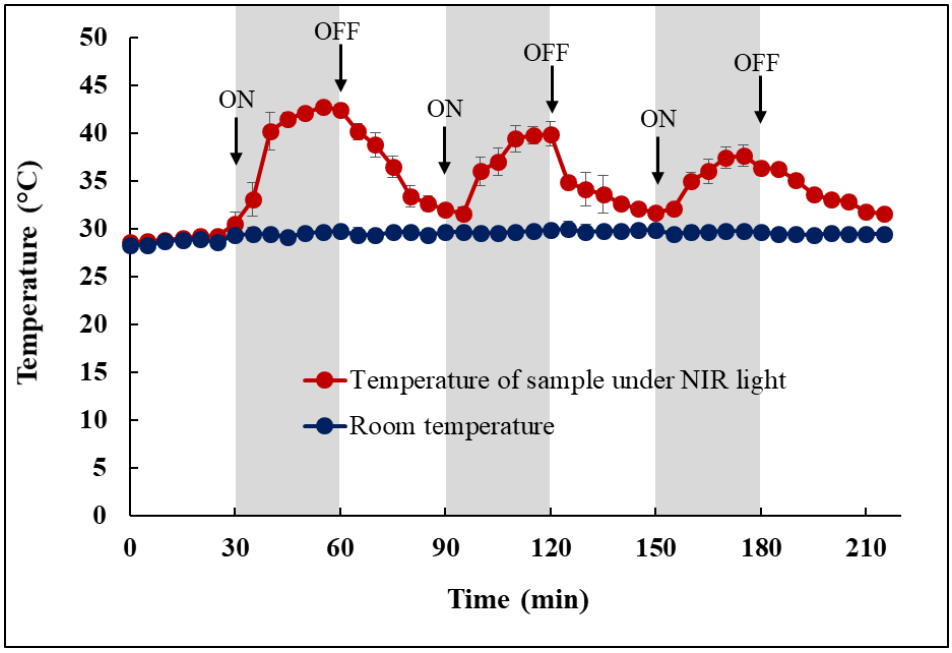

Figure 3.15 (A) Cumulative release profiles of amino compound from amino-CG@PDA microcomposites with and without NIR-light irradiation. (B) Time course of temperature profile of the suspension containing amino-CG@PDA microcomposites in the light-to-heat conversion experiment under NIR irradiation.

3.4 Conclusions

In summary, I fabricated novel amino-CG@PDA microcomposites that can be used as an NIR light-controlled release-targeted system for amino groups via gel-to-sol phase transition. The environmental temperature and external NIR irradiation have an obvious influence in photothermal-responsive release property. The release of amino groups from the phase transition of amino-CG@PDA microcomposites was enhanced by increasing temperature and more greatly under NIR-light irradiation. Thus, the photothermal-responsive behavior of carrageenan derivatives has very broad applicability in biomedical field. To create the new platform of control drug release, the combination of photothermal-sensitive material (amino-CG@PDA gel beads) and hydrogel was conducted. The detail of the temperature responsive drug release by using this system was descripted in chapter 4.

References

1. Roy, D.; Brooks, W. L. A.; Sumerlin, B. S., New directions in thermoresponsive polymers. *Chemical Society Reviews* **2013**, *42* (17), 7214-7243.

2. Liu, J.; Detrembleur, C.; Mornet, S.; Jerome, C.; Duguet, E., Design of hybrid nanovehicles for remotely triggered drug release: an overview. *Journal of Materials Chemistry B* **2015**, *3* (30), 6117-6147.

3. Hardy, J. G.; Palma, M.; Wind, S. J.; Biggs, M. J., Responsive Biomaterials: Advances in Materials Based on Shape-Memory Polymers. *Advanced materials* **2016**, *28* (27), 5717-5724.

4. Jochum, F. D.; Theato, P., Temperature- and light-responsive smart polymer materials. *Chemical Society Reviews* **2013**, *42* (17), 7468-7483.

5. Schmaljohann, D., Thermo- and pH-responsive polymers in drug delivery. *Advanced Drug Delivery Reviews* **2006,** *58* (15), 1655-1670.

6. Thornton, P. D.; Mart, R. J.; Webb, S. J.; Ulijn, R. V., Enzyme-responsive hydrogel particles for the controlled release of proteins: designing peptide actuators to match payload. *Soft Matter* **2008**, *4* (4), 821-827.

7. Hoffman, A. S., Stimuli-responsive polymers: Biomedical applications and challenges for clinical translation. *Advanced Drug Delivery Reviews* **2013**, *65* (1), 10-16.

8. Haq, M. A.; Su, Y.; Wang, D., Mechanical properties of PNIPAM based hydrogels: A review. *Materials science & engineering. C* **2017**, *70* (1), 842-855.

9. Yan, L.; Zhu, Q.; U. Kenkare, P., Lower critical solution temperature of linear PNIPA obtained from a Yukawa potential of polymer chains. *Jounal of Applied polymer Science* **2000**, *78* (11), 1971-1976.

10. Wang, X.; Qiu, X.; Wu, C., Comparison of the Coil-to-Globule and the Globule-to-Coil Transitions of a Single Poly(N-isopropylacrylamide) Homopolymer Chain in Water. *Macromolecules* **1998**, *31* (9), 2972-2976.

11. Kujawa, P.; Segui, F.; Shaban, S.; Diab, C.; Okada, Y.; Tanaka, F.; Winnik, F. M., Impact of End-Group Association and Main-Chain Hydration on the Thermosensitive Properties of Hydrophobically Modified Telechelic Poly(N-isopropylacrylamides) in Water. *Macromolecules* **2006**, *39* (1), 341-348.

12. Haider, M.; Megeed, Z.; Ghandehari, H., Genetically engineered polymers: status and prospects for controlled release. *Journal of Controlled Release* **2004**, *95* (1), 1-26.

13. Furgeson, D. Y.; Dreher, M. R.; Chilkoti, A., Structural optimization of a "smart" doxorubicin–polypeptide conjugate for thermally targeted delivery to solid tumors. *Journal of Controlled Release* **2006**, *110* (2), 362-369.

14. Kowalczyk, T.; Hnatuszko-Konka, K.; Gerszberg, A.; Kononowicz, A. K., Elastin-like polypeptides as a promising family of genetically-engineered protein based polymers. *World journal of microbiology & biotechnology* **2014**, *30* (8), 2141-2152.

15. Li, B.; Alonso, D. O. V.; Bennion, B. J.; Daggett, V., Hydrophobic Hydration Is an Important Source of Elasticity in Elastin-Based Biopolymers. *Journal of the American Chemical Society* **2001**, *123* (48), 11991-11998.

16. Meyer, D. E.; Shin, B. C.; Kong, G. A.; Dewhirst, M. W.; Chilkoti, A., Drug targeting using thermally responsive polymers and local hyperthermia. *Journal of Controlled Release* **2001**, *74* (1), 213-224.

17. Li, L.; Thangamathesvaran, P. M.; Yue, C. Y.; Tam, K. C.; Hu, X.; Lam, Y. C., Gel Network Structure of Methylcellulose in Water. *Langmuir* **2001,** *17* (26), 8062-8068.

18. Chenite, A.; Chaput, C.; Wang, D.; Combes, C.; Buschmann, M. D.; Hoemann, C. D.; Leroux, J. C.; Atkinson, B. L.; Binette, F.; Selmani, A., Novel injectable neutral solutions of chitosan form biodegradable gels in situ. *Biomaterials* **2000**, *21* (21), 2155-2161.

19. Daniel-da-Silva, A. L.; Ferreira, L.; Gil, A. M.; Trindade, T., Synthesis and swelling behavior of temperature responsive κ-carrageenan nanogels. *Journal of Colloid and Interface Science* **2011**, *355* (2), 512-517.

20. Xu, X.; Bai, B.; Wang, H.; Suo, Y., A Near-Infrared and Temperature-Responsive Pesticide Release Platform through Core–Shell Polydopamine@PNIPAm Nanocomposites. *ACS Applied Materials & Interfaces* **2017**, *9* (7), 6424-6432.

21. Zhang, H.; Guo, S.; Fu, S.; Zhao, Y., A Near-Infrared Light-Responsive Hybrid Hydrogel Based on UCST Triblock Copolymer and Gold Nanorods. *Polymers* **2017**, *9* (6), 1-9.

22. Tranquilan-Aranilla, C.; Nagasawa, N.; Bayquen, A.; Dela Rosa, A., Synthesis and characterization of carboxymethyl derivatives of kappa-carrageenan. *Carbohydrate Polymers* **2012**, *87* (2), 1810-1816.

23. Kale, R. N.; Bajaj, A. N., Ultraviolet Spectrophotometric Method for Determination of Gelatin Crosslinking in the Presence of Amino Groups. *Journal of Young Pharmacists : JYP* **2010**, *2* (1), 90-94.

24. Leong, K. H.; Chung, L. Y.; Noordin, M. I.; Mohamad, K.; Nishikawa, M.; Onuki, Y.; Morishita, M.; Takayama, K., Carboxymethylation of kappa-carrageenan for intestinal-targeted delivery of bioactive macromolecules. *Carbohydrate Polymers* **2011**, *83* (4), 1507-1515.

25. Turquois, T.; Acquistapace, S.; Vera, F. A.; Welti, D. H., Composition of carrageenan blends inferred from 13C-NMR and infrared spectroscopic analysis. *Carbohydrate Polymers* **1996**, *31* (4), 269-278.

26. Kačuráková, M.; Wilson, R. H., Developments in mid-infrared FT-IR spectroscopy of selected carbohydrates. *Carbohydrate Polymers* **2001**, *44* (4), 291-303.

27. Fujishima, M.; Matsuo, Y.; Takatori, H.; Uchida, K., Proton-conductive acid–base complex consisting of κ-carrageenan and 2-mercaptoimidazole. *Electrochemistry Communications* **2008**, *10* (10), 1482-1485.

28. Liew, J. W. Y.; Loh, K. S.; Ahmad, A.; Lim, K. L.; Wan Daud, W. R., Synthesis and characterization of modified κ-carrageenan for enhanced proton conductivity as polymer electrolyte membrane. *PloS one* **2017**, *12* (9), 1-15.

29. Liu, X.; Cao, J.; Li, H.; Li, J.; Jin, Q.; Ren, K.; Ji, J., Mussel-Inspired Polydopamine: A Biocompatible and Ultrastable Coating for Nanoparticles in Vivo. *ACS Nano* **2013**, *7* (10), 9384-9395.

30. Xu, H.; Liu, X.; Wang, D., Interfacial Basicity-Guided Formation of Polydopamine Hollow Capsules in Pristine O/W Emulsions – Toward Understanding of Emulsion Template Roles. *Chemistry of Materials* **2011**, *23* (23), 5105-5110.

31. Rochas, C.; Rinaudo, M., Mechanism of gel formation in k-Carrageenan. *Biopolymers* **1984**, *23*, 735–745.

32. Naim, S.; Samuel, B.; Chauhan, B.; Paradkar, A., Effect of potassium chloride and cationic drug on swelling, erosion and release from kappa-carrageenan matrices. *AAPS PharmSciTech* **2004**, *5* (2), 1-8.

33. MacArtain, P.; Jacquier, J. C.; Dawson, K. A., Physical characteristics of calcium induced κ- carrageenan networks. *Carbohydrate Polymers* **2003**, *53* (4), 395-400.

34. Santo, V. E.; Frias, A. M.; Carida, M.; Cancedda, R.; Gomes, M. E.; Mano, J. F.; Reis, R. L., Carrageenan-Based Hydrogels for the Controlled Delivery of PDGF-BB in Bone Tissue Engineering Applications. *Biomacromolecules* **2009**, *10* (6), 1392-1401.

35. Weng, L.; Gouldstone, A.; Wu, Y.; Chen, W., Mechanically strong double network photocrosslinked hydrogels from N,N-dimethylacrylamide and glycidyl methacrylated hyaluronan. *Biomaterials* **2008**, *29* (14), 2153-2163.

Chapter 4

Degradation of oxidized Dex-GMA by amino groups released from amino-CG@PDA and its application for drug delivery use

4.1 Introduction

Hydrogels are the hydrophilic polymer network which can hold large amounts of water or biological fluid. They may be chemically stable or can degrade and eventually disintegrate and dissolve [1]. Hydrogels are called reversible or physical gel when molecular entanglements and/or secondary forces such as ionic, H-bonding or hydrophobic forces are held together in forming network [2, 3]. In chemical gels, the network of covalent bonds are formed by crosslinking agent between macromolecule chains. The chemically charged hydrogels normally exhibit change in variation of temperature and pH. In case of physical gels, they are often reversible and show the possibility to dissolve when the environmental conditions (such as pH, ionic strength, or temperature) are changed [1]. The utilization of gel types depends on the application, the main areas are wound dressings, drug delivery systems, tissue engineering.

Hydrogels have been attracted for their use in drug delivery due to their unique properties such as high water absorption, high porosity, allowable drugs to be loaded, and sustained release. The release of drugs may go on through different mechanisms; diffusion controlled, swelling

controlled, chemically controlled and environmentally-responsive release [4, 5]. Some natural polymers can form hydrogel. Lin et al. [6] synthesized water-soluble chitosan derivative N-(2-carboxybenzyl)chitosan (CBCS) based pH sensitive hydrogel for colon-specific drug delivery system. The release of 5-fluorouracil (5-FU) was pH dependent for instance the release was much quicker in pH 7.4 buffer than in pH 1.0 solution. The carboxyl groups (COOH) in the hydrogels were the dominant part that would dissociate when increasing the osmotic pressure inside the hydrogels at higher pH, leading to gain swelling ratio and release drugs consequently. Dextran-based nanogels are fabricated by graft polyacrylic acid (PAA) on dextran (Dex) nanohydrogels (NGs) with covalent disulfide crosslinking (Dex-SS-PAA) for anti-cancer therapeutics [7]. The Dex-SS-PAA were subsequently conjugated with doxorubicin through an acid-labile hydrazone bond (Dex-SS-PAA-DOX). The results showed that fabricated dextran-based hydrogel exhibited pH- and redox-controlled drug release with strongly inhibited the growth of human breast cancer cells (MDA-MB-231) and reduce toxic of free DOX. Moreover, the control degradation of hydrogel has been become attention in drug delivery system, particularly control release of drug from hydrogel degradation.

Biodegradable hydrogels have been studied for many applications including drug delivery, tissue engineering, and cell encapsulation and culture. The release rates of the drugs which controlled by biodegradation kinetics of the polymers becomes attractive in drug delivery system. Two strategies are typically used to obtain degradable hydrogels, firstly, the backbone of polymer gel are designed to degrade by hydrolysis and/or enzymatic action. The second method involves introduction of degradable cross-linking points to systems that are comprised of non-degradable polymer chains [8, 9]. In previous report, Hyon et al. [10] prepared hydrogels by the reaction between aldehyde group in oxidized dextran and amino group in poly-L-lysine. The hydrogel showed degradation in the phosphate buffer solution (PBS) and the degradation time

can be controlled by the aldehyde introduction rate and amine concentration which were the crosslinking point of hydrogel. The mechanism behind the degradation was reported that the main chain of oxidized dextran was degraded by the Maillard reaction triggered by the Schiff base formation between aldehyde and amino groups. The degradation speed was found to depend on the amount of chemical crosslinking points during gelation. In addition, the degradation of hydrogel can be stimulated by various manners such as enzymes, chemical reactions, heat, and light depending on the type of hydrogels.

Light-responsive hydrogels are generally classified into two major types. First type, photodegradable hydrogels that possess photolabile moieties, such as o-nitrobenzyl [11] and azobenzene [12]), in their structures and thermo-sensitive hydrogels. Second type, thermo-sensitive hydrogels such as PNIPAM [13] that near infrared (NIR) materials (e.g., nanorods [14] and carbon nanotubes [15] are encapsulated into gel forming. The photodegradable hydrogels release drugs upon light-triggered degradation of their structures. In case of polysaccharide, k-carrageenan has been extensively used as gelling agent due to their biocompatibility and ability to form thermoreversible hydrogel. Temperature and NIR light responsive multi-walled carbon nanotube (MWCNT)-k-carrageenan hydrogel composites have been prepared [15]. Under NIR-light irradiation, the gel-to-sol transition MWCNT–k-carrageenan hydrogel composites (0.25 wt% CNTs) can be observed after 3.5 min exposure while for the unloaded hydrogel did not undergo any visible phase transition. Suggesting that hydrogel composites have potential in the development of remotely controlled light activated drug delivery systems.

In this study, the dispersion of amino-CG@PDA in oxidized Dex-GMA based hydrogel was prepared. NIR light was irradiated for amino release leading to react with aldehyde

remaining in hydrogel, consequently release of drugs loaded in hydrogel via hydrogel degradation.

4.2 Materials and methods

4.2.1 Materials

Doxorubicin hydrochloride (DOX) was obtained from Beijing Packbuy M&C Co., Ltd. The oxidized Dex-GMA based hydrogel and amino-CG were provided as descripted in Chapter 2 and 3. Glycine and other chemicals were purchased from Nacalai Tesque, Inc., (Kyoto, Japan). All chemicals were used without purification.

4.2.2 Mw determination of oxidized Dex-GMA by GPC

To investigate the Mw decreasing of oxidized Dex-GMA by amino groups addition, 2% (w/v) of oxidized Dex-GMA (24% oxidation, 23% DS of GMA) was mixed with the same volume of 5% (w/v) amino-CG solution (or glycine) and then incubated at 37 °C. To determine the molecular weight of oxidized Dex-GMA at the desired time after reaction, gel permeation chromatography (GPC) (Shimadzu, Japan, BioSep-s2000 column, Phenomenex, Inc., CA, USA) was utilized. PBS was used as the mobile phase (flow rate = 0.50 mL/min) and pullulan was used as the standard.

4.2.3 Drug loaded into oxidized Dex-GMA based hydrogel

DOX was dissolved in the solution of 10 wt% oxidized Dex-GMA (10% oxidation, 23% DS of GMA) in PBS with concentration of 0.05 mg/mL. The hydrogel loaded DOX was prepared, briefly, 0.5 mL of mixture solution of DOX and oxidized Dex-GMA, 0.5 mL of 1.36 wt% DTT, and 0.01 g of amino-CG@PDA were mixed in test tube and was then incubated at 37

°C for 30 min to allow the gelation, and the product was denoted as DOX@hydrogel. Here, we assumed that 100% of the drug was loaded into hydrogel.

4.2.4 Light-Responsive drug releasing test

For NIR-triggered drug release from hydrogel, the prepared DOX@hydrogel was immersed in 5 mL of PBS, and exposed to NIR light (808 nm, 1.0 W/cm^2) for 30 min. One milliliter of the solution was collected at different time points (0.5, 1.5, 2.5, 3.5, and 4.5 h) to analyze the DOX release by fluorescence spectroscopy (λ_{ex} 480 nm and λ_{em} 590 nm). Then, 1 mL of PBS was re-added the rest of the mix for further irradiation. The experimental setup is shown in Figure 4.1. The cumulative amount of Dox released from the hydrogel was calculated according to the following equation:

$$\text{DOX release efficiency (\%)} = (W_t/W_i) \times 100$$

Where W_i and W_t are the DOX content in the oxidized Dex-GMA based hydrogel and released from the loaded hydrogel at time t during the release process, respectively.

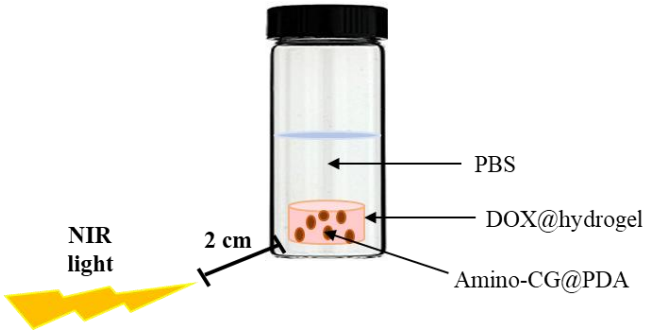

Figure 4.1 Experimental setup for light-responsive drug releasing test.

4.3 Results and discussion

4.3.1 Mw determination of oxidized Dex-GMA

In this study, the Mw decreasing of oxidized Dex-GMA after the reaction with amino-CG, and glycine solution was determined by the mixing solution of oxidized Dex-GMA and amino-CG (or glycine) at 37 °C. The Mw of various samples were recorded by GPC every 20 min for 3 h as shown in Figure 4.2, and the Mw of oxidized Dex-GMA (1% w/v) dramatically decreased in glycine solution (2.5% w/v) at the first 30 min and then gradually reduced until be stable over 3 h (red line).

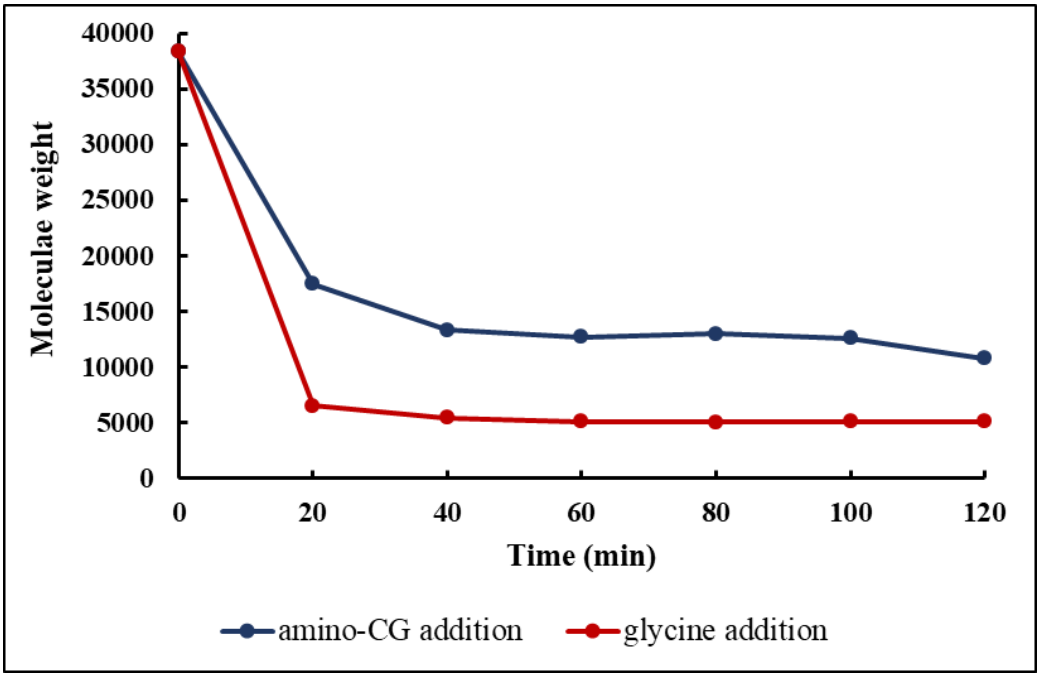

Figure 4.2 Mw decrease of oxidized Dex-GMA by amino-CG and glycine addition.

Similarly, the same trend of Mw decrease from 2.5% w/v amino-CG addition was detected, however, the higher Mw than that in glycine solution after degradation was observed (blue line). The reason behind this result is the amino content presented in amino-CG was lower than free amino groups from glycine solution, leading to the low power of degradation. Due to the ability to trigger the degradation of amino-CG, thus it was further used to control the degradation of hydrogel.

4.3.2 NIR light-responsive DOX release from hydrogel degradation test

Hydrogels provide a platform for achieving controlled therapeutic delivery to specific sites. The stimulus responsive hydrogels undergo changes (such as degradation) in response to environmental triggers. This property suggests the possible use of these materials for specific functions, especially drug release [16,17]. Doxorubicin is one of the most widely used commercial anticancer drugs in clinical application. Its derivative DOX•HCl is soluble in water, and hence it was used as a model drug to investigate the release from Ox-GMA-Dex based hydrogel. Figure 4.3A and 4.3B show the cumulative drug release from hydrogels loaded with 10 μg/ml drug over 5 h and 10 days in PBS, respectively. Only a very small amount of DOX was released in the absence of NIR light (black line), and it may come from free DOX liberated from the outer surface of hydrogel. In the presence of NIR light, we proposed a model of drug release as shown in Figure 4.4. The NIR light is irradiated on the DOX@hydrogel (step A), generating heat in the PDA of amino-CG@PDA microcomposites. This heating triggers the gel-to-sol phase transition of amino-CG to produce a flowing sol (step B) [18,19]. Then, the released amino-CG reacts with the remaining aldehyde on the hydrogel to form Schiff base in step C, initiating the degradation process which facilitates drug release (step D). In this experiment, the amino-CG@PDA gel beads started to transform to sol when irradiated under NIR light. After 4 h of

incubation the beads dissolved completely, suggesting that the Schiff base reaction occurred. The cumulative DOX release is significantly increased under NIR irradiation compared that with without NIR light. Thus, the release of drug from hydrogel can be controlled by NIR trigger, and drug release continues to some extent even after the NIR light was turned off. However, the cumulative DOX %release was only 5.5% over 5 h, and the hydrogel was not completely degraded. The release of DOX was likely to come from two factors: degradation and hydrogel swelling. The small amount of release may be explained as follows. First, the DOX molecules are positively charged and can be easily adsorbed on the negatively charged Ox-GMA-Dex chain by electrostatic interaction. Hence, the release of DOX by diffusion from the Ox-GMA-Dex hydrogel network was slow. The second reason was the low speed of hydrogel degradation, which is the critical step for drug release from the hydrogel. Because the amount of amino source used (5.4×10^{-6} mole $-NH_2$) was 11.5 times lower than the aldehyde content in oxidized Dex-GMA (6.2×10^{-5} mole), the degradation points (Shift base formation) was subsequently less quantity, hence the slow release of the drug. Figure 4.3B shows the cumulative DOX release profile over 10 days without NIR light irradiation after the first 5 h. We estimated that as much time as 10 days was required for main chain scission of DOX@hydrogel to enhance the DOX release. The main chain degradation of oxidized Dex-GMA hydrogel proceeded gently for the first 2 days to reach a DOX release of almost 10%. After that, the main chain scission was significantly accelerated, reaching a cumulative drug release of up to 83% over 7 days, and 100% release can be obtained for 10 day of incubation with complete degradation of hydrogel. These findings indicate that we can control the release of drug by hydrogel degradation triggered from NIR irradiation.

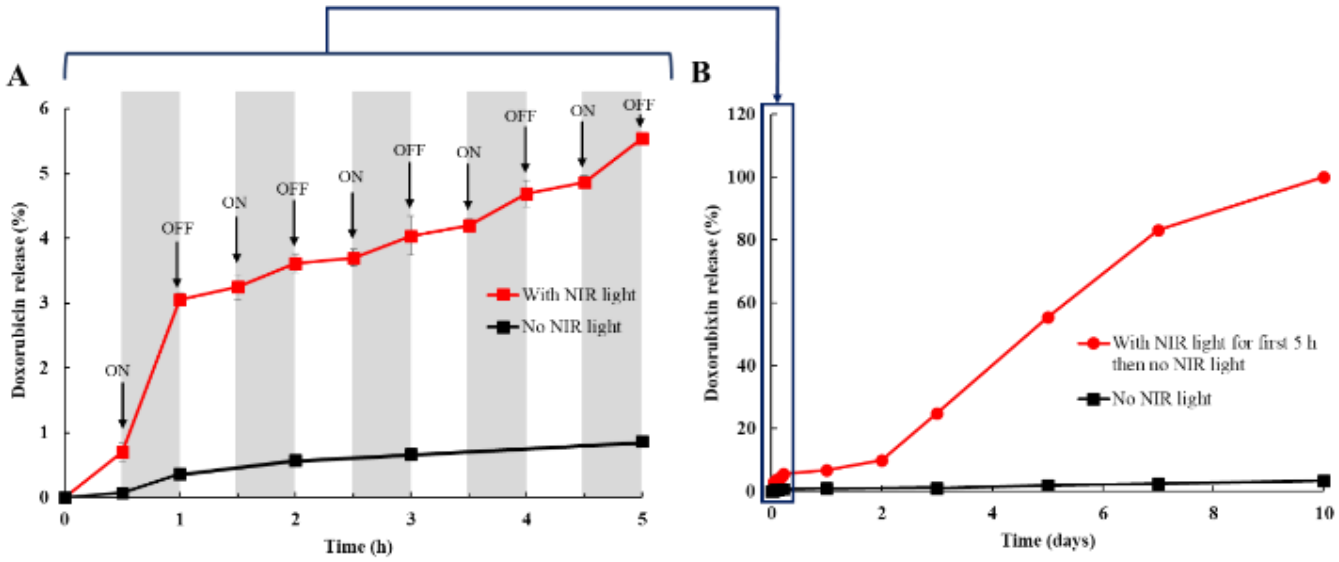

Figure 4.3 (A) Cumulative release profiles of DOX from hydrogel with and without NIR-light irradiation over 5 h. (B) Cumulative release profiles of DOX from hydrogel over 10 days.

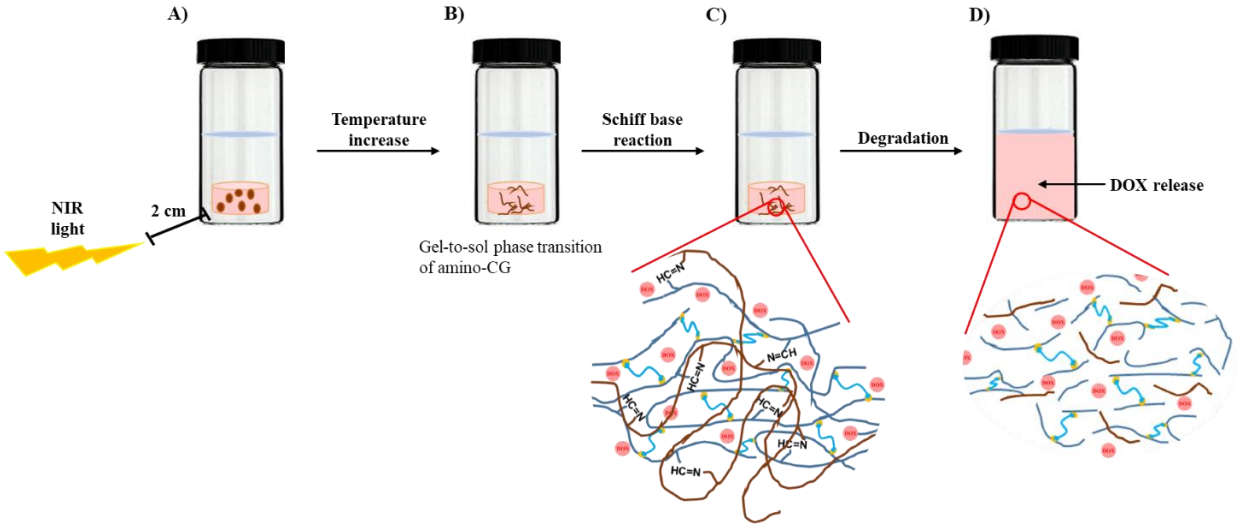

Figure 4.4 Schematic presentation of drug release under NIR irradiation.

4.4 Conclusion

The results revealed that the amino-CG provided the ability to be the amino source for the reaction with aldehyde groups from oxidized Dex-GMA to initiate the main chain degradation of oxidized Dex-GMA. The amino-CG@PDA gel beads were responsive to the temperature which can be changed by NIR light resulting the gel-to-sol phase transformation of amino-CG beads. The release of DOX from oxidized Dex-GMA based hydrogel was controlled under NIR irradiation due to the Schiff base reaction of amino compound from amino-CG and the preserved aldehyde on hydrogel, hence the degradation occurred and drug was able to be released. This kind of controlled drug release model can be regarded as a promising candidate for therapeutic hydrogels in drug delivery, although the rate of degradation should be considered.

References

1. Hoffman, A. S., Hydrogels for biomedical applications. *Advanced drug delivery reviews* **2002**, *54* (1), 3-12.

2. Campoccia, D.; Doherty, P.; Radice, M.; Brun, P.; Abatangelo, G.; Williams, D. F., Semisynthetic resorbable materials from hyaluronan esterification. *Biomaterials* **1998**, *19* (23), 2101-2127.

3. Prestwich, G. D.; Marecak, D. M.; Marecek, J. F.; Vercruysse, K. P.; Ziebell, M. R., Controlled chemical modification of hyaluronic acid: synthesis, applications, and biodegradation of hydrazide derivatives. *Journal of Controlled Release* **1998**, *53* (1), 93-103.

4. Xiong, X. Y.; Tam, K. C.; Gan, L. H., Polymeric nanostructures for drug delivery applications based on Pluronic copolymer systems. *Journal of nanoscience and nanotechnology* **2006**, *6* (9-10), 2638-2650.

5. Hoare, T. R.; Kohane, D. S., Hydrogels in drug delivery: Progress and challenges. *Polymer* **2008**, *49* (8), 1993-2007.

6. Lin, Y.; Chen, Q.; Luo, H., Preparation and characterization of N-(2-carboxybenzyl)chitosan as a potential pH-sensitive hydrogel for drug delivery. *Carbohydrate Research* **2007**, *342* (1), 87-95.

7. Wang, H.; Dai, T.; Zhou, S.; Huang, X.; Li, S.; Sun, K.; Zhou, G.; Dou, H., Self-Assembly Assisted Fabrication of Dextran-Based Nanohydrogels with Reduction-Cleavable Junctions for Applications as Efficient Drug Delivery Systems. *Scientific Reports* **2017**, *7*, 1-12.

8. Olde Damink, L. H.; Dijkstra, P. J.; van Luyn, M. J.; van Wachem, P. B.; Nieuwenhuis, P.; Feijen, J., In vitro degradation of dermal sheep collagen cross-linked using a water-soluble carbodiimide. *Biomaterials* **1996**, *17* (7), 679-684.

9. Eliaz, R. E.; Kost, J., Characterization of a polymeric PLGA-injectable implant delivery system for the controlled release of proteins. *Journal of biomedical materials research* **2000**, *50* (3), 388-936.

10. Hyon, S. H.; Nakajima, N.; Sugai, H.; Matsumura, K., Low cytotoxic tissue adhesive based on oxidized dextran and epsilon-poly-L-lysine. *Journal of biomedical materials research. Part A* **2014**, *102* (8), 2511-2520.

11. DeForest, C. A.; Anseth, K. S., Photoreversible patterning of biomolecules within click-based hydrogels. *Angewandte Chemie* **2012**, *51* (8), 1816-1819.

12. Tamesue, S.; Takashima, Y.; Yamaguchi, H.; Shinkai, S.; Harada, A., Photoswitchable supramolecular hydrogels formed by cyclodextrins and azobenzene polymers. *Angewandte Chemie* **2010**, *49* (41), 7461-7464.

13. Zhao, X.-q.; Wang, T.-x.; Liu, W.; Wang, C.-d.; Wang, D.; Shang, T.; Shen, L.-h.; Ren, L., Multifunctional Au@IPN-pNIPAAm nanogels for cancer cell imaging and combined chemo-photothermal treatment. *Journal of Materials Chemistry* **2011**, *21* (20), 7240-7247.

14. Shiotani, A.; Mori, T.; Niidome, T.; Niidome, Y.; Katayama, Y., Stable Incorporation of Gold Nanorods into N-Isopropylacrylamide Hydrogels and Their Rapid Shrinkage Induced by Near-Infrared Laser Irradiation. *Langmuir* **2007**, *23* (7), 4012-4018.

15. Estrada, A. C.; Daniel-da-Silva, A. L.; Trindade, T., Photothermally enhanced drug release by [small kappa]-carrageenan hydrogels reinforced with multi-walled carbon nanotubes. *RSC Advances* **2013**, *3* (27), 10828-10836.

16. Buwalda, S. J.; Vermonden, T.; Hennink, W. E., Hydrogels for Therapeutic Delivery: Current Developments and Future Directions. *Biomacromolecules* **2017**, *18* (2), 316-330.

17. Gao, L.; Sun, Q.; Wang, Y.; Zhu, W.; Li, X.; Luo, Q.; Li, X.; Shen, Z., Injectable poly(ethylene glycol) hydrogels for sustained doxorubicin release: Injectable Hydrogels for Drug Delivery. *Polymers for Advanced Technologies* **2016**, *28* (1), 35-40.

18. Pekcan, Ö.; Tari, Ö., A fluorescence study on the gel-to-sol transition of κ-carrageenan. *International Journal of Biological Macromolecules* **2004**, *34* (4), 223-231.

19. Kara, S.; Tamerler, C.; Bermek, H.; Pekcan, Ö., Cation effects on sol–gel and gel–sol phase transitions of κ-carrageenan–water system. *International Journal of Biological Macromolecules* **2003**, *31* (4), 177-185.

Chapter 5

General conclusion

Regarding to the objective of this research, the main goal of the study is to overcome the drawback of uncontrollable degradation timing of oxidized dextran-based hydrogel prepared by the reaction between aldehyde groups in oxidized dextran and amino groups. And the control release of amino source from the temperature-sensitive material by NIR stimulation was considered. In chapter 2, I introduced GMA into oxidized dextran and then forming a hydrogel with DTT while preserving the aldehyde to react with amine source. The finding showed that the degradation did not occur immediately after the hydrogels were formed. The addition of amine began a reaction with the remaining aldehyde, which triggering the degradation through a Maillard reaction via a Schiff base reaction. Moreover, the degradation could be controlled by the posteriori addition of an amine source, and interestingly, the degradation speed could be controlled independently of the mechanical properties of the hydrogel because the crosslinking points (both the GMA-thiol and aldehyde-thiol crosslinks) and degradation points (the reaction of aldehyde groups and amine) were different. In addition, the details of degradation mechanisms at the molecular level have been elucidated which can be helpful for the design of polymer materials in the precise degradation control.

Chapter 3, the themoresponsive material, amino-CG@PDA microcomposite was fabricated. It can be used as an NIR light-controlled release-targeted system for amino groups via gel-to-sol phase transition. The environmental temperature and external NIR irradiation have an obvious influence in photothermal-responsive release property that is, the release of amino groups from the transforming of amino-CG@PDA microcomposites gel beads to sol state was enhanced by increasing temperature and more greatly under NIR-light irradiation.

In chapter 4, amino-CG provides the ability to be the amino source for the reaction with aldehyde groups from oxidized Dex-GMA to initiate the main chain degradation of oxidized Dex-GMA. The amino-CG@PDA gel beads were suspended in drug-loaded oxidized dextran based-hydrogel. The release of drug from oxidized Dex-GMA based hydrogel was controlled under NIR irradiation due to the release of amino compound from amino-CG@PDA to react with the preserved aldehyde on hydrogel, leading to Schiff base formation. Hence, the degradation is started and drug can be released.

In this thesis, the controllable degradation of oxidized dextran-based hydrogels was accomplished. The release of amino compound was successfully controlled by NIR switching, subsequently react with the remaining aldehyde from oxidized dextran based-hydrogel and further initiated the main chain scission by Maillard reaction. For the future work, the animal implantation by this hydrogel should be considered. Hopefully, this platform can be regarded as a promising candidate for therapeutic hydrogels in drug delivery applications and tissue engineering.

Achievement

Research articles

Nonsuwan, P.; Puthong, S.; Palaga, T.; Muangsin, N., Novel organic/inorganic hybrid flower-like structure of selenium nanoparticles stabilized by pullulan derivatives. *Carbohydrate Polymers* **2018,** *184*, 9-19.

Nonsuwan, P; Matsukami, A; Hayashi, F; Hyon, S; Matsumura, K., Controlling the degradation of an oxidized dextran-based hydrogel independent of the mechanical properties. (accepted)

Conferences

Punnida Nonsuwan, Suong Hyu Hyon, Kazuaki Matsumura

9th International Conference on Fiber and Polymer Biotechnology, Osaka, Japan, 7-9 Sep 2016 (Best Poster Presentation)

Degradation control of multiple crosslinked dextran based hydrogel

Punnida Nonsuwan, Songchan Puthong, Nungnuj Muangsin

28th Annual Meeting of the European Society for Biomaterials (ESB 2017), Athens, Greece, 4-8 Sep 2017

Pullulan derivative for Stabilization and Control Shape of Nanoparticles

Punnida Nonsuwan, Suong Hyu Hyon, Kazuaki Matsumura

MRS Fall meeting 2017, Boston, USA, 26 Nov-1 Dec 2017

Control of degradation of oxidized dextran-based hydrogel formed via Michael addition

Punnida Nonsuwan, Suong Hyu Hyon, Kazuaki Matsumura

Hokuriku Biomaterials conference, Nagano, Japan, 15 Dec 2016

Degradation control of oxidized dextran-based hydrogel formed by hybrid cross-linking

Acknowledgements

This research could not be successful without the valuable advice of my advisor. I am highly thankful to Assoc. Prof. Kazuaki Matsumura for supporting, assistance, guidance, motivation and good suggestion for solving a problem through the completion of my doctoral study. I really appreciate all his contributions of time, opinion, and funding to make my Ph.D. experience productive and stimulating. Without his supports, I would have been imaginable this thesis could be completed and achieved. It is a great honor for me to be a member in Matsumura's laboratory.

I would like to express my appreciation to Dr. Fumiaki Hayashi from Division of Structural and Synthetic Biology, RIKEN Center for Life Science for NMR analysis. I also deeply appreciate the members of my committee: Prof. Masayuki Yamaguchi, Prof. Tatsuo Kaneko and Assoc. Prof. Takumi Yamaguchi. Further I would like to thank dual degree program (CU-JAIST) Scholarships for financial support during my doctoral study. Without these facilities and sponsorship, I would not be possible to conduct this research.

I am profoundly grateful to Prof. Nongnuj Muangsin for an encouragement and pushing me to apply CU-JAIST dual degree scholarship and also her valuable advice for minor research. Without her, I would not have been able to achieve and complete my study.

I really grateful to my family for their all along encourage, understanding, and greatest support and my friends for every spirit.

Finally, I would like to thank myself for my super power to send me pass many challenging and difficult experiences. I really grew up and can be held up a big smile on my face.